SPECTROELECTROCHEMICAL STUDIES OF HEME AND COPPER PROTEINS

Thesis by

Walther Robert Ellis, Jr.

In Partial Fulfillment of the Requirements

for the Degree of

Doctor of Philosophy

California Institute of Technology

Pasadena, California

1986

(Submitted May 19, 1986)

"Wir sehen in der Natur nicht Wörter, sondern immer nur Anfangsbuchstaben von Wörtern, und wenn wir alsdann lesen wollen, so finden wir, daß die sogenannten Wörter wiederum bloß Anfangsbuchstaben von anderen sind."

Georg Christoph Lichtenberg

ACKNOWLEDGEMENTS

In reviewing my graduate career at Caltech, I find that there is an extraordinary number of people to whom I owe a considerable debt. In many respects this thesis is not mine alone; it is due to the cumulative efforts of a cast of thousands, only some of whom can be singled out for mention below.

First and foremost, I am deeply indebted to my family. My parents have constantly encouraged me to relentlessly pursue my own interests in both the arts and sciences. They endured my protracted graduate career with considerable patience, tinged only occasionally with mild sarcasm. I think it's safe to say that we are all relieved that it's over. I wish my sister Karen well as she finishes her undergraduate studies. One day I hope to read her doctoral thesis.

The affluence and intellectual atmosphere at Caltech have made graduate school here a unique experience for me. At this time, I would like to acknowledge the example set by a number of chemistry faculty from whom I have learned much: Fred Anson, Sunney Chan, John Hopfield, Rudy Marcus, and Dick Marsh. Each of them has had a great influence on me and I am grateful for the opportunity of observing them work and for their patience in enduring my many naive questions. The staff of the divisional shops are rarely acknowledged in publications for their contributions and three of them, Delmer Dill, Tom Dunn, and Erich Siegel, certainly deserve mention.

I have found my graduate teaching duties to be personally rewarding. Hopefully Jeddi Master Tad Fox, my successor to the Ch 213 tutorship, will straighten out the mess that I created in revising the

course. David Beratan is warmly thanked for sharing with me the responsibilities incurred in creating and administering a new special topics course : Electron Transfer Reactions (Ch 140).

Being a member of the Gray group is an unforgettable experience. In particular, I would like to thank Vern, Les, Vanessa, Janet, Bob, Jon, Tom, Kathy, Ann, Tad, Vinnie, Miriam, Al, Jenny, Andy, Mike A., Mike H., Mary, Alison, Cindy, Dave, and Charlie for good times in and out of the lab. I would also like to thank a number of visiting faculty for many helpful discussions and valued friendship: Bo Malmström, Israel Pecht, Woody Woodruff, Milo Bordignon, George McLendon, and John Webb. As an unofficial member of the Chan group, I have acquired an appreciation of the "mysteries" of cytochrome oxidase. The thousands of hours spent with Dave Blair and Hsin Wang on the oxidase project will be long (and painfully) remembered.

It is a great pleasure to be able to thank Harry Gray for having served as my research advisor. His good humor, élan, infectious enthusiasm for science, and catholic research interests make his research group an exciting place to scientifically mature. Harry has never tired of reminding me that I am a "legend in my own mind" and a "second-rate drinker." I plead guilty to the first charge and defer rebuttal of the second to a future social outing. At one time I was somewhat dismayed by his policy of "rule by benign neglect." Now I realize that this hands-off treatment, having been mastered by many of his students, is in large part responsible for Harry's present status as one of the godfathers of contemporary inorganic chemistry. Happy 50^{th}, Padrone.

ABSTRACT

A complete characterization of the redox thermodynamics of a metalloprotein involves the determination of the effects of pH, ionic strength, and temperature. In particular, variable-temperature reduction potential measurements yield the enthalpic and entropic contributions to E^{o}, which, in turn, are related to kinetic activation parameters.

In Chapter II of this thesis, the design of a versatile spectroelectrochemical apparatus for high precision measurements of metalloprotein reduction potentials is described. A stainless steel shroud, necessary for anaerobic measurements, is used to house either of two types of spectroelectrochemical cells: a thin-layer optically transparent electrode cell, or a two cm. stirred cell (useful for observing weak chromophores). Both types of cells are suitable for variable-temperature measurements using either absorption or circular dichroism spectroscopy. The latter offers a useful alternative to absorption spectroscopy since redox mediators, which are almost always necessary for electrochemical experiments on metalloproteins, are generally not optically active and therefore will not interfere with the acquisition of protein circular dichroism spectra.

Spectroelectrochemical measurements for a selection of paradigmatic hemoproteins are presented in Chapter III. Horse heart cytochrome _c_ is shown to yield redox thermodynamic parameters in excellent agreement with results of calorimetric determinations. Data for _R. palustris_ cytochrome _c′_ and myoglobin are also presented and discussed with reference to extant spectroscopic and kinetic data, and

crystal structure determinations for these proteins. ΔS^o does not correlate with protein surface charge, unlike the well-known correlation of ΔS^o with charge for transition metal complexes. Instead, it is suggested that ΔS^o is (at least in part) determined by redox-linked protein conformational changes. Next, redox thermodynamic parameters for the azurins from A. denitrificans and A. faecalis are presented. The azurin data show that proton uptake (in the region $pK_a^{ox} < pH < pK_a^{red}$) accompanying the reduction of the copper site decreases ΔS^o slightly. This observation is discussed in light of crystallographic studies on "blue" copper proteins.

Chapter IV discusses the problems of temperature and metal-metal interactions associated with the equilibrium redox behavior of multi-site metalloproteins. An analogy between allosteric ligand binding and allosteric electron binding (i.e., reduction) is used to analyze Nernst plots exhibiting unusual slopes. In interactive situations, the conventionally defined reduction potential is not a simple thermodynamic quantity. This formalism is used in a discussion of the equilibrium redox interactions displayed by the optically visible metal centers (Cu_A, Fe a, Fe a_3) in cytochrome c oxidase. The commonly accepted "neoclassical" model, which only incorporates interaction between Fe a and Fe a_3, is shown to be incorrect. The importance of temperature (leading to varying entropies of reduction for different metal sites in a protein) is illustrated by a $(NH_3)_5Ru$(His-48)-derivative of sperm whale myoglobin. Kinetic and thermodynamic data for this two-site protein lead to an estimate of 20 kcal/mol for the reorganizational enthalpy of the iron heme in myoglobin. This value

is substantially larger than the 7-8 kcal/mol estimate for horse cytochrome _c_, and is most likely due to a ligation change upon reduction of myoglobin wherein the axial water molecule dissociates from the iron center.

A detailed discussion of the pH, ionic strength, and temperature dependences of the formal reduction potentials of the Cu_A, Fe _a_, and Fe $_{a_3}$ centers in cytochrome oxidase is the topic of Chapter V. These results are compared with values for other protein copper and heme sites and are discussed within the context of the known structural features and reactivity of the enzyme.

TABLE OF CONTENTS

CHAPTER I

OVERVIEW

BIOENERGETIC ROLES OF METALLOPROTEINS

By definition, bioenergetics (1,2) is concerned with the transformations of energy in biological systems. Three fundamental mechanisms of energy extraction and storage have been identified (3) in living organisms: glycolysis, respiration, and photosynthesis. The process of glycolysis involves the fermentation of glucose to produce lactic acid, which has a lower free energy content and is eliminated as waste products. In respiration, energy is extracted from organic compounds by combining them with an oxidant such as sulfate, nitrate, or molecular oxygen. Photosynthesis is a process whereby solar energy is trapped and then stored as carbon dioxide is reduced to produce molecules of high free energy content.

All of these processes involve electron transfer reactions, and proteins are needed to accept electrons and pass them on. Such proteins (4) contain redox-active prosthetic groups of both an organic and an inorganic nature, e.g., flavins, ubiquinone, nicotinamide adenine dinucleotide (NAD), iron hemes, copper ions, and iron-sulfur clusters. The proteins and protein complexes involved in mitochondrial oxidative phosphorylation (5,6) and photosynthesis (7,8) have been objects of intense scrutiny for at least thirty years, yet the functions of these electron transfer proteins are not presently understood in any detail.

Electron transfer chains play a central role in biological energy transduction. A feature of them all is that they contain transition metal ions in unusual chemical environments. The recognition of this circumstance has led to renewed interest in preparative coordination

chemistry, with the goal of modeling coordination sites in metalloproteins (9).

The mammalian respiratory assembly serves as an illustration of the current understanding of metalloprotein structure and redox function. Oxidative phosphorylation is carried out by respiratory assemblies located in the inner membrane of mitochondria. Figure 1 depicts a simplified view of the flow of electrons from NADH to dioxygen via a series of electron carriers: flavins, iron-sulfur clusters, quinones, and iron hemes. Except for the quinones, these electron carriers are prosthetic groups of proteins. The net reaction

$$1/2\ O_2 + NADH + H^+ \longrightarrow H_2O + NAD^+ \qquad (1)$$

is accompanied by a free energy decrease of 53 kcal/mol.

The mitochondrial electron transfer chain has been resolved into a series of protein complexes that are linked by the electron carriers ubiquinone and cytochrome _c_. It has been recently shown (10) that a structurally ordered chain of electron transfer proteins is not required for rapid and sequential electron transfer from NADH to O_2. Freeze-fracture microscopy and laser fluorescence studies indicate that the respiratory components diffuse laterally and independently over the inner mitochondrial membrane. The complexes of the respiratory chain are: NADH dehydrogenase (Complex I), succinate dehydrogenase (Complex II), ubiquinol-cytochrome _c_ reductase (Complex III, containing cytochromes _b_ and $_{c_1}$), and cytochrome _c_ oxidase (Complex IV, containing cytochrome _a_). All of these protein complexes

Figure 1. A simplified view of the release of free energy as electrons flow from NADH to molecular oxygen in the mitochondrial oxidative phosphorylation chain. At three points the standard free energy decrease is especially large in order to provide energy for ATP synthesis. E_{FMN} represents NADH dehydrogenase and CoQ is coenzyme Q (ubiquinone).

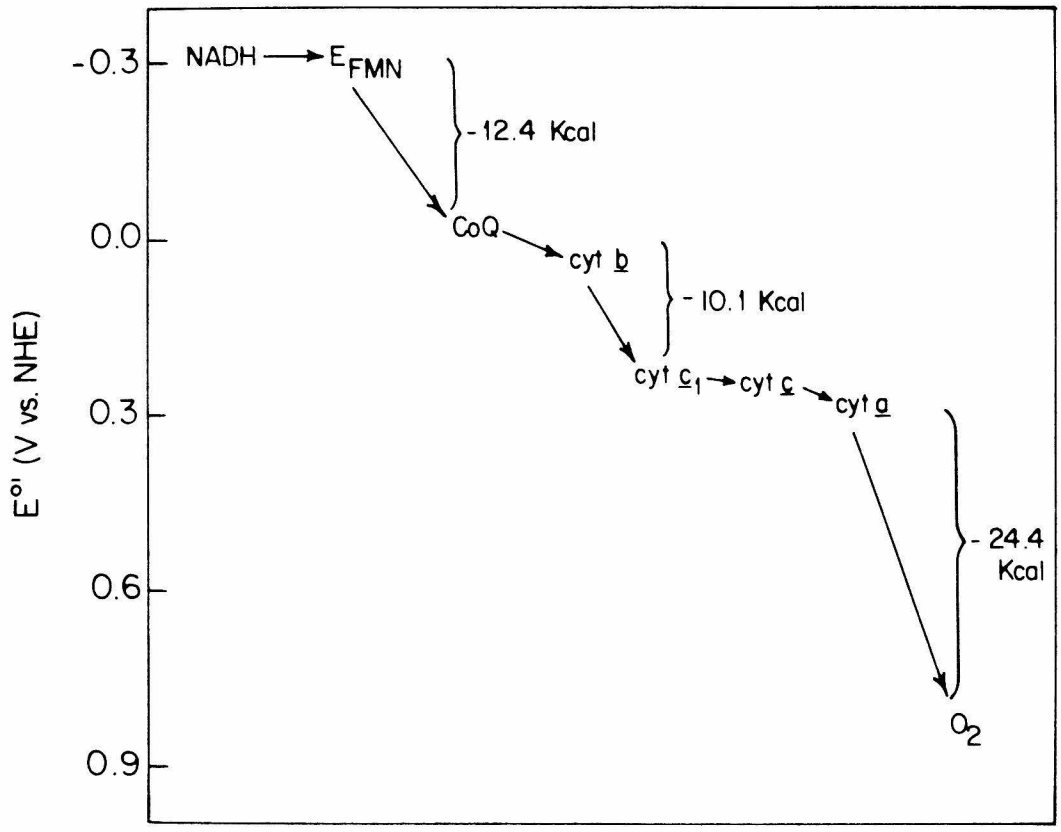
-0.3
0.0
0.3
0.6
0.9
E°' (V vs. NHE)
NADH → E FMN
- 12.4 Kcal
CoQ
cyt b
- 10.1 Kcal
cyt c1 → cyt c → cyt a
- 24.4 Kcal
O2

span the membrane bilayer. Ubiquinone (or coenzyme Q) is a lipid-soluble quinone. Cytochrome _c_, finally, is a water-soluble peripheral membrane protein.

Flavins and iron-sulfur clusters are present as the redox-active prosthetic groups of Complexes I and II, which are poorly understood. Complex III transfers electrons from ubiquinol to cytochrome _c_ and possesses four redox centers: two _b_-type cytochromes, one (2Fe-2S) unit and one cytochrome c_1 (11,12). Complex IV, the terminal component of the respiratory chain and more commonly known as cytochrome _c_ oxidase, contains two copper centers and two heme _a_ centers. Cytochrome _c_ oxidase will be discussed at length in Chapters IV and V of this thesis. Out of the approximately 20 protein-bound redox centers associated with the mitochrondrial electron transport chain, only one of them, cytochrome _c_, is understood in any detail (13). This situation is largely due to preparative difficulties and a lack of structural (i.e., crystallographic) information for the protein components.

The electron transfer steps that figure prominently in oxidative phosphorylation thus frequently involve protein-bound metal ions that are separated by relatively large distances (10 Å or greater). Thermodynamic constraints clearly play an important role in determining the rates of intramolecular electron transfer reactions in proteins and protein complexes (14).

EQUILIBRIUM THERMODYNAMIC ASPECTS OF REDOX REACTIONS

The application of electrochemical techniques to the study of

biological systems finds its roots in work done more than fifty years ago (15-17). This early work, based primarily on potentiometric studies, provided extensive thermodynamic information for a number of naturally-occurring compounds. Reliable determinations of the reduction (or formal) potential of a redox couple are dependent upon the observation of responses which are Nernstian. For the redox process given by

$$Ox + ne^- \underset{k_r}{\overset{k_f}{\rightleftharpoons}} Red \qquad (2)$$

where k_f and k_r are the forward and reverse heterogeneous electron transfer rate constants, respectively, the Nernst equation

$$E = E^o + (2.303RT/nF)\log(Ox/Red) \qquad (3)$$

where E^o is the formal potential of the redox couple and all other terms have their usual definitions, will be obeyed if diffusion control rather than heterogeneous electron transfer is the rate-determining step. In practical terms, this means that when an increment of reducing of oxidizing equivalents is added to a sample containing Ox and Red the redox concentration ratio given in Equation (3) must be stoichiometrically shifted and rapidly result in an invariant potentiometric response that is in agreement with the Nernst equation. At 25 ^oC a plot of $E_{applied}$ vs. log(Ox/Red) must be linear and have a slope of $(59/n)$ mV and an intercept equal to the formal potential of the redox couple.

In biology several liberties must be taken with standard conditions. The activities of components in membranes are unknown and even using concentrations it is not possible to approach standard conditions either in concentration, or if the proton is involved, in pH. The E^{o}, if it was directly measurable, would be a value obtained using concentrations much less than standard activities or concentrations. Further, determinations at pH 0 cannot generally be done with biomolecules, and in most cases there is insufficient information to make a reliable extrapolation back to pH 0 from higher, more physiologically relevant pH values. In this thesis the symbol $E^{o'}$ will be used to denote determinations done near pH 7.0, in accordance with biochemical convention.

Metalloprotein redox reactions are frequently accompanied by ion (especially proton) uptake or release. The reduction potential, and nearly every other property (18,19) of a metalloprotein (exclusive of its primary amino acid sequence) can be shown to vary with the pH and mobile ion concentration of the solvent. The effect of ion binding on redox energetics can be predicted using the Nernst equation. Consider the following reaction:

$$RedH \rightleftharpoons Ox + e^{-} + H^{+} \qquad (4)$$

The Nernst equation for this reaction (25 ^{o}C) is

$$E = E^{o} + 0.059\log[(Ox)(H^{+})/(RedH)] \qquad (5)$$

Upon simplification, Equation (5) yields

$$E = E^{O} + 0.059\log[(Ox)/(RedH) - 0.059pH \quad (6)$$

Equation (6) indicates that the reduction potential will shift -59 mV for every unit increase in pH. The underlying reason for this behavior is that the oxidized and reduced forms of a redox couple may have very different proton affinities. For most redox couples this proton transfer would be limited by two pK_as, one for the oxidized form and the other, at higher pH, for the reduced form. Many redox couples of biological interest possess pK_as in the physiological range and therefore pH-dependent behavior cannot be ignored. Typically, pK_as for redox proteins are inferred from redox titrations done as a function of pH. NMR titration curves are frequently helpful in identifying the amino acid residue responsible for the pH-dependent electrochemical behavior. At alkaline pH values, coordinated water may deprotonate as well. Figure 2 illustrates a plot of E^{O} vs. pH. The pK_as are revealed because, above and below the pK_as, proton transfer becomes insignificant and the value of E^{O} loses its dependence on the solution pH. Three distinct regions occur in the plot. At pH values >> pK_a^{red} the predominant redox reaction is

$$Red^{-} \rightleftharpoons Ox + e^{-} \quad (7)$$

Equation (4) describes the reaction occurring at pH values between pK_a^{ox} and pK_a^{red}. At pH values << pK_a^{ox} the reaction is

Figure 2. Plot of the reduction potential (E^o) of a hypothetical redox couple vs. solution pH when the couple has pK_as of 2 and 8. Three regions are illustrated: pH < pK_a^{ox}; pK_a^{ox} < pH < pK_a^{red}, where E^o decreases by 59 mV per pH unit increase; and pH > pK_a^{red}. The predominant redox species are indicated in each region. E^o is 196 mV at pH 5.0. Dashed lines extrapolate to the respective pK_as.

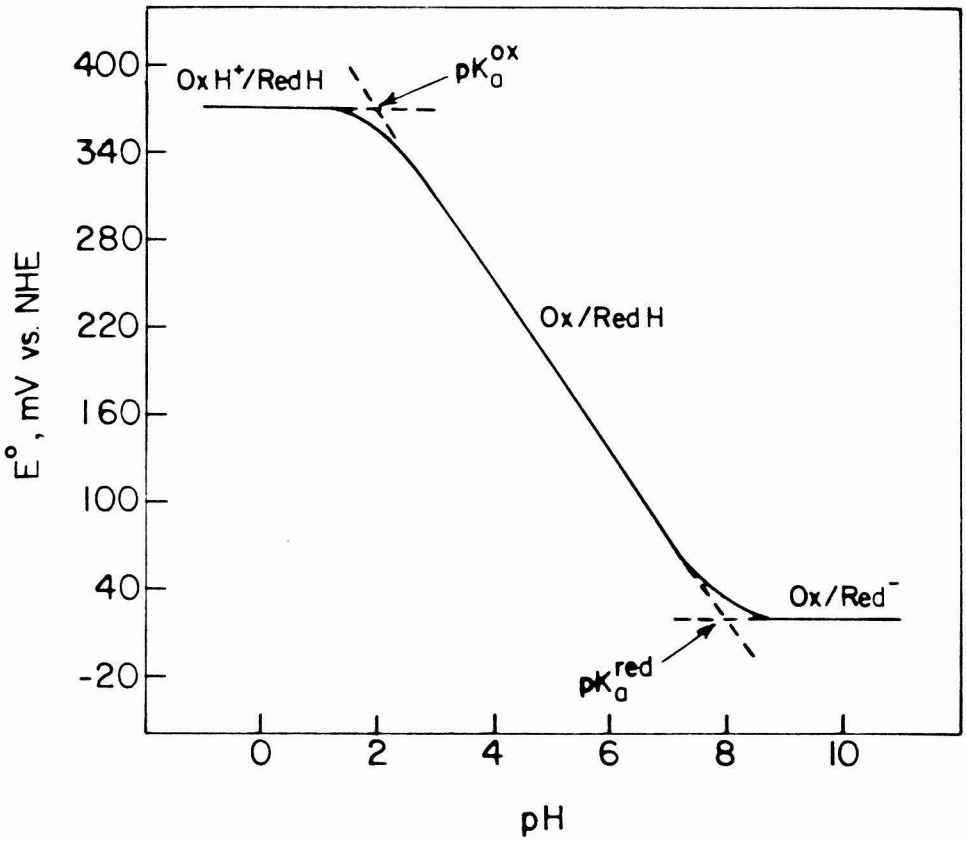
400
340
280
220
160
100
40
-20
E°, mV vs. NHE
Ox H⁺/Red H
pK$_a^{ox}$
Ox/Red H
Ox/Red⁻
pK$_a^{red}$
0
2
4
6
8
10
pH

$$RedH \rightleftharpoons OxH^{+} + e^{-} \qquad (8)$$

Figure 3 illustrates the appropriate thermodynamic cycle for this situation.

Equations for the measured E^{o} for redox couples with multiple *n* values and the stepwise binding of several protons can be derived using the above approach. This analysis can be easily extended to the asymmetric binding of the oxidized and conjugate reduced forms of a protein couple to a ligand. The ligand can be anything from a membrane phospholipid or another protein to a small molecule (a buffer component or exogenous ligand, for example).

The complete characterization of the redox thermodynamics of a metalloprotein involves the determination of the effects of pH, ionic strength, and temperature on the value of E^{o}. The temperature dependence of the reduction potential (20) yields the enthalpic (ΔH^{o}) and entropic (ΔS^{o}) components of the free energy change associated with the metalloprotein half reaction. Two electrochemical cell configurations are commonly used (Figure 4). If the reference electrode and the solution containing the redox couple of interest are always maintained at the same temperature, the cell is said to be in an isothermal configuration (21). Such isothermal cells suffer from a disadvantage relating to the fact that, once the temperature is changed, most reference electrodes return to equilibrium very slowly. If the reference electrode is held at constant temperature while the temperature of the solution containing the redox couple of interest is varied, the cell is said to be in a nonisothermal configuration.

Figure 3. Thermodynamic cycle for the coupled electron- and proton-transfer reactions displaying the potentiometric behavior illustrated in Figure 2.

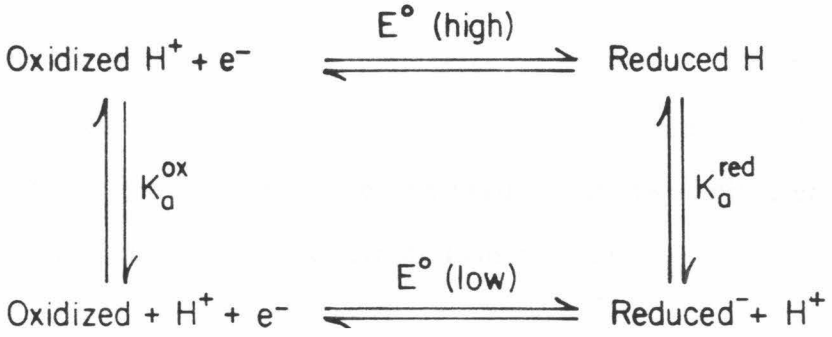
Oxidized $H^+ + e^-$
E° (high)
Reduced H
K_a^{ox}
K_a^{red}
Oxidized + $H^+ + e^-$
E° (low)
Reduced$^-$ + H^+

Figure 4. Isothermal and nonisothermal electrochemical cells. In the isothermal case, the temperature of the reference electrode changes along with that of the sample. The apparent temperature dependence of the sample E^o must therefore be corrected for the contribution of the temperature dependence of the reference electrode. The nonisothermal configuration requires that the working (i.e., protein sample) and reference electrode compartments be maintained at two different temperatures, with that of the reference electrode held constant.

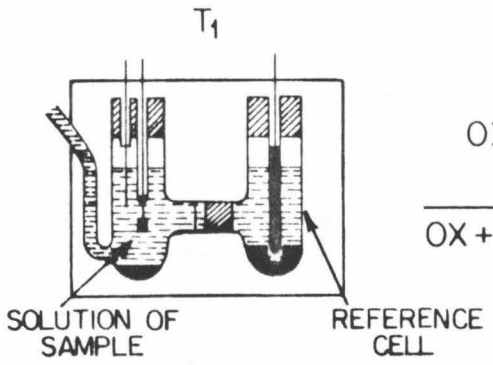

ISOTHERMAL

$$OX + E^- \rightleftharpoons RED$$
$$\tfrac{1}{2}\cdot H_2 \rightleftharpoons H^+ + E^-$$
$$OX + \tfrac{1}{2}\cdot H_2 \rightleftharpoons RED + H^+$$

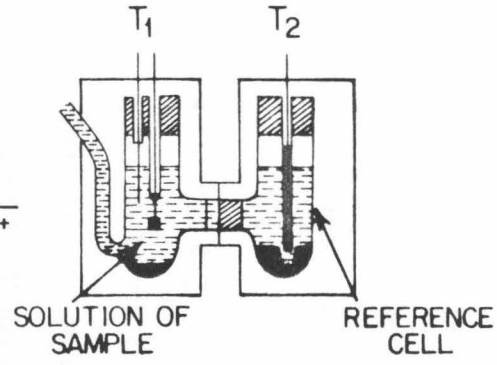

NONISOTHERMAL

$$\Delta S^0_{iso} = (S^0_{red} + S^0_{H^+}) - (S^0_{ox} + \tfrac{1}{2}\cdot S^0_{H_2})$$

$$S^0_{H_2} = 31.2 \text{ eu}$$

$$S^0_{H^+} = 0 \text{ (BY CONVENTION)}$$

$$S^0_{red} - S^0_{ox} = \Delta S^0_{iso} + 15.6 \text{ eu}$$

$$\Delta S^0_{rc} = \Delta S^0_{iso} + 15.6 \text{ eu}$$

T_2 IS HELD FIXED WHILE
T_1 IS VARIED

$$S^0_{red} - S^0_{ox} = F\cdot(dE^0/dT)$$

$$\Delta S^0_{rc} = F\cdot(dE^0/dT)$$

Weaver and coworkers (22) have noted that the use of nonisothermal cells circumvents the reference electrode problem associated with isothermal cells. If the temperature coefficients of certain thermal junction potentials can be made either negligible or constant relative to the overall temperature coefficient of the nonisothermal cell, (dE^o/dT), this method provides a direct measure of entropy changes for half-cell reactions, ΔS_{rc}^o: $\Delta S_{rc}^o = S_{red}^o - S_{ox}^o = nF(dE^o/dT)$. Effects due to temperature gradients can be made sufficiently small that no serious error results in neglecting them in cases where (dE^o/dT) is at least 0.2 mV/deg (21).

The net entropy change for the complete cell reaction, referenced to the NHE, is given by $\Delta S_{cell}^o = \Delta S_{rc}^o + (nS_{H^+}^o - 1/2\, nS_{H_2}^o)$, where the S^o terms represent partial molal entropies. The entropy difference due to the reference electrode may be separated from that due to the redox couple of interest using third law considerations. Using 31.2 eu for the partial molal entropy of H_2 and Latimer's convention (23) of zero for $S_{H^+}^o$, the reaction entropy for $n = 1$ processes may be written as

$$\Delta S_{rc}^o = \Delta S_{cell}^o + 15.6 \text{ eu} \qquad (9)$$

Thus, the reaction entropy (obtainable via the nonisothermal experiment) is equal to the entropy change for the overall cell reaction (obtainable via the isothermal experiment) plus 15.6 eu.

Two additional experimental methods are useful in determining redox thermodynamic parameters. Temperature-dependent relaxation amplitudes

obtained from temperature-jump experiments on redox systems can be analyzed using the van't Hoff equation to obtain ΔH^o for redox couples (24-26). Calorimetry is actually the method of choice for obtaining ΔH^o for a redox reaction (27,28). These two methods complement electrochemical and chemical redox titrations since the latter yield ΔS^o directly from the data while the former yield ΔH^o. The thermodynamic relation $\Delta G^o = \Delta H^o - T\Delta S^o$ is used to obtain the missing parameter. Of course, calorimetry cannot be used to obtain ΔH^o values for individual redox centers in multisite systems since the measured reaction heat cannot be uniquely apportioned amongst the titrating centers.

Electrostatic charge effects and specific ligand solvation appear to dominate the reaction entropies exhibited by transition metal complexes (22,29-46). Negatively charged redox couples tend to have negative reaction entropies and positively charged couples display positive reaction entropies, as seen in Figure 5. Bulky, hydrophobic ligands (phen and bipy, for example) depress the magnitude of the observed ΔS_{rc}^o. Metalloprotein couples (47-52), on the other hand, tend to have negative reaction entropies that do not correlate with protein charge. A knowledge of the thermodynamics of electron transfer reactions is needed in order to adequately understand these reactions. The large body of kinetic data for metalloprotein redox reactions has unfortunately not been supplemented with a similarly extensive thermodynamic database. The reaction entropy has been shown to correlate with the solvent reorganization energy for outer-sphere self-exchange reactions of transition metal couples (53). Marcus and

Figure 5. Reaction entropies for selected transition metal and metalloprotein couples. Values taken from References 39, 43, 47, 49, and 50.

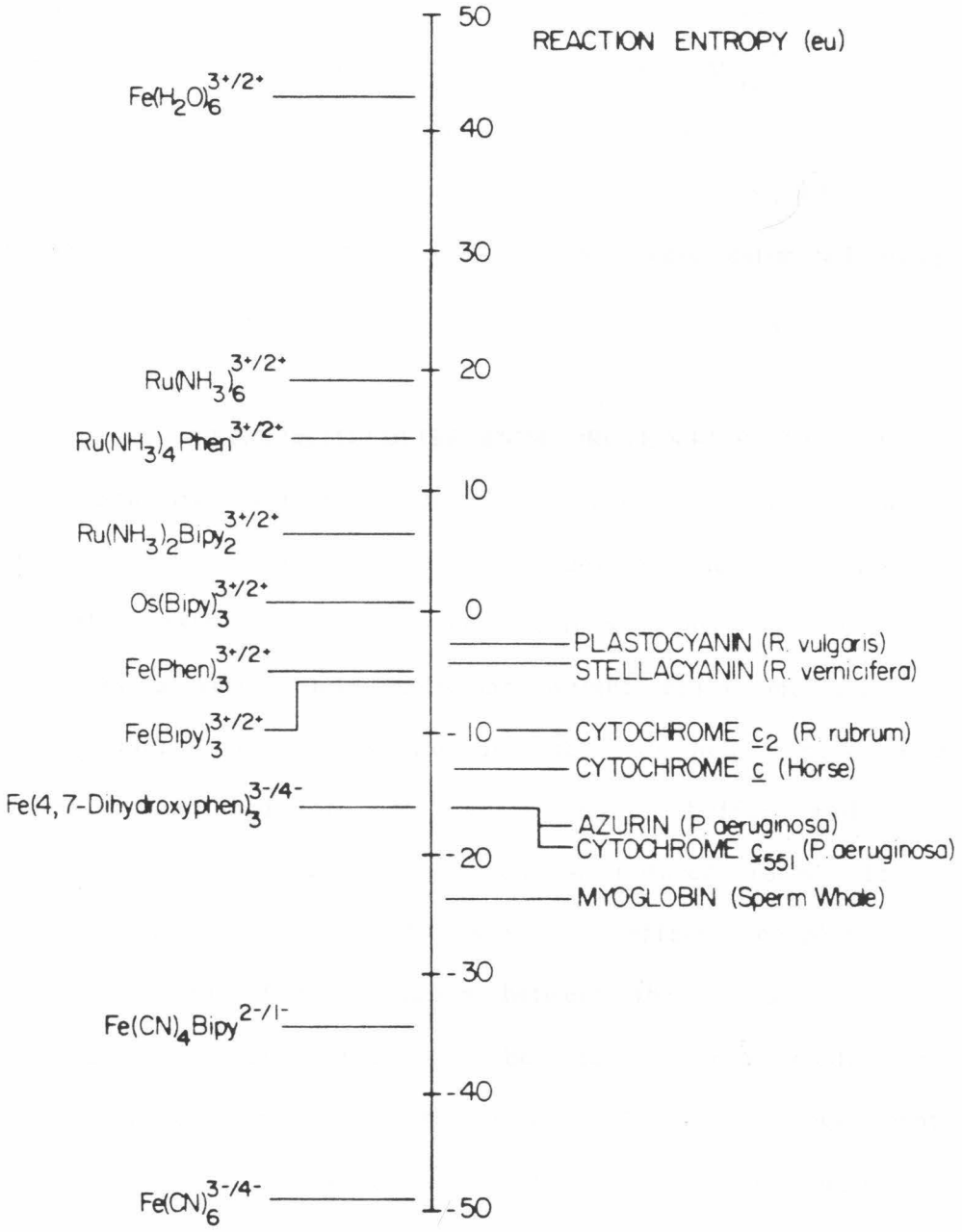
50
REACTION ENTROPY (eu)
$Fe(H_2O)_6^{3+/2+}$
40
30
$Ru(NH_3)_6^{3+/2+}$
20
$Ru(NH_3)_4Phen^{3+/2+}$
10
$Ru(NH_3)_2Bipy_2^{3+/2+}$
$Os(Bipy)_3^{3+/2+}$
0
PLASTOCYANIN (R. vulgaris)
STELLACYANIN (R. vernicifera)
$Fe(Phen)_3^{3+/2+}$
$Fe(Bipy)_3^{3+/2+}$
-10
CYTOCHROME c_2 (R rubrum)
CYTOCHROME c (Horse)
$Fe(4,7\text{-Dihydroxyphen})_3^{3-/4-}$
AZURIN (P. aeruginosa)
CYTOCHROME c_{551} (P. aeruginosa)
-20
MYOGLOBIN (Sperm Whale)
-30
$Fe(CN)_4Bipy^{2-/1-}$
-40
$Fe(CN)_6^{3-/4-}$
-50

Sutin (54) have presented a thermodynamic analysis of the classical Marcus model of electron transfer in which the standard entropy (ΔS_{12}^{o}) and enthalpy (ΔH_{12}^{o}) changes for a cross reaction were shown to contribute to the kinetic activation entropy ($\Delta S_{12}^{\neq}$) and enthalpy ($\Delta H_{12}^{\neq}$), respectively. The enthalpic reorganizational barriers for electron transfer in horse heart cytochrome c (55), P. aeruginosa azurin (56), and sperm whale myoblobin (50) were estimated using the theory outlined in reference 54.

ELECTROCHEMICAL METHODS FOR DETERMINING PROTEIN REDUCTION POTENTIALS

The fundamental problem in determination of E^{o} and the number of electrons transferred per molecule (*n* value) of metalloproteins is the generally slow rate of heterogeneous electron transfer at an indicator electrode. As a result, low molecular weight redox mediators (57-60) are usually added to the solution in order to help rapidly establish equilibrium. The mediator acts as a redox buffer and is most effective near a 1:1 ratio of oxidized to reduced form. The redox protein and indicator electrode are, in effect, coupled by the mediator (Figure 6). The interaction between the mediator and protein may on occasion cause problems, because required mediator-protein complex formation can affect the protein E^{o} value. As mentioned previously, the classical method for determination of protein redox potentials is potentiometric titration, which is still used in a variety of ways. The principle of this method is that the potential of an inert electrode, typically Pt, is measured against a suitable reference electrode with respect to the fraction (Ox)/(Red) of the

Figure 6. Use of a mediator titrant (MT) to couple a redox protein to an indicator electrode. Here, the mediator titrant accepts electrons from the electrode and transfers them via an outer-sphere electron transfer mechanism to the protein in a reductive titration.

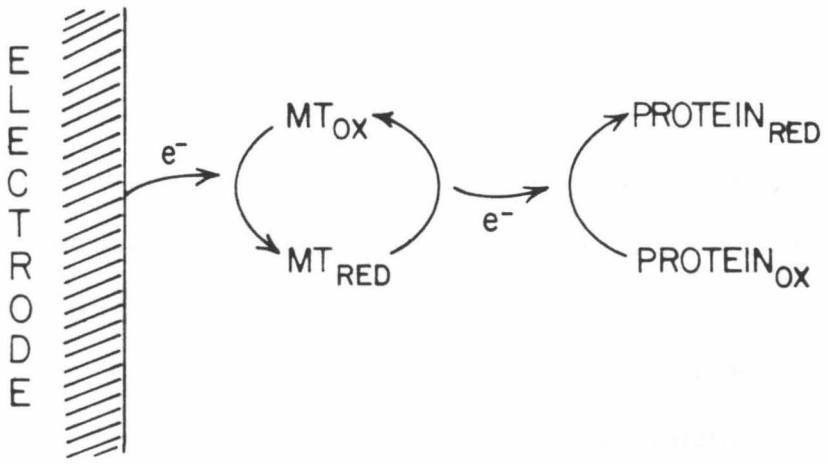
ELECTRODE
e⁻
MT OX
MT RED
e⁻
PROTEIN RED
PROTEIN OX

system of interest. The measured potential is E^{o} when (Ox) = (Red), as dictated by the Nernst equation. The ratio of (Ox)/(Red) may be varied by mixing the oxidized and reduced forms, photoreduction of Ox by a dye, or titration of the completely reduced sample with an oxidant (or vice versa). A concern in this type of experiment is the agreement between successive reductive and oxidative titrations of the same protein sample. During a chemical titration, the volume of the sample changes and spent titrant accumulates in the sample. Successive reductive and oxidative titrations of a sample can give rise to hysteresis in the potentiometric responses that may be due to these effects.

An alternative to relying on potentiometric measurements alone during a chemical redox titration of a metalloprotein involves optically monitoring the change in the redox state of the protein during the titration. The protein redox state, (Ox)/(Red), is determined from the optical absorption data together with the measured potentiometric response at each point in the titration. Agreement between these two sets of data expressed in terms of the Nernst equation provides more confidence in the measured thermodynamic parameters of a redox protein.

Certain advantages arise in the use of electrochemical techniques compared to chemical redox titrations in the determination of redox thermodynamic parameters of proteins. These newer methods include indirect coulometric titrations, the use of optically transparent thin-layer electrodes (OTTLEs), and electrode modification to obtain direct (i.e., unmediated) electrochemistry. The advantage of these

methods lies in the fact that redox equivalents are added directly by electrochemcal charge injection on nanoequivalent levels, instead of by chemcal reagents as in potentiometric titrations.

In the indirect coulometric titration (61-67), the titrant is electrochemically generated by the reduction of a low molecular weight mediator. The reduced mediator then transfers electrons to the protein sample until equilibrium is reached. This process involves a two step mechanism:

$$M_{ox} + ne^- \longrightarrow M_{red} \text{ (electrode reaction)} \qquad (10)$$

$$M_{red} + P_{ox} \longrightarrow M_{ox} + P_{red} \text{ (solution reaction)} \qquad (11)$$

The sample volume remains constant during repetitive titrations. The formal potential of the mediator in this type of titration should be far removed from that of the protein so that the equilibrium constant for Equation (11) is large. By measuring the charge associated with the electrolysis of the mediator titrant (Equation 10), under the same conditions, the charge associated with reduction of the protein is indirectly known.

The technique of OTTLE electrochemistry (67,68) was first applied to redox proteins by Heineman et al. (69). The unique features of the OTTLE arise from the very short distances over which molecules must diffuse to undergo electron transfer at the electrode surface (70-72) and from the facility for acquiring optical data to monitor the redox state of the solution resident species which is provided by an

optically transparent electrode (73-78). The major liability in using OTTLEs is the requirement that the optically monitored species exhibit a large difference molar absorptivity. Further, a mediated OTTLE study of a given redox protein will require access to a mediator having the desired formal potential and optical properties in both the oxidized and reduced forms which do not interfere with the optical response of the sample. The most difficult step in OTTLE experiments is frequently the search for appropriate mediators. As the succeeding chapters in this thesis amply illustrate the construction and use of OTTLE cells, this method will not be further elaborated here.

Within the last ten years, an interesting development in bioelectrochemistry has appeared: the advent of methods for obtaining direct electrochemistry using small molecules referred to as "redox promoters" (instead of mediator titrants) to modify the electrode surface. These methods have largely been developed in the laboratory of H.A.O. Hill at Oxford University. Cytochrome c was the first system studied (79-81). In the presence of 4,4′-bipyridyl, the protein was shown to undergo quasi-reversible heterogeneous electron transfer at gold electrodes. A survey (82) of a large number of bifunctional organic molecules suggested that redox promoters bind to the electrode surface via a heteroatom (N, P, or S) and provide a second functional group that can hydrogen-bond to the lysine residues around the heme crevice on cytochrome c. This bears a striking resemblance to the manner in which cytochrome c interacts with its physiological redox partners.

Detailed kinetic studies confirmed the suggestion that cytochrome

c rapidly and reversibly binds to the electrode and that this binding interaction is an essential feature of the overall electrode reaction (80). Continued research along these lines has resulted in modified electrodes designed to electrostatically promote rapid charge transfer. Mg^{2+} ions promote the direct electrochemistry of plastocyanin at edge-oriented pyrolytic graphite electrodes (83). Several other proteins that carry a net negative charge (rubredoxin, C. pasteuranium ferredoxin, and flavodoxin) also exhibit rapid electron transfer at pyrolytic graphite electrodes when multivalent cations such as Mg^{2+} or $Cr(NH_3)_6^{3+}$ are present (84). While direct electrochemistry of large redox enzymes such as cytochrome c oxidase will probably not be possible, new results for other small, water-soluble redox proteins will almost surely be forthcoming in the near future.

OUTLINE OF THIS THESIS

The application of spectroelectrochemical methods to the study of a number of metalloproteins is described in this thesis. Chapter II presents spectroelectrochemical cell designs together with machining specifications for a stainless steel shroud, useful in situations where anaerobic measurements are necessary. Structurally characterized metalloproteins containing blue coppers or iron hemes as prosthetic groups are the topic of Chapter III. Redox thermodynamic parameters are presented and discussed for Alcaligenes azurins and three hemoproteins containing distinctive sites (myoglobin, cytochrome c, and cytochrome c′). Chapter IV discusses two factors that

complicate the equilibrium redox behavior of multisite redox metalloproteins: temperature and allosteric interactions. Data for a $(NH_3)_5Ru$(His-48)-myoglobin derivative are reviewed and the problem of site-site interactions in cytochrome _c_ oxidase is discussed in detail. Cytochrome _c_ oxidase is the subject of Chapter V, wherein redox thermodynamic data for the three spectrally visible metal centers (Cu_A, cytochrome _a_, and cytochrome $_{a_3}$) are presented and discussed with respect to the mechanisms of electron transfer and proton pumping by the enzyme. The final chapter contains concluding remarks and suggestions for further work.

REFERENCES

1. Blondin, G.A., and Green, D.E. (1975) *Chem. & Eng. News* **53**, 26 (November 10 issue).

2. Ernster, L., ed. (1984) *Bioenergetics*, Elsevier, Amsterdam.

3. Jones, C.W. (1981) *Biological Energy Conservation, 2nd Edition*, Chapman and Hall, London.

4. Dreyer, J.L. (1984) *Experientia* **40**, 653.

5. Hatefi, Y. (1985) *Ann. Rev. Biochem.* **54**, 1015.

6. Dixit, B.P.S.N., and Vanderkooi, J.M. (1984) *Curr. Top. Bioenergetics* **13**, 159.

7. Michel-Beyerle, M.E., ed. (1985) *Antennas and Reaction Centers of Photosynthetic Bacteria*, Springer-Verlag, Berlin.

8. Govindjee, ed. (1982) *Photosynthesis: Energy Conversion by Plants and Bacteria, Volume 1*, Academic Press, New York.

9. Ibers, J.A., and Holm, R.H. (1980) *Science* **209**, 223.

10. Hackenbrock, C.R. (1981) *Trends Biochem. Sci.* **6**, 151.

11. Rich, P.R. (1984) *Biochim. Biophys. Acta* **768**, 53.

12. Trumpower, B.L. (1981) *Biochim. Biophys. Acta* **639**, 129.

13. Moore, G.R., Eley, C.G.S., and Williams, R.J.P. (1984) *Adv. Inorg. Bioinorg. Mech.* **3**, 1.

14. Marcus, R.A., and Sutin, N. (1985) *Biochim. Biophys. Acta* **811**, 265.

15. Clark, W.M. (1960) *Oxidation-Reduction Potentials of Organic Systems*, Williams and Wilkins Co., Baltimore.

16. Dutton, P.L. (1978) *Meth. Enzymol.* **54**, 411.

17. Dutton, P.L., and Wilson, D.F. (1974) *Biochim. Biophys. Acta* **346**, 165.

18. Matthew, J.B. (1985) *Ann. Rev. Biophys. Biophys. Chem.* **14**, 387.

19. Matthew, J.B., Gurd, F.R.N., Garcia-Moreno E., B., Flanagan, M.A., March, K.L., and Shire, S.J. (1985) *CRC Crit. Rev. Biochem.* **18**,91.

20. Eastman, E.D. (1928) *J. Am. Chem. Soc.* **50**, 292.

21. de Bethune, A.J., Licht, T.S., and Swendeman, N. (1959) *J. Electrochem. Soc.* **106**, 616.

22. Yee, E.L., Cave, R.J., Guyer, K.L., Tyma, P.D., and Weaver, M.J. (1979) *J. Am. Chem. Soc.* **101**, 1131.

23. Latimer, W.M. (1952) *The Oxidation States of the Elements and Their Potentials in Aqueous Solutions, 2nd Edition*, Prentice-Hall, Englewood Cliffs, N.J.

24. Czerlinski, G.H. (1966) *Chemical Relaxation*, Marcel Dekker, New York.

25. Strehlow, H., and Knoche, W. (1977) *Fundamentals of Chemical Relaxation* Verlag Chemie, Weinheim, F.R.G.

26. Rosen, P., and Pecht, I. (1976) *Biochemistry* **15**, 775.

27. Edsall, J.T., and Gutfruend, H. (1983) *Biothermodynamics*, Wiley, Chichester, U.K.

28. Sturtevant, J.M. (1974) *Ann. Rev. Biophys. Bioeng.* **3**, 35.

29. Wawrousek, E.F., and McArdle, J.V. (1982) *J. Inorg. Biochem.* **17**, 169.

30. Tsou, Y.-M., and Anson, F.C. (1984) *J. Electrochem. Soc.* **131**, 595.

31. Hupp, J.T., and Weaver, M.J. (1984) *J. Electrochem. Soc.* **131**, 619.

32. Lieber, C.M., and Lewis, N.S. (1986) *J. Phys. Chem.* **90**, 1002.

33. Schmitz, J.E.J., and van der Linden, J.G.M. (1984) *Inorg. Chem.* **23**, 117.

34. Ogino, H., and Ogino, K. (1983) *Inorg. Chem.* **22**, 2208.

35. Schmitz, J.E.J., and van der Linden, J.G.M. (1984) *Inorg. Chem.* **23**, 3298.

36. Weaver, M.J., and Nettles, S.M. (1980) *Inorg. Chem.* **19**, 1641.

37. Hupp, J.T., and Weaver, M.J. (1984) *Inorg. Chem.* **23**, 3639.

38. Youngblood, M.P., and Margerum, D.W. (1980) *Inorg. Chem.* **19**, 3068.

39. Yee, E.L., and Weaver, M.J. (1980) *Inorg. Chem.* **19**, 1077.

40. George, P., Hanania, G.I.H., and Eaton, W.A. (1966) in *Hemes and Hemoproteins*, Chance, B., ed., Academic Press, New York, p. 267.

41. Kratochvil, B., and Knoeck, J. (1966) *J. Phys. Chem.* **70**, 944.

42. George, P., Hanania, G.I.H., and Irvine, D.H. (1957) *J. Chem. Soc. (London)*, 3048.

43. Hanania, G.I.H., Irvine, D.H., Eaton, W.A., and George, P. (1967) *J. Phys. Chem.* **71**, 2022.

44. Kadish, K.M., Thompson, L.K., Beroiz, D., and Bottomley, L.A. (1977) in *Electrochemical Studies of Biological Systems*, Sawyer, D.T., ed., Amer. Chem. Soc., Washington, D.C., p. 51.

45. Borchardt, D., and Wherland, S. (1984) *Inorg. Chem.* **23**, 2537.

46. Borchardt, D., and Wherland, S. (1982) *Inorg. Chem.* **21**, 93.

47. Taniguchi, V.T., Sailasuta-Scott, N.S., Anson, F.C., and Gray, H.B. (1980) *Pure & Appl. Chem.* **52**, 2275.

48. Reid, L.S., Taniguchi, V.T., Gray, H.B., and Mauk, A.G. (1982) *J. Am. Chem. Soc.* **104**, 7516.

49. Taniguchi, V.T., Ellis, W.R., Jr., Cammarata, V., Webb, J., Anson, F.C., and Gray, H.B. (1982) in *Electrochemical and Spectrochemcal Studies of Biological Redox Components*, Kadish, K.M., ed., Amer. Chem. Soc., Washington, D.C., p. 51.

50. Crutchley, R.J., Ellis, W.R., Jr., and Gray, H.B. (1985) *J. Am. Chem. Soc.* **107**, 5002.

51. Taniguchi, V.T., Malmström, B.G., Anson, F.C., and Gray, H.B. (1982) *Proc. Natl. Acad. Sci. U.S.A.* **79**, 3387.

52. Margalit, R., and Schejter, A. (1970) *FEBS Lett.* **6**, 278.

53. Sutin, N., Weaver, M.J., and Yee, E.L. (1980) *Inorg. Chem.* **19**, 1098.

54. Marcus, R.A., and Sutin, N. (1975) *Inorg. Chem.* **14**, 213.

55. Nocera, D.G., Winkler, J.R., Yocom, K.M., Bordignon, E., and Gray, H.B. (1984) *J. Am. Chem. Soc.* **106**, 5145.

56. Margalit, R., Kostić, N.M., Che, C.-M., Blair, D.F., Chiang, H.-J., Pecht, I., Shelton, J.B., Shelton, J.R., Schroeder, W.A,, and Gray, H.B. (1984) *Proc. Natl. Acad. Sci. U.S.A.* **84**, 6554.

57. Fultz, M.L., and Durst, R.A. (1982) *Anal. Chim. Acta* **140**, 1.

58. Prince, R.G., Linkletter, S.J.G., and Dutton, P.L. (1981) *Biochim. Biophys. Acta* **635**, 132.

59. Wilson, G.S. (1978) *Meth. Enzymol.* **54**, 396.

60. Johnson, J.M., Halsall, H.B., and Heineman, W.R. (1983) *Anal. Biochem.* **133**, 186.

61. Su, C.-H., and Heineman, W.R. (1981) *Anal. Chem.* **53**, 594.

62. Hawkridge, F.M., and Kuwana, T. (1973) *Anal. Chem.* **45**, 1021.

63. Watt, G.D. (1979) *Anal. Biochem.* **99**, 399.

64. Steckhan, E., and Kuwana, T. (1974) *Ber. Bunsenges. Phys. Chem.* **78**, 253.

65. Yates, D.M., Szentirmay, R., and Kuwana, T. (1980) *Anal. Biochem.* **102**, 271.

66. Szentirmay, R., Yeh, P., and Kuwana, T. (1977) in *Electrochemical Studies of Biological Systems*, Sawyer, D.T., ed., Amer. Chem. Soc., Washington, D.C., p. 143.

67. Kuwana, T., and Winograd, N. (1974) *Electroanal. Chem.* **7**, 1.

68. Heineman, W.R., Hawkridge, F.M., and Blount, H.N. (1984) *Electroanal. Chem.* **13**, 1.

69. Heineman, W.R., Norris, B.J., and Goelz, J.F. (1975) *Anal. Chem.* **47**, 79.

70. Reilley, C.N. (1968) *Rev. Pure Appl. Chem.* **18**, 137.

71. Hubbard, A.T. (1973) *CRC Crit. Rev. Anal. Chem.* **3**, 201.

72. Hubbard, A.T., and Anson, F.C. (1971) *Electroanal. Chem.* **4**, 129.

73. Heineman, W.R. (1983) *J. Chem. Educ.* **60**, 305.

74. Anderson, J.L. (1979) *Anal. Chem.* **51**, 2312.

75. Brewster, J.D., and Anderson, J.L. (1982) *Anal. Chem.* **54**, 2560.

76. Jones, E.T.T., and Faulkner, L.R. (1984) *J. Electroanal. Chem.* **179**, 53.

77. Smith, D.A., Elder, R.C., and Heineman, W.R. (1985) *Anal. Chem.* **57**, 2361.

78. Heineman, W.R., Anderson, C.W., Halsall, H.B., Hurst, M.M. Johnson, J.M., Kreishman, G.P., Norris, B.J., Simone, M.J., and Su, C.-H. (1982) in *Electrochemical and Spectrochemical Studies of Biological Redox Components*, Kadish, K.M., ed., Amer. Chem. Soc., Washington, D.C. p. 1.

79. Eddowes, M.J., and Hill, H.A.O. (1979) *J. Am. Chem. Soc.* **101**, 4461.

80. Albery, W.J., Eddowes, M.J., Hill, H.A.O., and Hillman, A.R. (1981) *J. Am. Chem. Soc.* **103**, 3904.

81. Eddowes, M.J., and Hill, H.A.O. (1982) in *Electrochemical and Spectrochemical Studies of Biological Redox Components*, Kadish, K.M., ed., Amer. Chem. Soc., Washington, D.C., p. 173.

82. Allen, P.M., Hill, H.A.O., and Walton, N.J. (1984) *J. Electroanal. Chem.* **178**, 69.

83. Armstrong, F.A., Hill, H.A.O., Oliver, B.N., and Whitford, D. (1985) *J. Am. Chem. Soc.* **107**, 1473.

84. Armstrong, F.A., Hill, H.A.O., Oliver, B.N., and Walton, N.J. (1984) *J. Am. Chem. Soc.* **106**, 921.

CHAPTER II

DESIGN AND EVALUATION OF A SPECTROELECTROCHEMICAL APPARATUS

INTRODUCTION

Spectroelectrochemistry has been used with increasing frequency to characterize the redox properties of biomolecules. During the last decade, numerous (1-17) designs have been reported for spectroelectrochemical cells incorporating specific features that are desirable in titrating biological redox components: small sample volume, large electrode surface area, ability to monitor weak chromophores, accurate cell temperature measurement and control, anaerobic operation, and the ability to spectrally monitor the sample by means other than standard absorption spectroscopy. Cell designs reported to date do not meet more than a few of these criteria. The anaerobicity criterion is especially serious when studying metalloproteins that are destroyed by oxygen (e.g., most iron-sulfur proteins) or redox enzymes (cytochrome c oxidase, for example), for which oxygen acts as a substrate. Additionally, many metalloproteins are slowly denatured by hydrogen peroxide that is generated in solutions containing dissolved oxygen.

Designs for optically transparent thin-layer electrode (OTTLE) and long-path spectroelectrochemistry cells are presented in this chapter. The problem of O_2 exclusion is overcome by the use of a stainless steel shroud for the cells (18,19).

MATERIALS AND METHODS

Protein solutions. C. vinosum HiPIP was gift from Drs. T.E. Meyer, R.G. Bartsch, and M.D. Kamen (20), and was purified by ion-exchange chromatography to a final purity ratio (A_{283}/A_{388}, reduced) of 2.51. Tris(1,10-phenanthroline)cobalt(III)perchlorate was prepared by the

method of Schilt and Taylor (21). All other materials were of reagent quality and used without further purification.

OTTLE cell construction. The OTTLE cell is adapted from a design of Heineman and coworkers (13), with modifications to enable convenient use and reassembly. Machining specifications for the clear lucite cell body are given in Figure 1. The working cell compartment (2 x 2 cm) is contained in the lower portion of the cell body. Gold electroformed mesh (500 lines/inch, minigrid, 60% transmittance) serves as the working electrode material and is available from Interconics, St. Paul, MN. Optical path lengths may be varied from 0.12 to 0.89 mm (with 0.1 mm Teflon tape, Dilectrix Corp., Farmingdale, NY), with multiple minigrids used in the thicker cells. The cell body contains separate ports and solution paths from the thin-layer cavity to the reference and counter electrodes.

The first step in assembling the cell is installation of the bottom quartz (21 x 21 x 1.5 mm) window by epoxying it onto the lower portion of the lucite body. Next, U-shaped Teflon spacers and 17 x 35 mm pieces of gold minigrid are layered on top of the window. The top window is then affixed with epoxy, taking care not to allow the epoxy to seep into the thin-layer cavity. A piece of 18-gauge copper wire is then attached (using solder or conducting epoxy) to the portion of the minigrid(s) portruding from the bottom of the cell. After making the electrical contact, the minigrid(s) and wire are gently rolled up and epoxied to the base of the cell body. All four edges of the thin-layer cavity are then coated with epoxy to make the cell more durable. The working cell compartment can be rebuilt simply by softening the

Figure 1. Machining specifications for the OTTLE cell body (clear lucite). (A) Front view; (B) side view; and (C) thermocouple plug (machined to fit loosely into the thermocouple port). All dimensions are in mm.

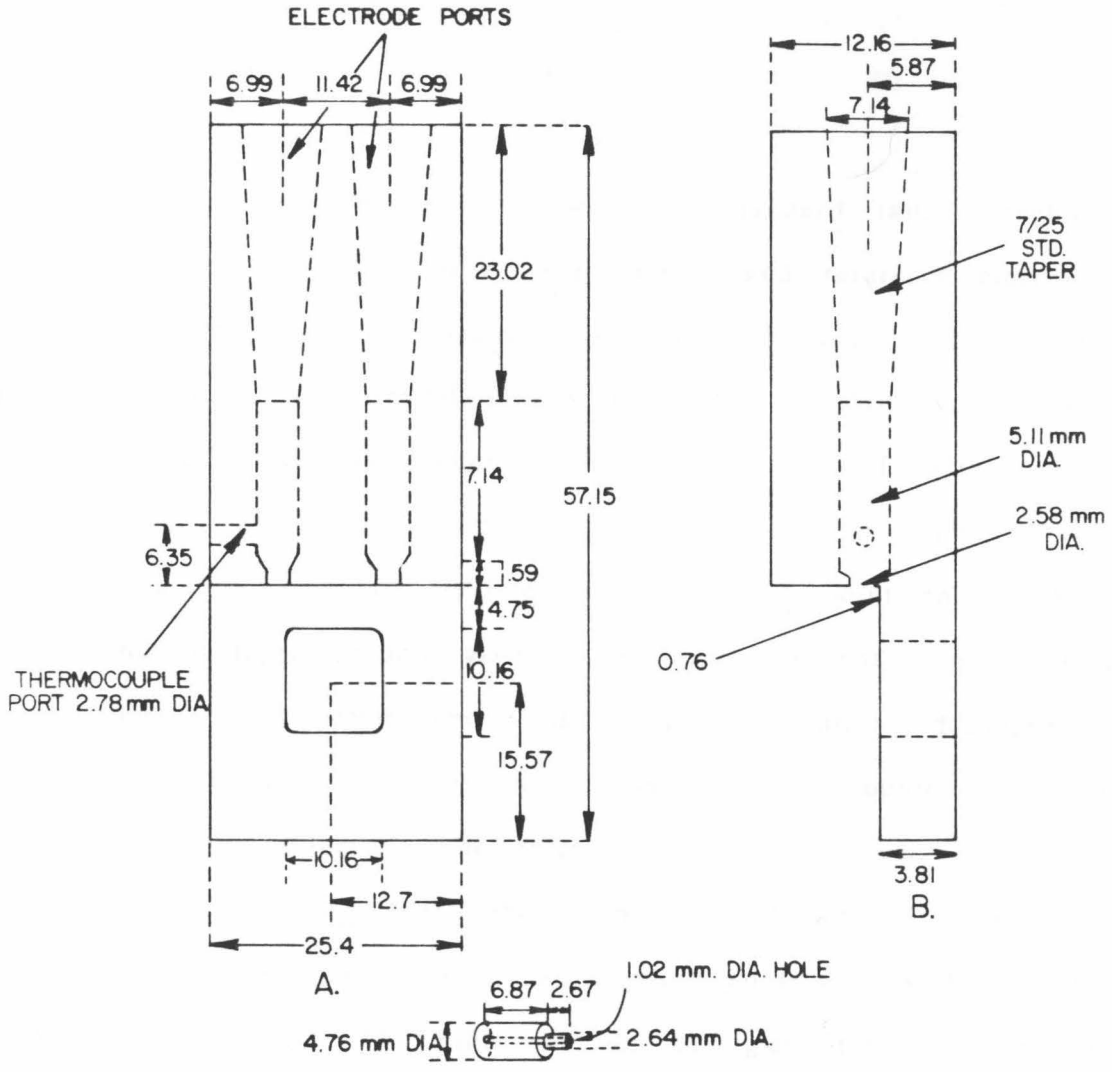

C. THERMOCOUPLE PLUG

epoxy sealant with methanol and cutting it away with a sharp scalpel.

The tip of the microthermocouple (copper-constan, Omega Engineering, available from B.J. Wolfe Enterprises, North Hollywood, CA) is epoxied into a lucite plug (Figure 1C) which is machined slightly undersize. The plug assembly is then inserted into the thermocouple port and epoxied to the cell body on the outside only.

The lucite cell body contains two 7/25 standard tapers machined lengthwise into the top to house the counter and reference electrodes. The counter (or auxiliary) electrode is a 9 inch length of 0.02 inch diameter platinum wire sealed into a tube of soft glass with a 5/20 standard taper outer glass joint, leaving ca. 1 inch of wire exposed at both ends. This is supported in a 2.25 inch long compartment consisting of a 5/20 standard taper ground glass inner joint on top of a 7/25 standard taper ground glass outer joint, terminated by a fine porous frit. This compartment is used to contain deoxygenated supporting electrolyte and serves to isolate the counter electrode from the protein solution. The reference electrode consists of a 0.25 x 9.5 inch tube of soft glass, the bottom end of which is terminated by a 7/25 standard taper ground glass outer joint with a Pt junction (0.25 inch) sealed in. The other end of the glass tube is flared to receive a Sargent-Welch (miniature, Pt junction, #S-30080-17) saturated calomel electrode (SCE). The tube serves as a salt bridge and is filled with degassed saturated KCl solution.

Long-path spectroelectrochemical cell construction. A 2 cm optical path spectroelectrochemical cell, Figure 2, was designed for the study of weakly absorbing chromophores. The working electrode consists of a

0.005 inch thick sheet of gold foil (Electronic Space Products, Los Angeles, CA) epoxied to the bottom and sides of the working electrode compartment. A 0.030 inch diameter gold wire is attached to the gold foil by means of conducting epoxy. Two 21 x 21 x 1.5 mm quartz windows complete the cell. Due to the large cell dimensions, a miniature stir bar is required for operation of this cell. The reference and counter electrodes previously described for use with the OTTLE cell may be used with this cell as well.

Shroud assembly. The spectroelectrochemical cell bodies are machined from clear lucite and are unsuitable for studies that require maintenance of anaerobic conditions over an extended time period, since lucite is permeable to oxygen. A stainless steel shroud was therefore designed to house the cells. This apparatus (Figures 3-8) requires approximately 100 hours of construction time by an experienced machinist. The bottom and flange are welded to the cannister. Both window housings (also welded in place) contain double O-ring-sealed fused quartz windows (Heraeus-Amersil). All of the connections through the faceplate (to a waterbath, potentiostat, and digital thermometer) are gas-tight: O-ring seals, Cajon ultratorr fittings, Eccobond high-vacuum epoxy (Emerson & Cuming, Gardena, CA) and an Oxford Instruments high-vacuum 10 pin electrical feed-through are used. A spectrophotometer mount (machine specifications not shown) is used to support the shroud. The base of the mount contains a pneumatic stirrer (required when using the long-path cell) similar to that previously described (22). The entire apparatus is depicted in Figure 9. On the left, an OTTLE cell fitted with electrodes is shown

Figure 2. Machining specifications for a long-path spectroelectrochemical cell (clear lucite). All dimensions are in mm.

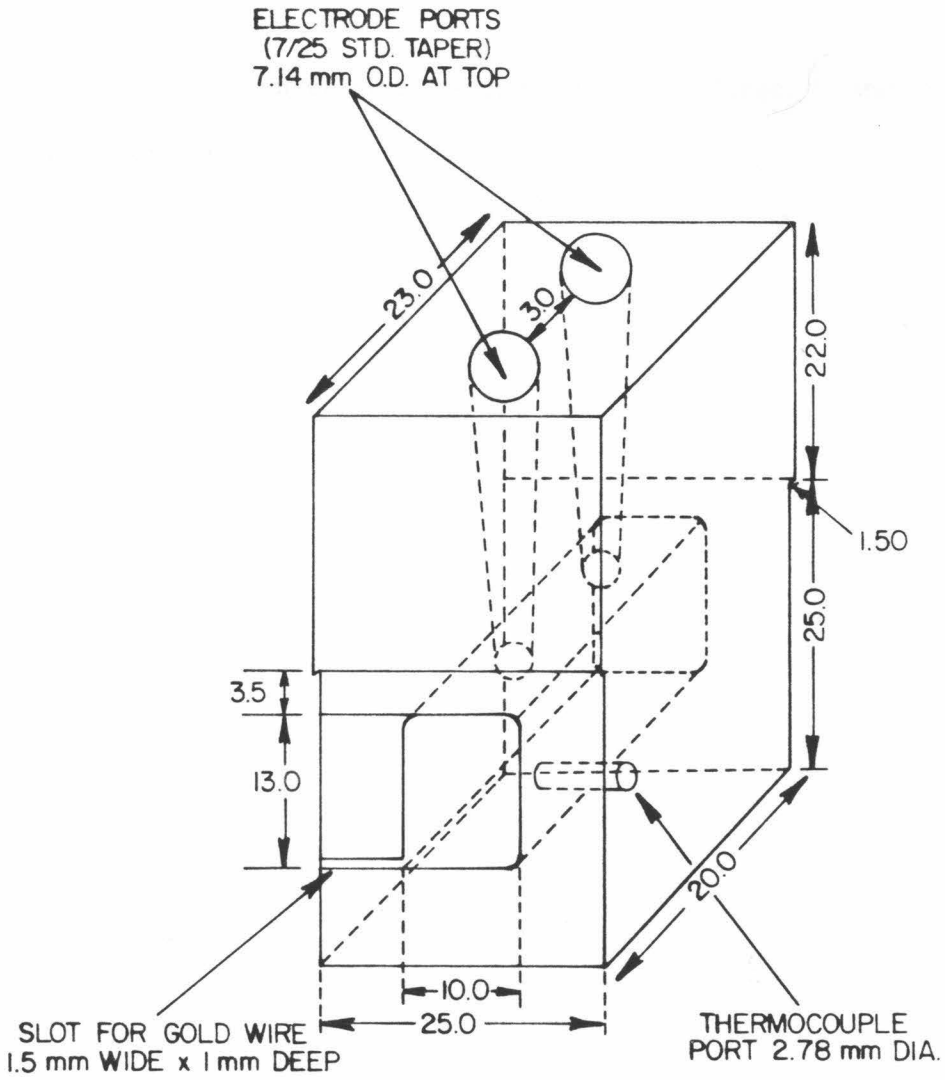
ELECTRODE PORTS
(7/25 STD. TAPER)
7.14 mm O.D. AT TOP
23.0
3.0
22.0
1.50
25.0
3.5
13.0
20.0
10.0
25.0
SLOT FOR GOLD WIRE
1.5 mm WIDE x 1 mm DEEP
THERMOCOUPLE
PORT 2.78 mm DIA.

Figure 3. Shroud machining specifications: flange. Material: 0.5 inch stainless steel plate.

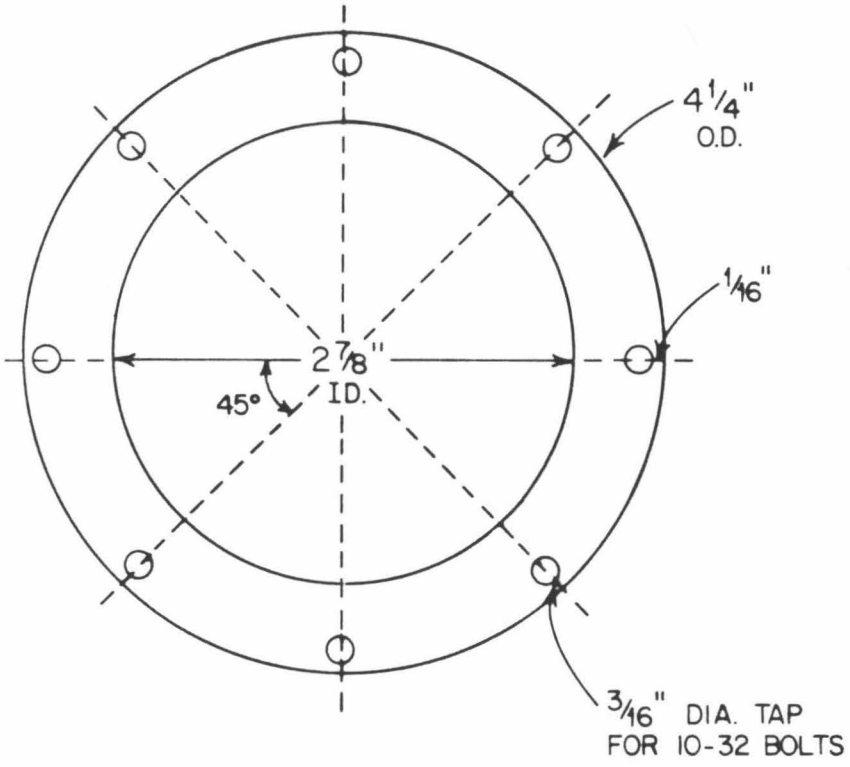
4 1/4"
O.D.
1/16"
2 7/8"
I.D.
45°
3/16" DIA. TAP
FOR 10-32 BOLTS

Figure 4. Shroud machining specifications: cannister. The end cap and flange are welded in place. Material: stainless steel.

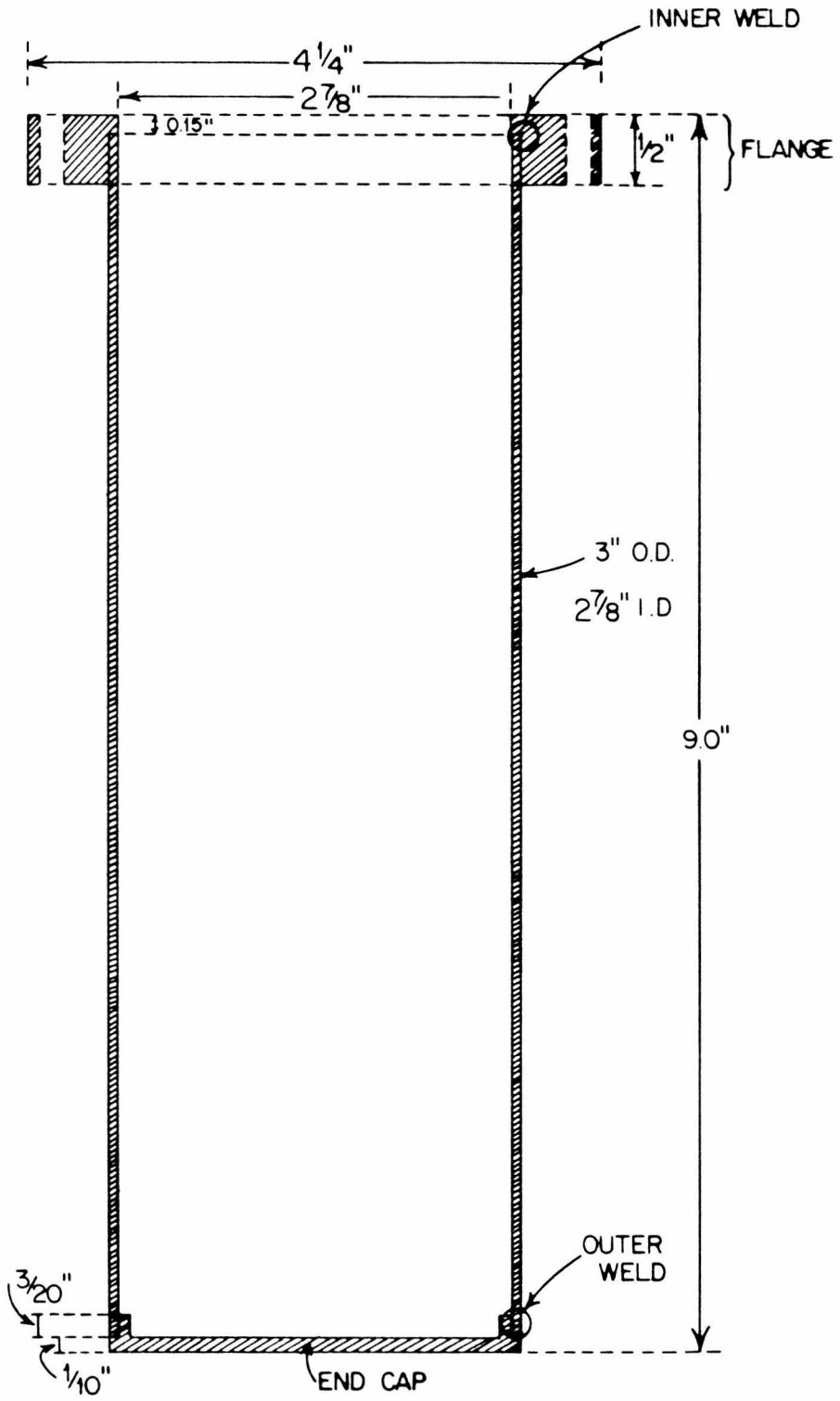
INNER WELD
4 1/4"
2 7/8"
± 0.15"
1/2"
FLANGE
3" O.D.
2 7/8" I.D
9.0"
OUTER WELD
3/20"
1/10"
END CAP

Figure 5. Shroud machining specifications: window housings. The housings are fitted onto the cannister and welded in place. Heavy lines indicate weld joints. Material: stainless steel.

A. BOTTOM VIEW

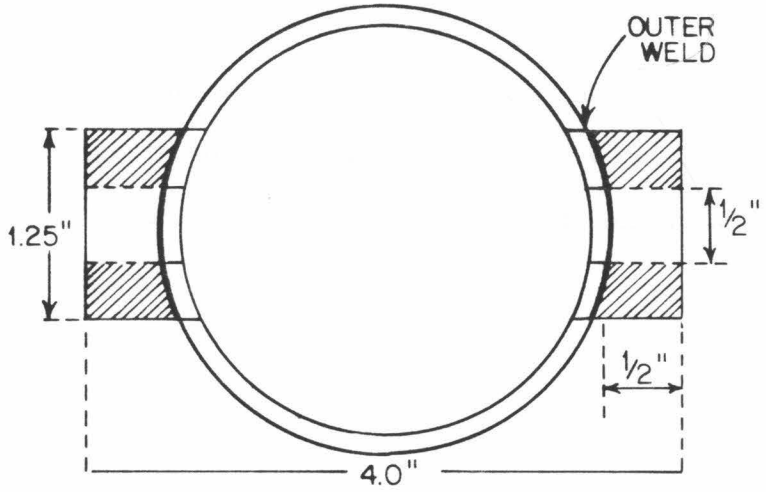

B. SIDE VIEW

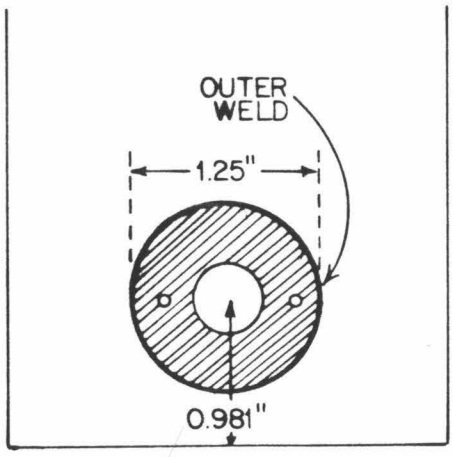

BOTTOM OF CANNISTER
(END CAP IN PLACE)

Figure 6. Shroud machining specifications: expanded cut-away view of a window housing. The window is sandwiched between two O-rings to maintain a gas-tight seal and prevent strain when the assembly is tightened (which would cause optical depolarization problems). Material: stainless steel.

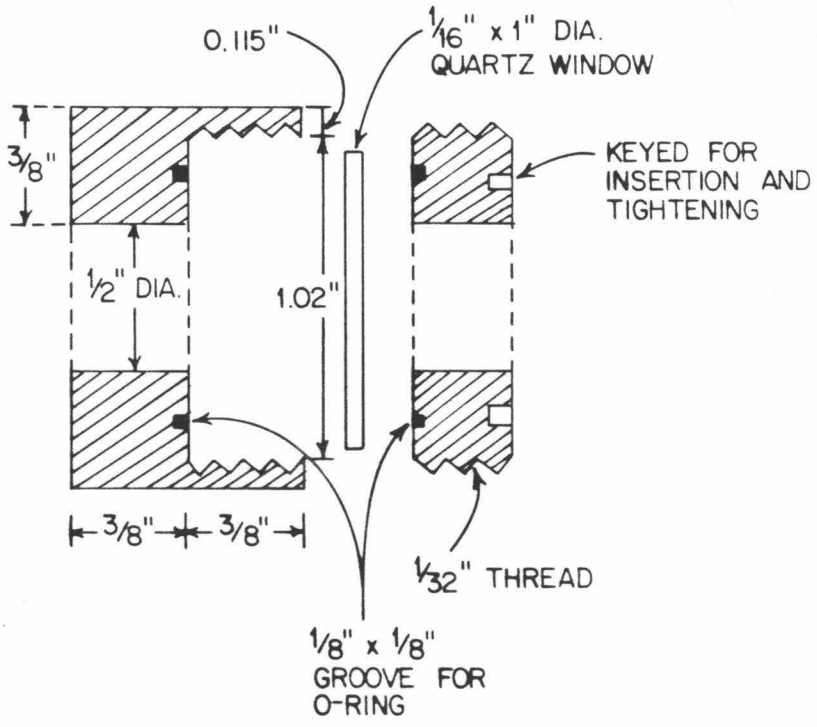
0.115"
1/16" x 1" DIA.
QUARTZ WINDOW
3/8"
KEYED FOR
INSERTION AND
TIGHTENING
1/2" DIA.
1.02"
3/8"
3/8"
1/32" THREAD
1/8" x 1/8"
GROOVE FOR
O-RING

Figure 7. Shroud machining specifications: faceplate. Placement of the fittings and O-ring are illustrated. Dotted lines indicate the placement of a suspension arm (perpendicular to the window axis). Material: 7/16 inch stainless steel plate.

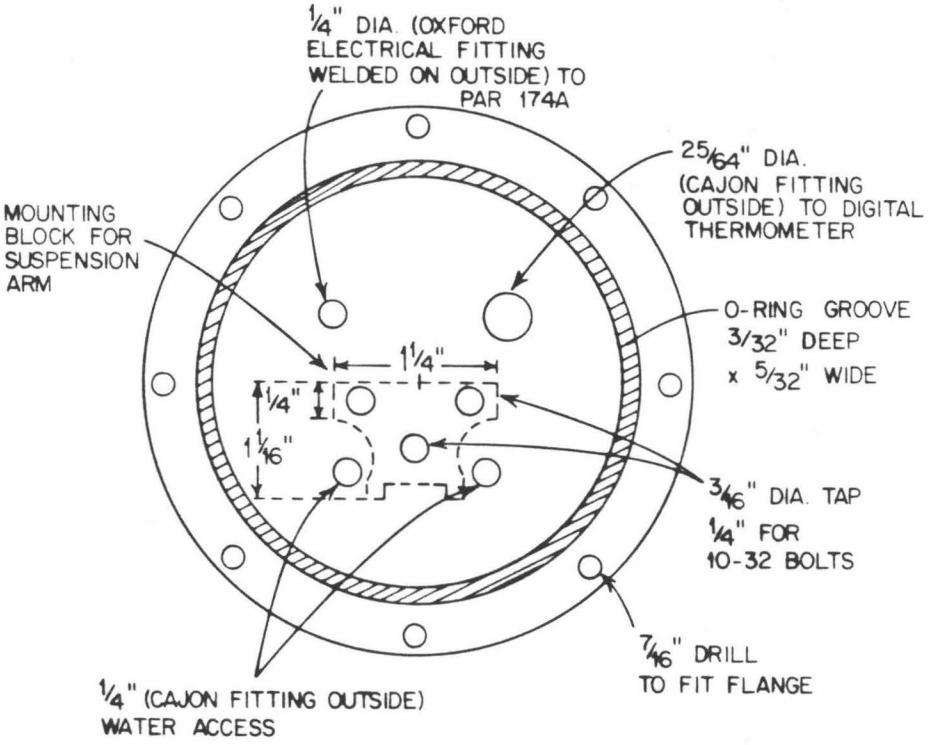
1/4" DIA. (OXFORD ELECTRICAL FITTING WELDED ON OUTSIDE) TO PAR 174A
25/64" DIA. (CAJON FITTING OUTSIDE) TO DIGITAL THERMOMETER
MOUNTING BLOCK FOR SUSPENSION ARM
O-RING GROOVE 3/32" DEEP x 5/32" WIDE
1 1/4"
1/4"
1 1/16"
3/16" DIA. TAP 1/4" FOR 10-32 BOLTS
7/16" DRILL TO FIT FLANGE
1/4" (CAJON FITTING OUTSIDE) WATER ACCESS

Figure 8. Shroud machining spcifications: thermostatting block. Spectroelectrochemical cells are clamped (using the mounting tabs) to this block, which is mounted on a 7.75" x 1.0" x 0.125" stainless steel suspension arm (not shown) that is attached to the underside of the faceplate. A piece of 0.25" o. d. copper tubing (not shown) is soldered to the block (for temperature control). Material: copper.

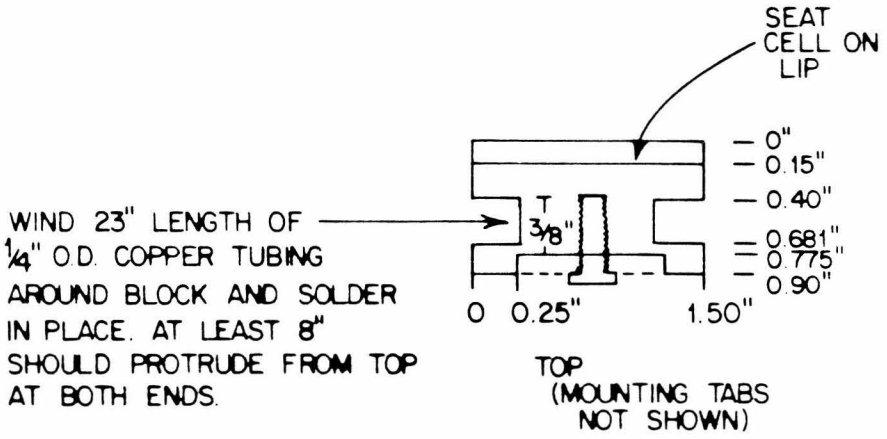
SEAT CELL ON LIP
WIND 23" LENGTH OF 1/4" O.D. COPPER TUBING AROUND BLOCK AND SOLDER IN PLACE. AT LEAST 8" SHOULD PROTRUDE FROM TOP AT BOTH ENDS.
T 3/8"
0"
0.15"
0.40"
0.681"
0.775"
0.90"
0
0.25"
1.50"
TOP
(MOUNTING TABS NOT SHOWN)

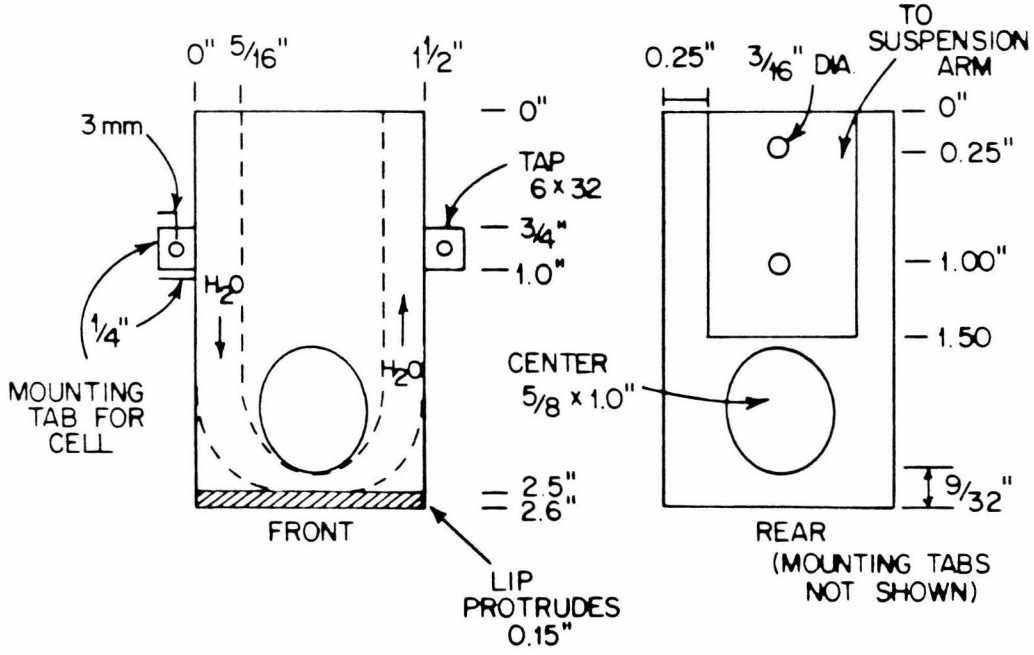
0"
5/16"
1 1/2"
3 mm
TAP 6 x 32
3/4"
1.0"
H2O
1/4"
MOUNTING TAB FOR CELL
2.5"
2.6"
FRONT
LIP PROTRUDES 0.15"
0.25"
3/16" DIA.
TO SUSPENSION ARM
0"
0.25"
1.00"
1.50
CENTER 5/8 x 1.0"
9/32"
REAR
(MOUNTING TABS NOT SHOWN)

Figure 9. View of the disassembled shroud. On the left, an OTTLE cell fitted with Pt counter and saturated calomel reference electrodes is shown clamped to the thermostatting block. The cannister is clamped onto the spectrophotometer mount on the right.

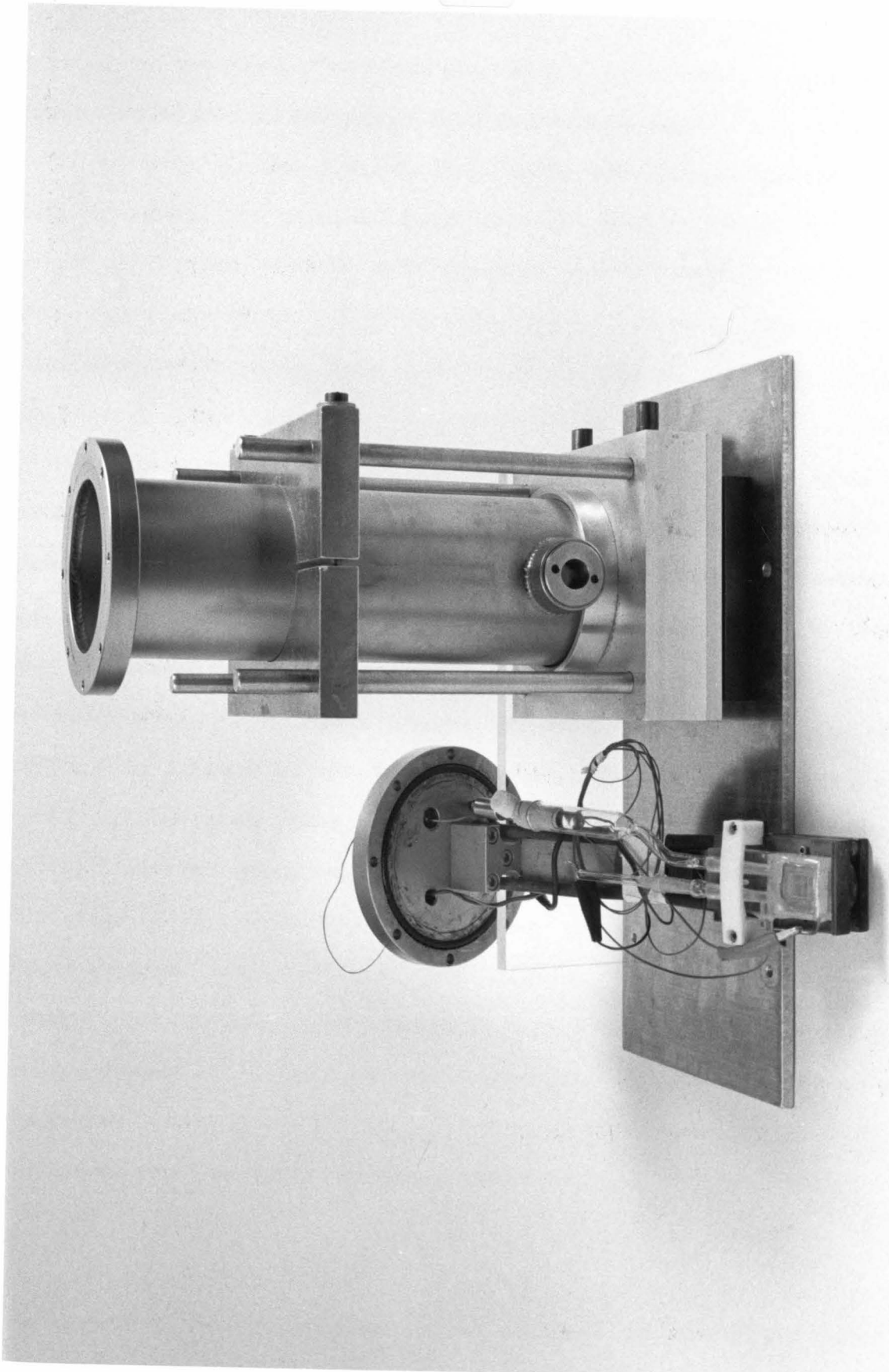

clamped to the shroud thermostatting block. The shroud cannister is shown clamped onto the spectrophotometer mount on the right.

A Princeton Applied Research Model 174A polarographic analyzer was used to control the potential across the cells and precise (± 0.1 mV) values of the cell potential were measured with a Keithley 177 microvolt digital multimeter. Cell temperatures were varied using a constant temperature water bath and measured directly with an Omega Engineering, Inc. precision microthermocouple (plus Fluke 2175A Digital Thermometer, ± 0.2 ^{o}C) situated in the protein solution. Formal reduction potentials were determined by sequentially applying a series of potentials, $E_{applied}$, across the spectroelectrochemical cell. Each potential was maintained until electrolysis ceased so that the equilibrium value of the ratio of concentrations of oxidized to reduced forms of all redox couples in solution, (Ox/(Red), was established as defined by the Nernst equation. Redox couples were converted in increments from one oxidation state to the other by the series of applied potentials, for which each value of (Ox)/(Red) was determined from the corresponding overlay spectra. Absorption spectra were obtained with a Cary 219 recording spectrophotometer and circular dichroism spectra were obtained with a JASCO J-500C recording spectropolarimeter. Formal reduction potentials and n values were determined from plots of $E_{applied}$ vs. log(Ox)/(Red). At least 6-7 data points were included in each Nernst plot.

RESULTS AND DISCUSSION

The shroud was designed to contain an inert atmosphere and hence

there is no need for continuous flushing with argon or nitrogen. Instead, the protein solution is loaded into a spectroelectrochemical cell (inside a Vacuum Atmospheres inert atmosphere box), the reference and counter electrodes are sealed into the cell body (using Apiezon H grease), and the assembled cell is then clamped to the thermostatting block of the shroud. The spectroelectrochemical system may be brought out of the inert atmosphere box and seated onto the spectrophotometer mount after making the electrical connections and bolting the face-plate onto the flange of the shroud. The anaerobic performance of the sealed system was evaluated in two ways. First, solid chromous acetylacetonate (donated by Prof. C.A. Reed) was placed into the shroud and periodically checked for evidence of oxidation (color change from orange to grey-green); no detectable change was observed after six days. Second, a solution of reduced iron-molybdenum protein of Azotobacter vinelandii nitrogenase, donated by Prof. C.E. McKenna, was placed (inside an inert atmosphere box) into the shroud, which was then sealed and brought out into the laboratory atmosphere for 12 hours. The shroud was subsequently taken back into the inert atmosphere box, and the protein was removed for assay (performed by Dr. M.-C. McKenna, using acetylene as the substrate). Essentially complete (> 95%) retention of the enzyme activity was observed. This protein is rapidly (within 10 minutes) destroyed upon exposure to oxygen concentrations in excess of 5-10 ppm.

The cells previously described can be used with the shroud for anaerobic measurements of E^{o} as a function of temperature. In order to accommodate the assembled cells within the shroud, both the

reference and counter electrodes must be shortened to 6.5 inches or less. Careful temperature measurements of the working electrode solution and reference SCE indicate that the SCE is partially thermostated when used with an OTTLE cell in the shroud. The long-path spectroelectrochemical cell, when in the shroud, is in a completely isothermal configuration. Hence, the temperature dependence of the SCE (23) must be taken into consideration when using the shroud for variable-temperature measurements.

When rigorously anaerobic measurements are not necessary, the cell body may be clamped onto a thermostatting block with the extended (9 inch) reference electrode salt bridge in place to maintain the cell in a nonisothermal configuration. This experimental setup allows one to collect variable-temperature data at a much faster rate, since the reference electrode is kept at 25 ^{o}C. Chapters III, IV, and V present results obtained by absorption spectroelectrochemistry that illustrate the capabilities of this equipment.

With few exceptions, metalloproteins undergo very slow heterogeneous electron transfer at an electrode. For this reason, low molecular weight redox mediators (see Reference 25 for a compilation) are used to maintain properly poised cell potentials. Many potentially useful redox mediators unfortunately interfere with spectral measurements when absorption spectroscopy is used. Since most mediators are not optically active, circular dichroism (CD) measurement offers a useful alternative. A set of overlay CD spectra obtained for the C. vinosum HiPIP(Ox)/HiPIP(Red) couple using thin-layer spectroelectrochemistry is shown in Figure 10. A Nernst plot of the

Figure 10. Overlay circular dichroism spectra of C. vinosum HiPIP at different values of the applied potential in mV vs. NHE. Solution conditions: pH 7.5, 0.245 M ionic strength phosphate buffer, 25 ^{o}C. Mediator titrant: $K_3[Fe(CN)_6]$, 1 equivalent.

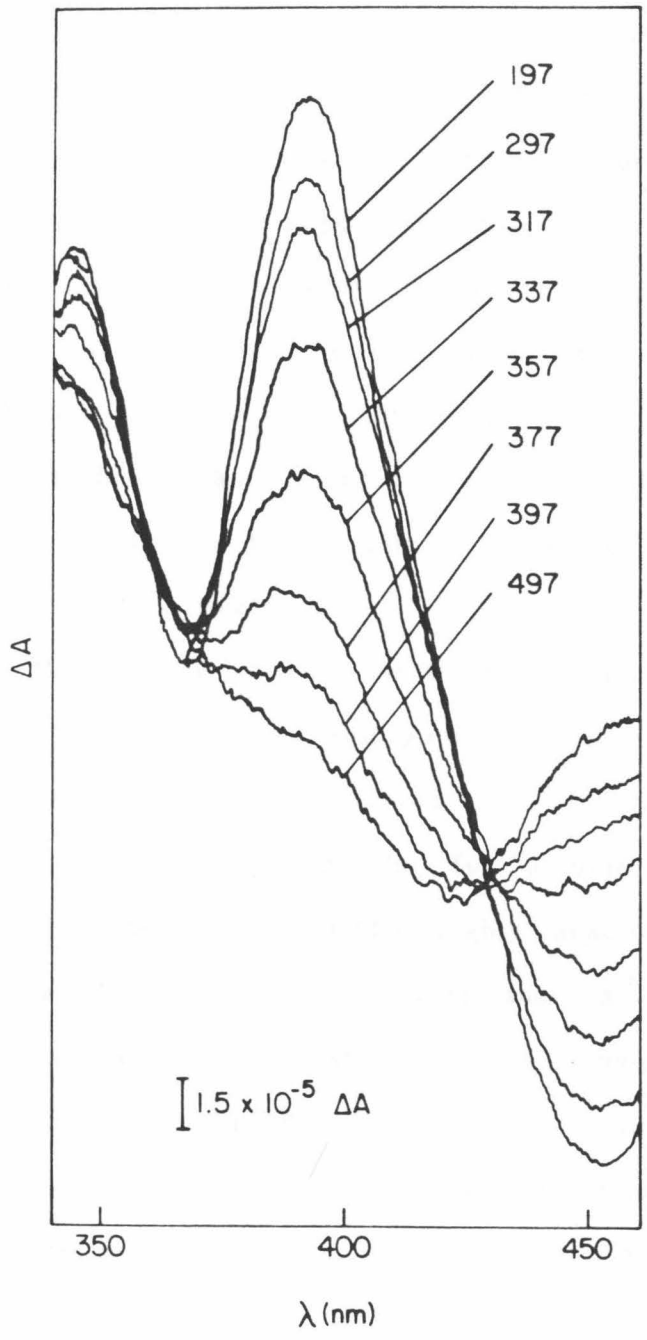
197
297
317
337
357
377
397
497
ΔA
1.5 x 10⁻⁵ ΔA
350
400
450
λ (nm)

data (at 400 nm) is displayed in Figure 11. Essentially identical results were obtained (n = 1.0 ± 0.05 and $E^{0\prime}$ = 348 ± 2 mV vs. NHE) from CD and absorption experiments carried out under the same conditions. Both $K_3[Fe(CN)_6]$ and $[Co(phen)_3](ClO_4)_3$ were used as redox mediators, with no difference in the results. These results are in good agreement with the literature value of 356 mV vs. NHE (25). It is important that high quality fused quartz be used for the cell windows. Additionally, it is imperative that the entire spectroelectrochemical cell does not cause depolarization effects, whether through strain or from multiple reflections at the optically transparent gold electrodes. This can be monitored by comparing the CD of a solution containing $NiSO_4$ and potassium d-tartrate placed before and then after the cell. The nickel tartrate CD spectra will be superposable if the cell is optically satisfactory.

All six of the design criteria mentioned in the introduction to this chapter have been met. Both absorption and CD may be monitored using this spectroelectrochemistry apparatus. The OTTLE and long-path cells both incorporate microthermocouples for accurate protein temperature measurement. The shroud enables highly anaerobic measurements to be undertaken; oxygen-sensitive proteins such as nitrogenase and oxidases can now be routinely studied. The long-path cell makes spectroelectrochemical experiments on proteins containing weakly absorbing chromophores (Type II copper, for example) possible. The OTTLE cell possesses a small sample volume (ca. 0.4 mL); the thermocouple can be removed to decrease the volume to ca. 0.2 mL when protein availability is a problem. Finally, both cells contain gold

Figure 11. Nernst plot calculated from the spectra displayed in Figure 10. The solid line is a least-squares fit (56 mV slope) to the data at 400 nm.

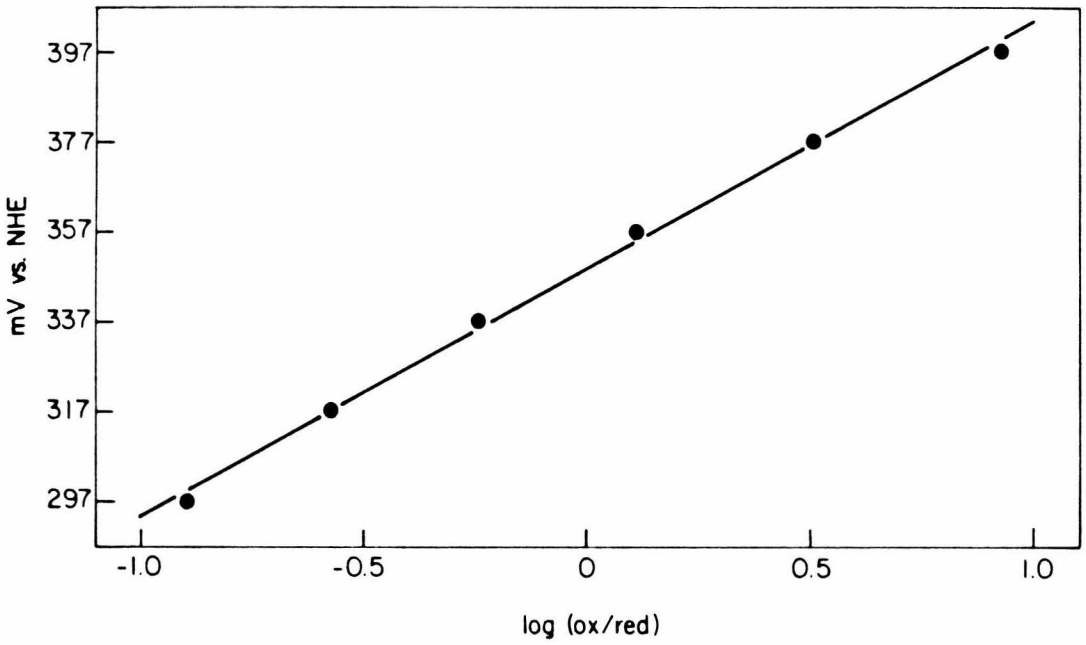
397
377
357
337
317
297
mV vs. NHE
-1.0
-0.5
0
0.5
1.0
log (ox/red)

working electrodes with large surface areas (greater than 4 cm^2 for the long-path cell) to minimize electrolysis time.

REFERENCES

1. Rossi, P., McCurdy, C.W., and McCreery, R.L. (1981) *J. Am. Chem. Soc.* **103**, 2524.

2. Anderson, J.L., and Kincaid, J.R. (1978) *Appl. Spect.* **32**, 356.

3. Finklea, H.O., Boggess, R.K., Trogdon, J.W., and Schultz, F.A. (1983) *Anal. Chem.* **55**, 1177.

4. Hawkridge, F.M., and Ke, B. (1977) *Anal. Biochem.* **78**, 76.

5. Simone, M.J., Heineman, W.R., and Kreishman, G.P. (1982) *Anal. Chem.* **54**, 2382.

6. Anderson, J.L. (1979) *Anal. Chem.* **51**, 2312.

7. Brewster, J.D., and Anderson, J.L. (1982) *Anal. Chem.* **54**, 2560.

8. Heineman, W.R., Norris, B.J., and Goelz, J.F. (1975) *Anal. Chem.* **47**, 79.

9. Norris, B.J., Meckstroth, M.L., and Heineman, W.R. (1976) *Anal. Chem.* **48**, 630.

10. Rubinson, K.A., and Mark, H.B., Jr. (1982) *Anal. Chem.* **54**, 1204.

11. Hawkridge, F.M., and Kuwana, T. (1973) *Anal. Chem.* **45**, 1021.

12. Heineman, W.R., Meckstroth, M.L., Norris, B.J., and Su, C.-H. (1979) *J. Electroanal. Chem.* **104**, 577.

13. Anderson, C.W., Halsall, H.B., and Heineman, W.R. (1979) *Anal. Biochem.* **93**, 366.

14. Stankovich, M.T. (1980) *Anal. Biochem.* **109**, 295.

15. Huang, Y.-Y., and Kimura, T. (1983) *Anal. Biochem.* **133**, 385.

16. Jones, E.T.T., and Faulkner, L.R. (1984) *J. Electroanal. Chem.* **179**, 53.

17. Condit, D.A., Herrera, M.E., Stankovich, M.T., and Curran, D.J. (1984) *Anal. Chem.* **56**, 2909.

18. Taniguchi, V.T., Ellis, W.R., Jr., Cammarata, V., Webb, J., Anson, F.C., and Gray, H.B. (1982) in *Electrochemical and Spectrochemical Studies of Biological Redox Components*, Kadish, K.M., ed., Amer. Chem. Soc., Washington, D.C., p. 51.

19. Ellis, W.R., Jr., Morgan, T.V., Taniguchi, V.T., Stephens, P.J., and Gray, H.B., *Anal. Biochem.*, to be submitted for publication.

20. Bartsch, R.G. (1978) *Meth. Enzymol.* **53**, 329.

21. Schilt, A.A., and Taylor, R.C. (1959) *J. Inorg. Nucl. Chem.* **9**, 211.

22. Hamilton, R., Maguire, D., and McCabe, M. (1979) *Anal. Biochem.* **93**, 386.

23. Wingfield, B., and Acree, S.F. (1937) *J. Res. Nat. Bur. Stand.* **19**, 163.

24. Fultz, M.L., and Durst, R.A. (1982) *Anal. Chim. Acta* **140**, 1.

25. Mizrahi, I.A., Meyer, T.E., and Cusanovich, M.A. (1980) *Biochemistry* **19**, 4727.

CHAPTER III

REDOX THERMODYNAMIC PARAMETERS FOR SELECTED SINGLE-SITE HEME AND COPPER METALLOPROTEINS

INTRODUCTION

Metalloproteins containing a single redox prosthetic group can be divided into two general classes: electron carriers and proteins involved in the transport or activation of small molecules. A fundamental question concerns how a simple prosthetic group, like heme, can exhibit such a wide range of reduction potentials and functional diversity. Essentially the same heme group occurs in such functionally diverse proteins as a-, b-, c-, and c′-cytochromes, peroxidases, catalase, cytochrome P-450, and myoglobin.

Adman (1) has identified some of the factors that are characteristic of electron transport proteins: (a) possession of a cofactor to act as an electron sink; (b) placement of the cofactor close enough to the protein surface to allow electron entrance and/or egress; (c) existence of a hydrophobic shell adjacent to, but perhaps not always entirely surrounding, the cofactor; (d) small structural changes accompanying electron transfer (to minimize the inner-sphere reorganizational energy); and (e) a flexible architecture which permits expansion or contraction in preferred directions upon electron transfer.

In 1968 Vallee and Williams suggested (2) that the environment of a metal center in a protein may give rise to an "entatic state," a strained geometry unlike those associated with conventional coordination complexes. This "entatic state" hypothesis was advanced in order to rationalize ORD, absorption and EPR spectra, and reduction potentials of certain copper, iron, and cobalt proteins which did not appear to be explicable in the context of the properties of typical

complexes of these metal ions. During the intervening years it has become clear that, with the possible exception of "blue" copper centers (3), there is nothing "strained" about the environments of electron transfer proteins. This point has been repeatedly demonstrated by the synthesis of low molecular weight models for protein coordination sites (4,5). Metalloproteins that function as "electron transferases" typically place their prosthetic groups in a hydrophobic environment and provide occasional hydrogen bonds to stabilize one or both metal oxidation states. Severe inner-sphere reorganizational problems are apparently avoided by dictating a coordination environment that is a compromise between ones favored by the oxidized and reduced metal ions (6).

Redox thermodynamic parameters for several paradigmatic hemoproteins (cytochrome _c_, myoglobin, and cytochrome _c_′) and two azurins are presented in this chapter. The results are discussed with respect to the known structural features and reactivities of these proteins, and provide reference points for the results presented in Chapter V for the cytochrome and Cu_A centers in cytochrome _c_ oxidase.

MATERIALS AND METHODS

Horse heart cytochrome _c_ (Type VI from Sigma Chemical Co.) was purified by cation-exchange chromatography (pH 7.0) on Whatman CM-52 cellulose (7). Sperm whale myoglobin (Type II from Sigma Chemical Co.) was also chromatographed (pH 7.8) on Whatman CM-52 cellulose prior to use. Crystals of _Rhodopseudomonas palustris_ cytochrome _c_′ were generously donated by Drs. R.G. Bartsch, T.E. Meyer, and M.D.

Kamen. Azurin samples from Alcaligenes denitrificans and Alcaligenes faecalis were supplied by Professors E.N. Baker and I. Pecht, respectively, and did not require further purification.

$[Ru(NH_3)_5py](ClO_4)_3$ was prepared as previously described (8). $[Ru(NH_3)_6]Cl_3$ was purchased from Alfa Products and purified prior to use, as described by Pladziewicz et al. (9). $[Co(phen)_3](ClO_4)_3$ was prepared by the method of Schilt and Taylor (10). The sodium salt (indicator grade) of 2,6-dichloroindophenol (Aldrich Chem. Co.) was used as received. All protein and buffer solutions were prepared using deionized water purified by a Barnstead NANOpure water purifier and analytical grade reagents. The spectroelectrochemical apparatus and methods employed in these experiments were described in Chapter II.

RESULTS AND DISCUSSION

Horse heart cytochrome c. As mentioned in Chapter I, cytochrome c occupies a prominent place in the mitochondrial electron transport chain. Its water solubility, low molecular weight (12,400 daltons), and ease of purification have led to a large number of experiments, which, when taken together, present a detailed picture of the structure and biological function of this electron carrier (11-14). Figure 1 illustrates a ribbon drawing of the structure of tuna ferricytochrome c, as viewed from the exposed heme edge (15). The lower portion of this figure depicts the structural details in the vicinity of the heme site for the oxidized and reduced proteins (16,17). Several mechanisms for the interaction of cytochrome c with its

Figure 1. Structural features of cytochrome c. Top illustration, taken from Reference 15: a schematic representation of the structure of tuna cytochrome c, which is known to closely resemble the horse heart protein. Propionate-6 is located at the lower front (outer) position of the heme pocket and propionate-7 is at the lower back position. His-18 and Met-80 provide the axial ligands to the iron center. Lower illustration, taken from Reference 16: schematic drawing (not to scale) of side-chain motion in the vicinity of the heme. Heavy lines indicate the reduced molecule, and light lines the oxidized molecule. Note the motion of the buried water molecule on the left.

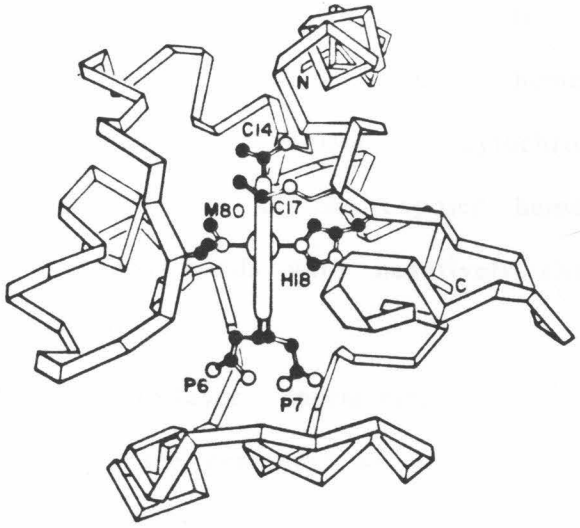
N
C14
C17
M80
H18
C
P6
P7

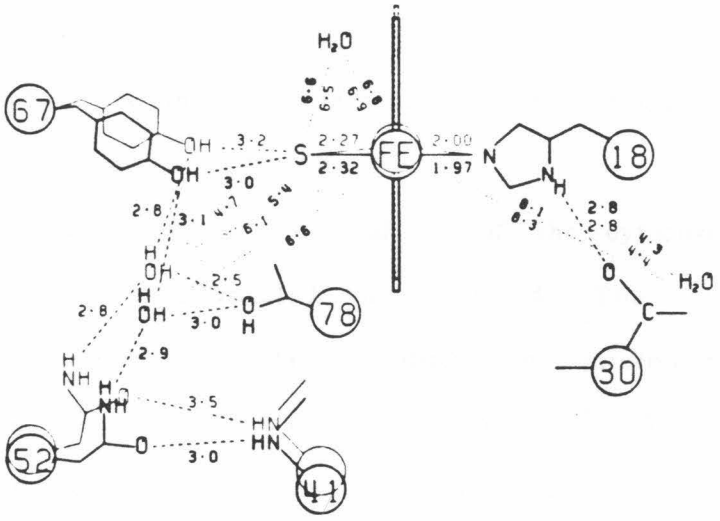
H2O
67
OH
3·2
S
2·27
2·32
FE
2·00
1·97
N
NH
18
OH
3·0
2·8
3·1
4·7
5·4
6·1
6·6
6·8
6·5
6·8
6·3
6·1
2·8
2·8
4·3
4·4
O
C
H2O
30
H
OH
2·5
O
H
78
2·8
OH
3·0
2·9
NH
NH
3·5
HN
HN
52
O
3·0
41

physiological redox partners have been proposed during the last 25 years. Results of kinetic studies (principally from the Margoliash, Millett, and Bosshard laboratories) all point to electron transfer into and out of the protein via the exposed heme edge. This is presently the accepted reaction mechanism for cytochrome c; a number of lysine residues in the vicinity of the exposed heme edge appear to form intermolecular hydrogen bonds with negatively charged residues of protein redox partners (18-20).

The results of a thin-layer spectroelectrochemical titration (21) of cytochrome c (24.4 ^{o}C) are presented as a set of overlay absorbance spectra in Figure 2. The inset to this figure illustrates the rapid reestablishment of equilibrium conditions subsequent to each change in the applied potential. The absorbance changes at 550 nm were used to determine the Nernst plot (Figure 3) for this titration. The solid line is a least-squares fit to the data (n = 1.0, $E^{o'}$ = 262 ± 2 mV vs. NHE). This result is in good agreement with previous determinations (22,23) of the formal potential (250-270 mV).

Results for the temperature dependence of the cytochrome c formal reduction potential are illustrated in Figure 4. The solid line is a least-squares fit to the data, yielding an interpolated reduction potential (25 ^{o}C) of 260 ± 2 mV vs. NHE and $dE^{o'}/dT$ = -5.61 ± 0.5 x 10^{-4} V/^{o}C. The redox thermodynamic parameters (25 ^{o}C) derived from these nonisothermal experiments are as follows: $\Delta G^{o'}$ = -6.00 ± 0.05 kcal/mol, $\Delta H^{o'}$ = -14.5 ± 0.4 kcal/mol, and $\Delta S^{o'}$ = -28.5 ± 1.2 eu. Importantly, the results of two calorimetric determinations of the enthalpy of reduction (pH 7.0, 25 ^{o}C) for horse heart cytochrome c are

Figure 2. Thin-layer spectroelectrochemistry of horse heart cytochrome c (0.13 mM), ionic strength 0.1 M, pH 7.0 phosphate buffer, 24.4 ^{o}C, 0.65 mM $[Ru(NH_3)_5py](ClO_4)_3$. Overlay spectra and absorbance changes at 550 nm as a function of time at different values of $E_{applied}$ in mV vs. NHE are shown. The mediator is observed to spectrally interfere below 502 nm, causing the lack of isosbestic behavior in this region.

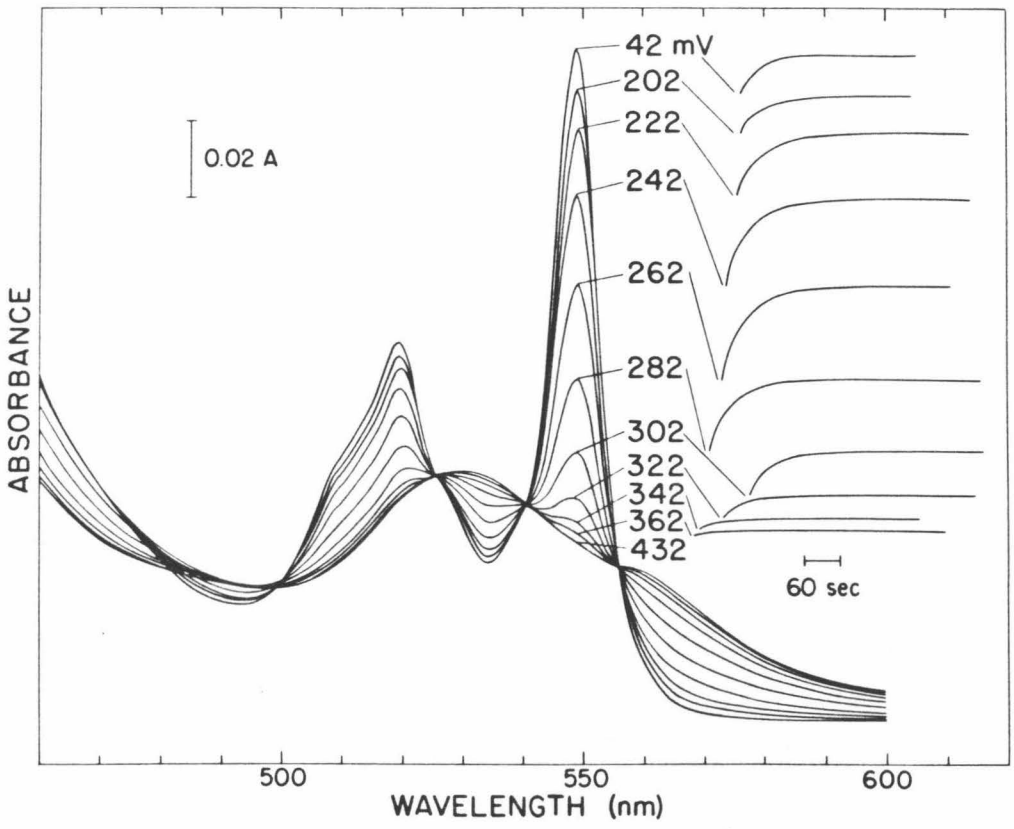
42 mV
202
222
242
262
282
302
322
342
362
432
0.02 A
60 sec
ABSORBANCE
500
550
600
WAVELENGTH (nm)

Figure 3. Nernst plot of the data (at 550 nm) presented in Figure 2. The least-squares fit (solid line) yields a 59 mV slope and $E^{o'}$ = 262 ± 2 mV vs. NHE.

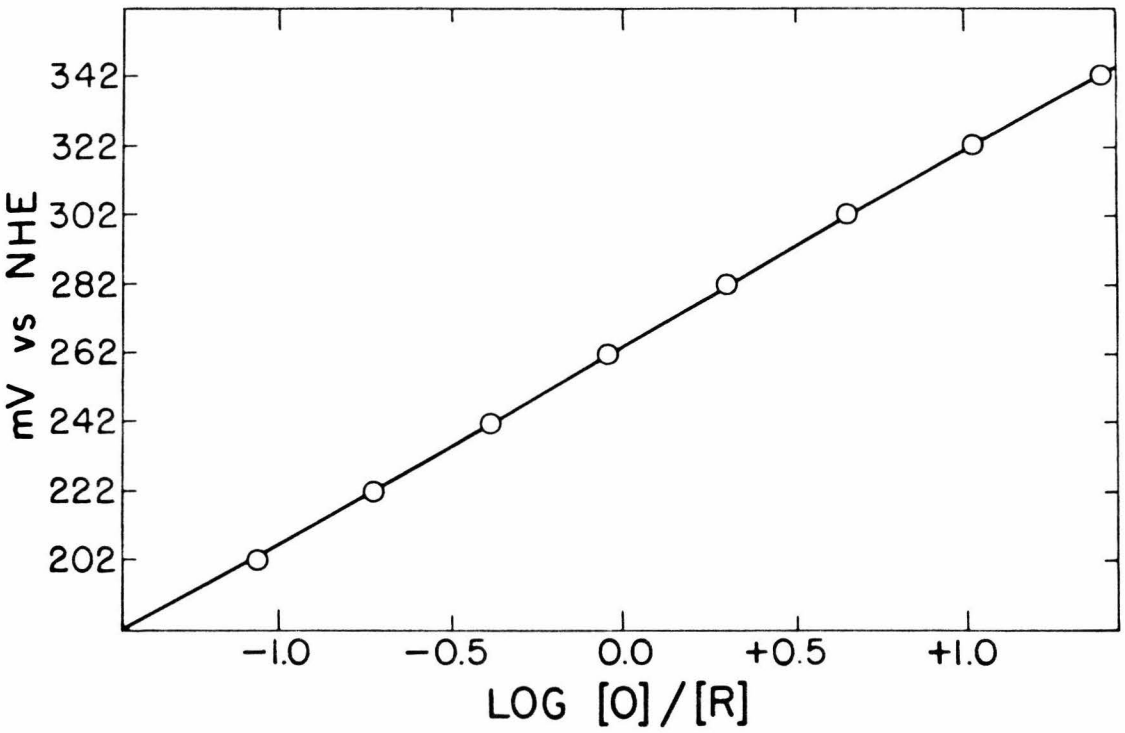
342
322
302
282
262
242
222
202
mV vs NHE
−1.0
−0.5
0.0
+0.5
+1.0
LOG [O] / [R]

Figure 4. Temperature dependence of $E^{o'}$ for horse heart cytochrome _c_ using nonisothermal thin-layer spectroelectrochemistry, where $E^{o'}(25\ ^{o}C) = 260 \pm 2$ mV vs. NHE and $dE^{o'}/dT = -5.61 \pm 0.5 \times 10^{-4}$ V/^{o}C. Solution conditions as in Figure 2. Key: (O) $[(NH_3)_5pyRu]^{3+/2+}$; and (Δ) 2,6-dichloroindophenol.

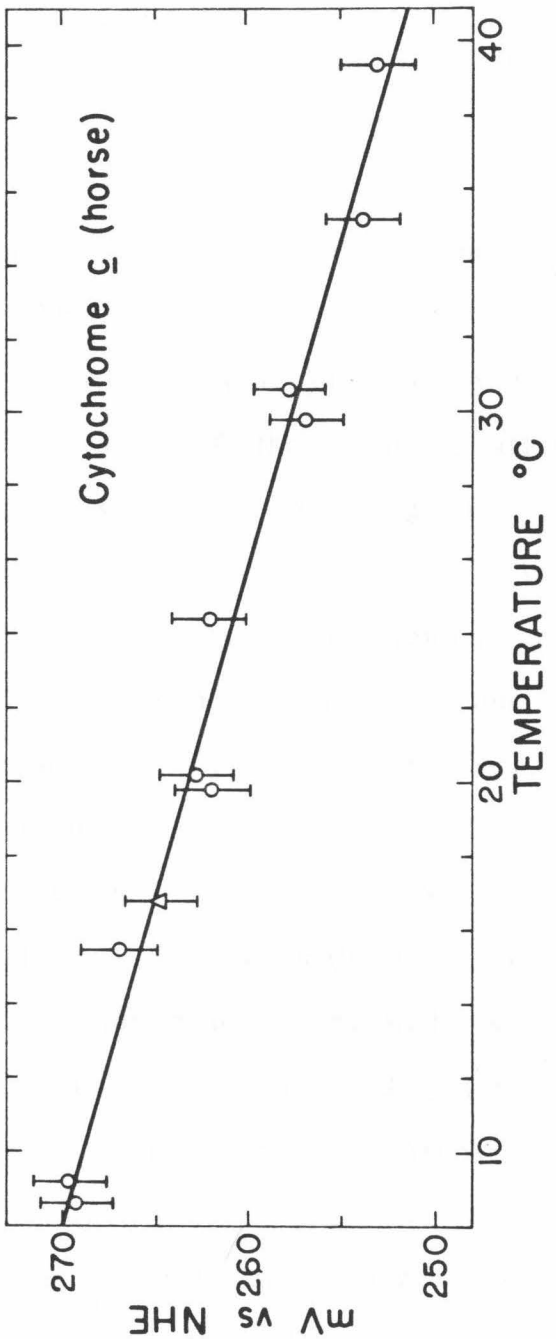
Cytochrome c (horse)
mV vs NHE
270
260
250
10
20
30
40
TEMPERATURE °C

in excellent agreement with the value reported here: $\Delta H^{o\prime}$ = -14.1 kcal/mol (Watt and Sturtevant, Ref. 24) and $\Delta H^{o\prime}$ = -14.5 ± 1.5 kcal/mol (George et al., Ref. 25).

Cytochrome c is a highly basic protein (pI = 10.05); at pH 7.0, the surface charge q is +7 (26). By analogy with transition metal complexes, one might expect the ΔS_{rc}^{o} to be slightly positive (the hydrophobic environment is expected to reduce the magnitude of ΔS_{rc}^{o}); the observed ΔS_{rc}^{o} is -12.9 ± 1.2 eu, however.

Lysine residues constitute most of the protein's cationic side chains. Chemical modification of these residues affords an opportunity to alter the properties of the ε-amino groups directly involved in anion binding (27-30). Margoliash and coworkers (30) have mapped a number of anion binding sites on ferricytochrome c via the use of carboxydinitrophenyl modification of lysine residues. This study revealed the presence of one high-affinity phosphate binding site near Lys-87 with an estimated $K_d \sim 2 \times 10^{-4}$ M and another site of lower affinity located in the vicinity of Lys-25, His-26, and Lys-27. Other anions, such as chloride (28), carbonate (30), and citrate (30) are known to bind to the oxidized protein as well. A notable exception is cacodylate, which was found to be non-binding (28). No indications of small cation binding to either ferro- or ferricytochrome c have been obtained to date.

In order to determine whether ion binding to horse heart cytochrome c has a significant effect on the redox thermodynamics of the protein, experiments were performed (pH 7.0, I = 0.1 M) using sodium cacodylate buffer instead of sodium phosphate buffer. These results are

displayed in Figure 5. The thermodynamic parameters (25 ^{o}C) for cytochrome c in cacodylate buffer are as follows: $\Delta G^{o'}$ = -6.3 ± 0.05 kcal/mol, $\Delta H^{o'}$ = -15.2 ± 0.33 kcal/mol, $\Delta S^{o'}$ = -29.8 ± 1.2 eu, and $\Delta S_{rc}{}^{o'}$ = -14.2 ± 1.2 eu. Similar results (31) were obtained for the heme iron site in cytochrome c labeled with $[Ru(NH_3)_5]^{3+/2+}$ at His-33 ($\Delta S_{rc}{}^{o'}$ = -13.6 ± 0.8 eu). Within experimental error, the reaction entropy is insensitive to the binding of ions on the surface of the molecule. Charge-induced outer-sphere (i.e., solvent) reorganization can only be a small factor in this entropy change since only 4% of the heme surface is exposed to the solvent.

It has been known for several decades that cytochrome c exhibits several pH-dependent conformational states. An alkaline transition with a pK_a ~ 9.1 has been observed for ferricytochrome c. This transition is believed to be associated with the dissociation of Met-80; the reduction potential falls dramatically (23) and the 695 nm absorption band, associated with a sulfur→iron LMCT transition, disappears. The ^{2}H NMR resonance due to Met-80 in the deuterium-enriched oxidized protein disappears from its hyperfine-shifted upfield position without line broadening and reappears coincident with the Met-65 methyl resonance (32). In contrast, ferrocytochrome c maintains an ordered structure over the pH range 4 to 11 (33). The heme iron remains low-spin throughout this transition and a new strong field ligand must therefore replace Met-80. It has been frequently suggested that an ε-amino nitrogen of a nearby lysine provides the new donor atom, but this remains a subject of controversy (34). Regardless, it is clear that reduction of ferricytochrome c at alkaline pH values below 11

Figure 5. Temperature dependence of the reduction potential of horse heart cytochrome c in a nonbinding cacodylate buffer medium. Conditions: pH 7.0; 0.1 M ionic strength; 1 equivalent $[(NH_3)_5pyRu]^{3+/2+}$ present.

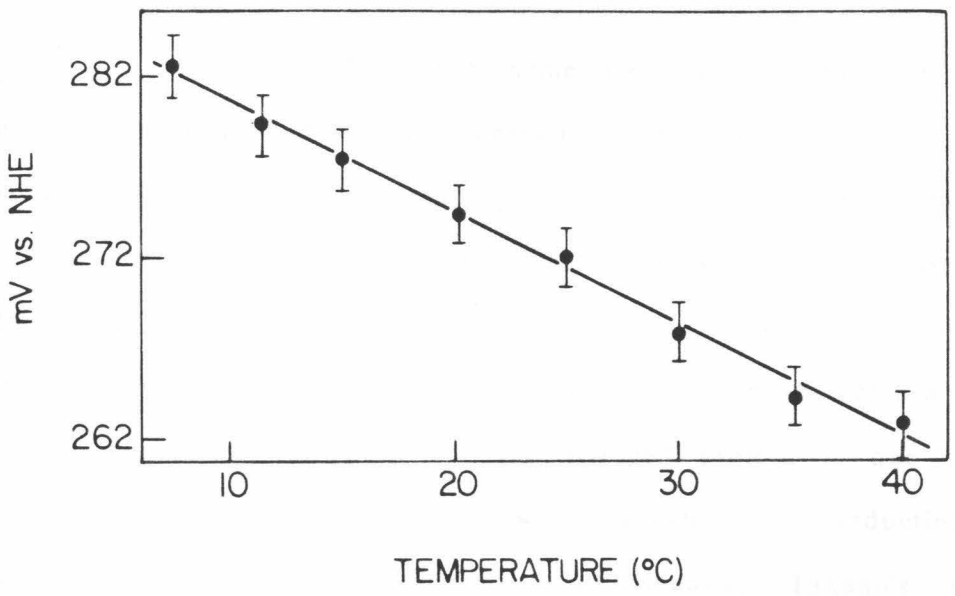
282
272
262
mV vs. NHE
10
20
30
40
TEMPERATURE (°C)

causes a drastic conformational change at the heme site. The unknown sixth ligand must be displaced by Met-80 in order for the reduced protein to assume a structure similar to the one at neutral pH. Figure 6 displays a plot of ΔS^{o} vs. pH. The points on this plot were calculated using the potentiometric and calorimetric data in References 23 and 24, respectively. As the pH increases, ΔS^{o} drastically decreases, as expected for a situation in which reduction is accompanied by a large change in molecular geometry (35).

Sperm whale myoglobin (36). The heme iron in myoglobin is high-spin in both oxidation states, in contrast to the low-spin heme iron in cytochrome c. As expected (37) on the basis of X-ray structures of iron porphyrin complexes, the iron atom is significantly displaced from the heme plane in both oxidation states: 0.40Å out-of-plane in aquometmyoglobin (38) and 0.55Å out-of-plane in deoxymyoglobin (39). The further displcement observed for the reduced protein is due to an increase in atomic radius, which is well-established for reduction of high-spin Fe(III) to high-spin Fe(II). Additionally, Takano's structures (38,39) confirm Pauling's suggestion (40) that the axial water molecule in aquometmyoglobin dissociates from the iron upon reduction of the protein.

Figure 7 presents a set of overlay absorbance spectra obtained during an anaerobic thin-layer spectroelectrochemistry experiment (pH 7.0, 25 ^{o}C). The corresponding Nernst plot is displayed in Figure 8. Myoglobin functions as an O_2 carrier; hence, the shroud was used to maintain anaerobic conditions and prevent formation of oxymyoglobin upon reduction of the protein.

Figure 6. pH dependence of ΔS^{o} for horse heart cytochrome c. Calculated from the data in References 23 and 24. Selected values of the surface charge (q) are shown to emphasize the lack of a correlation between q and ΔS^{o}.

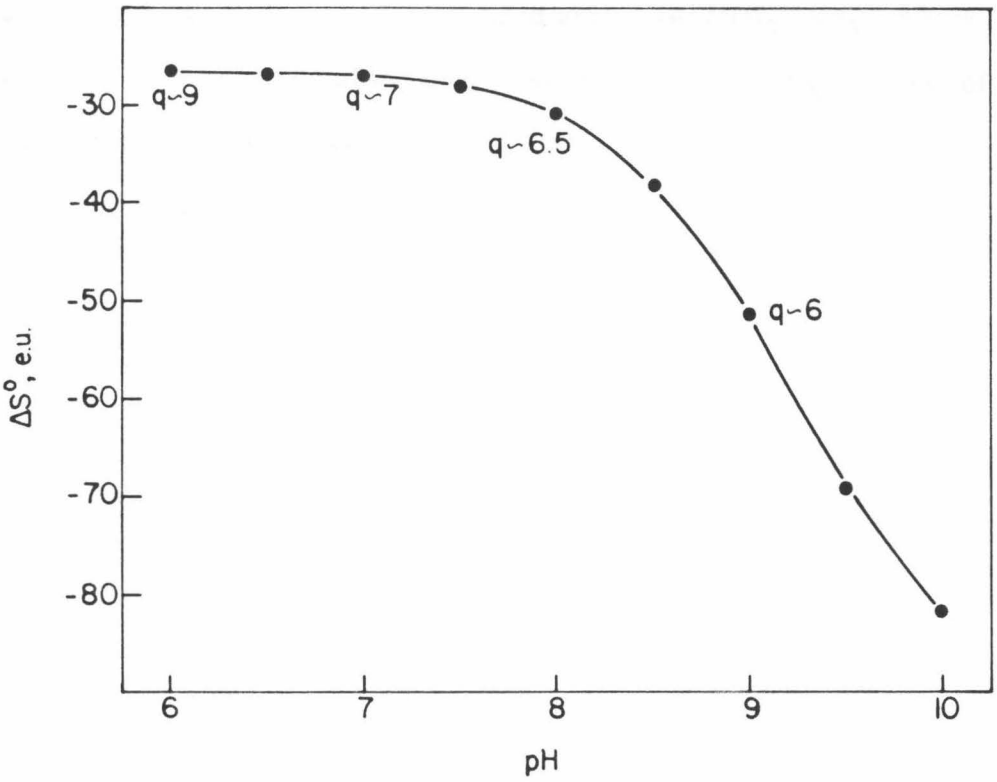
q~9
q~7
q~6.5
q~6
-30
-40
-50
-60
-70
-80
ΔS°, e.u.
6
7
8
9
10
pH

Figure 7. Thin-layer spectroelectrochemistry of native sperm whale myoglobin (pH 7.0, I = 0.1 M, phosphate buffer, 25 ^{o}C). Protein concentration: 8.3 x 10^{-4} M. Redox mediator: $[Ru(NH_3)_6]Cl_3$, 8.3 x 10^{-4} M. Overlay spectra and absorbance changes at different values of the applied potential in mV vs. NHE.

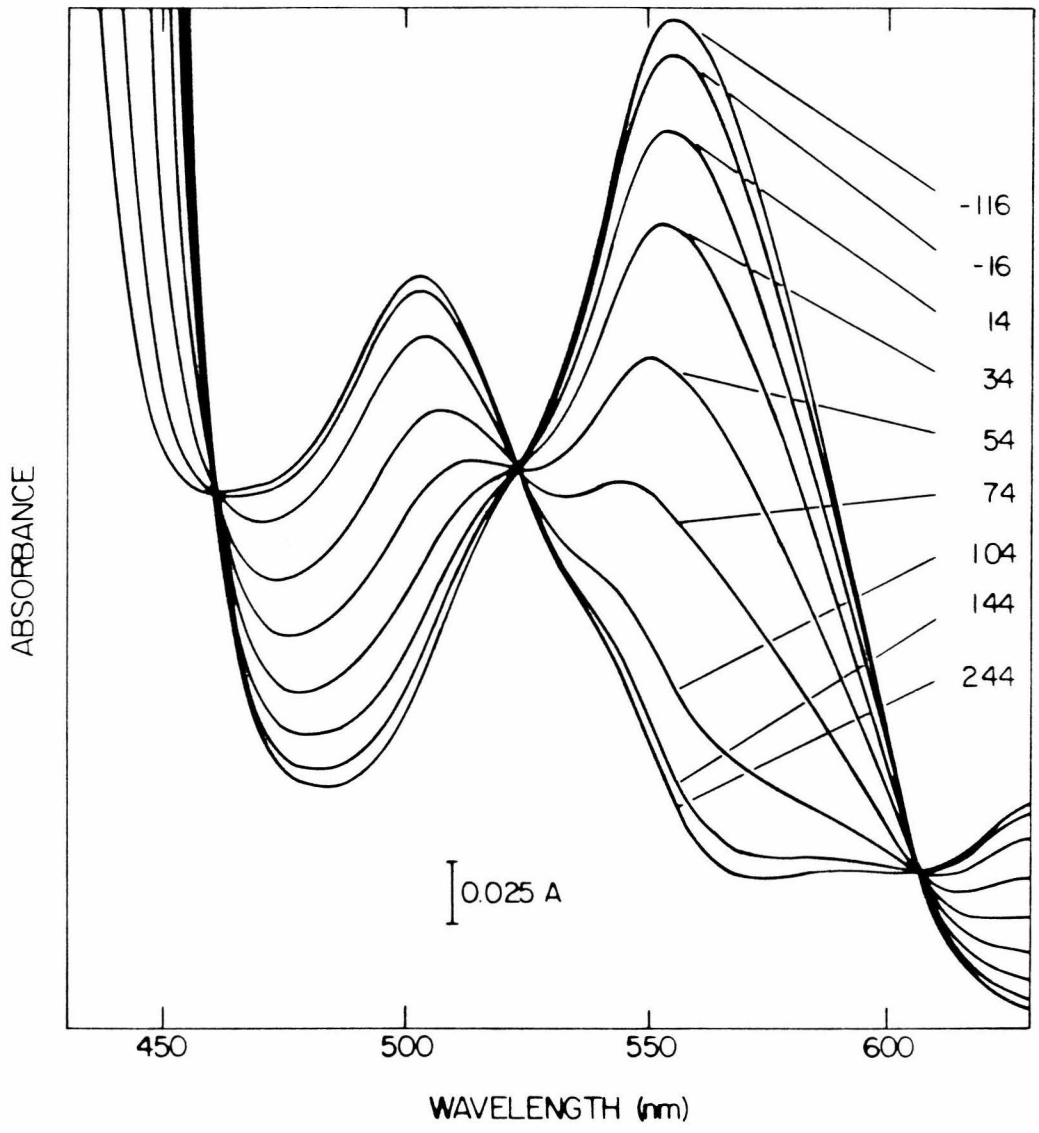
ABSORBANCE
-116
-16
14
34
54
74
104
144
244
0.025 A
450
500
550
600
WAVELENGTH (nm)

Figure 8. Nernst plot of the data in Figure 7. The solid line is a least-squares (58 mV slope) fit to the data at 556 nm.

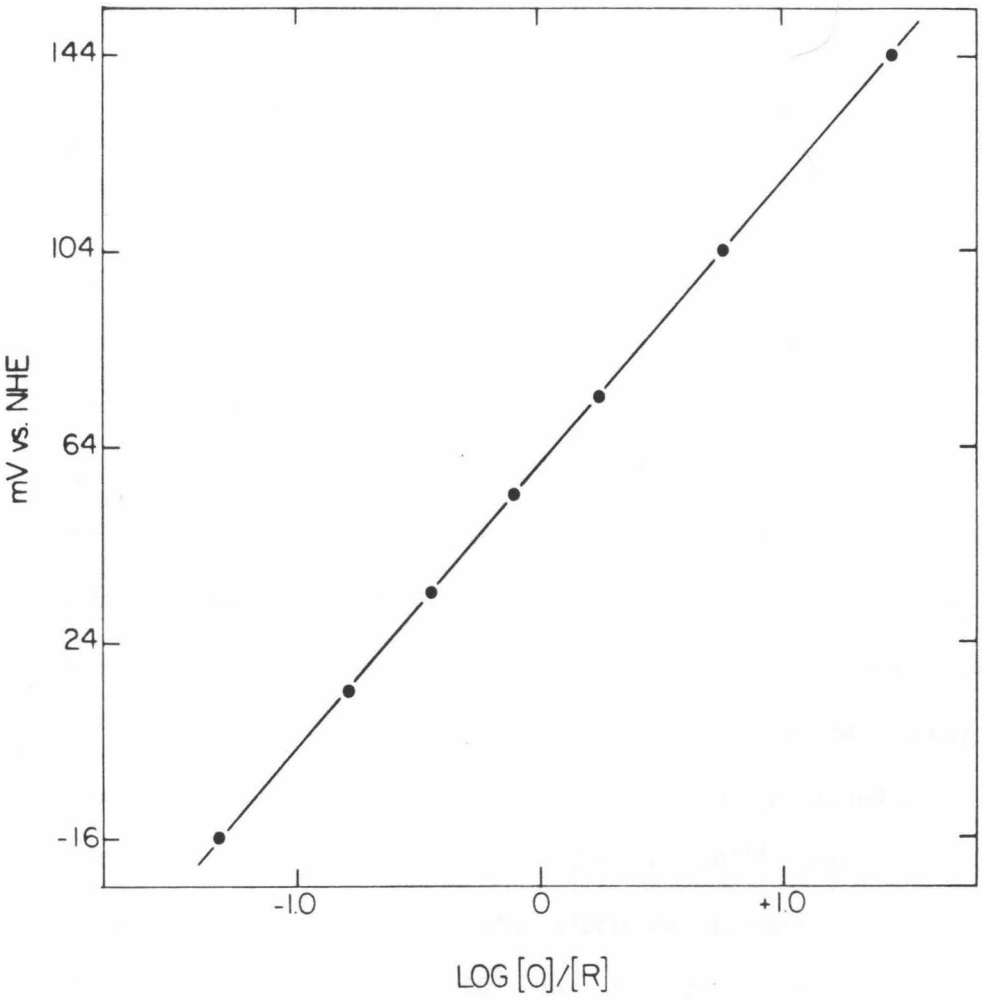
144
104
64
24
-16
mV vs. NHE
-1.0
0
+1.0
LOG [O]/[R]

The temperature dependence of the myoglobin reduction potential (after correction for the temperature dependence of the SCE) is displayed in Figure 9. The following redox thermodynamic parameters (25 ^{o}C) are derived from these experiments: $\Delta G^{o'}$ = -1.36 ± 0.05 kcal/mol, $\Delta H^{o'}$ = -13.0 ± 0.4 kcal/mol, and $\Delta S^{o'}$ = -39.2 ± 1.2 eu. These values should replace those derived from less precise data reported by Brunori et al. (41). Potentiometric results (pH 5.9, I = 0.25 M, Ref. 42) for horse heart myoglobin are in fair agreement with the present results: ΔG^{o} = -2.77 kcal/mol, ΔH^{o} = -14 kcal/mol, and ΔS^{o} = -38 eu. Loss of the axial H_2O should lead to a positive ΔS_{rc}^{o}. Thus, the observed negative ΔS_{rc}^{o} may reflect greater thermal motion for deoxymyoglobin than for metmyoglobin.

The change in molecular geometry upon reduction of the heme site is expected to result in high kinetic activation energies and hence slow electron transfer rates. Methyl viologen modified gold minigrid electrodes have been used to determine (43,44) heterogeneous electron transfer rate constants (pH 7.0 phosphate buffer, 0.1 M NaCl) via potential step chronoabsorptiometry for cytochrome c (0.6-1.0 x 10^{-5} cm/sec) and sperm whale myoglobin (3.9 x 10^{-11} cm/sec). (These proteins most likely interact with the electrode surface via the heme crevice.) This difference of ca. 10^{5} in rate points to a larger reorganizational energy for myoglobin. Experimental results yielding an estimate of the enthalpic component of the myoglobin reorganizational energy are presented in Chapter IV.

Rhodopseudomonas palustris cytochrome c′. The cytochromes c′ are mono- and diheme proteins found in denitrifying and photosynthetic

Figure 9. Temperature dependence of the formal reduction potential of sperm whale myoglobin (i.e., metmyoglobin→deoxymyoglobin). Conditions as in Figure 7. The data points have been corrected for the temperature dependence of the SCE, which was experimentally measured (5-50 ^{o}C) using a dual water-jacketed H-cell and two SCEs. One SCE was thermostatted at 25 ^{o}C. Each time the temperature of the second SCE was changed, approximately 4-8 hours was required for the potential measured across the two SCEs to stabilize (± 0.2 mV).

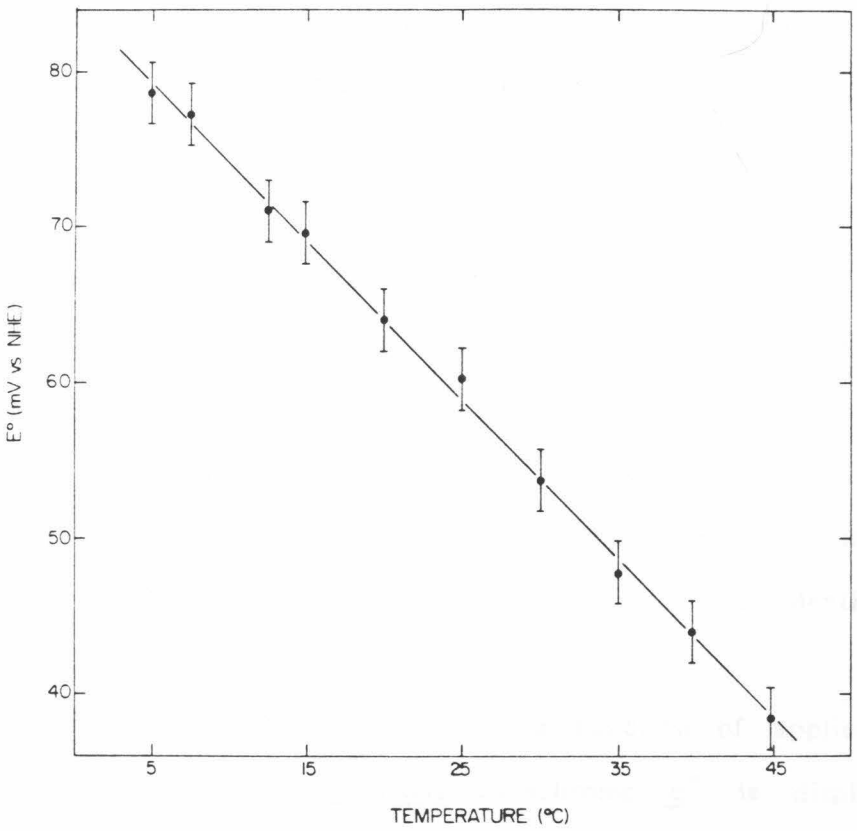
80
70
60
50
40
E° (mV vs NHE)
5
15
25
35
45
TEMPERATURE (°C)

bacteria, and comprise the largest class of bacterial cytochromes known (45-47). These proteins presumably function as electron carriers, although a precise cellular role has not yet been established. These proteins are similar to the low-spin cytochromes _c_ in their heme-binding sequence pattern (-Cys-X-Y-Cys-His-), but exhibit optical spectra resembling that of high-spin myoglobin. Ferricytochromes _c′_ are characterized by paramagnetic susceptibilities intermediate between those of high-spin and low-spin hemoproteins (48,49).

X-ray crystallographic studies (50-52) of _R. molischianum_ ferricytochrome _c′_, presently at 1.67Å resolution, have established earlier suggestions that the heme iron is pentacoordinate with a histidyl imidazole group providing the single axial ligand to the heme iron. A ribbon drawing of the monomer structure is given in Figure 10. (Note that dimeric _c′_ cytochromes consist of two identical subunits.)

A set of overlay absorption spectra as a function of applied potential for the monomeric _R. palustris_ cytochrome _c′_ is displayed in Figure 11, with the corresponding Nernst plot presented in Figure 12. The formal reduction potential (pH 7.0, 25 ^{o}C) determined from the Nernst plot is 88 ± 2 mV vs. NHE. The pH dependence of the reduction potential is displayed in Figure 13. A nonlinear least-squares fit of the data in this plot yields pK_{a1}^{ox} = 8.2 and pK_{a2}^{red} = 4.8, in fair agreement with Barakat and Strekas' values (53) of 8.0 and 5.4, respectively. Cytochrome _c′_, like cytochrome _c_, is observed to undergo an alkaline transition. Weber (54) has suggested, on the basis of

Figure 10. Ribbon Drawing (taken from Ref. 50) of the R. molischianum ferricytochrome c′ monomer. Note that the sixth coordination site of the heme iron is vacant. In contrast to cytochrome c, this protein is largely composed of four nearly parallel α-helices.

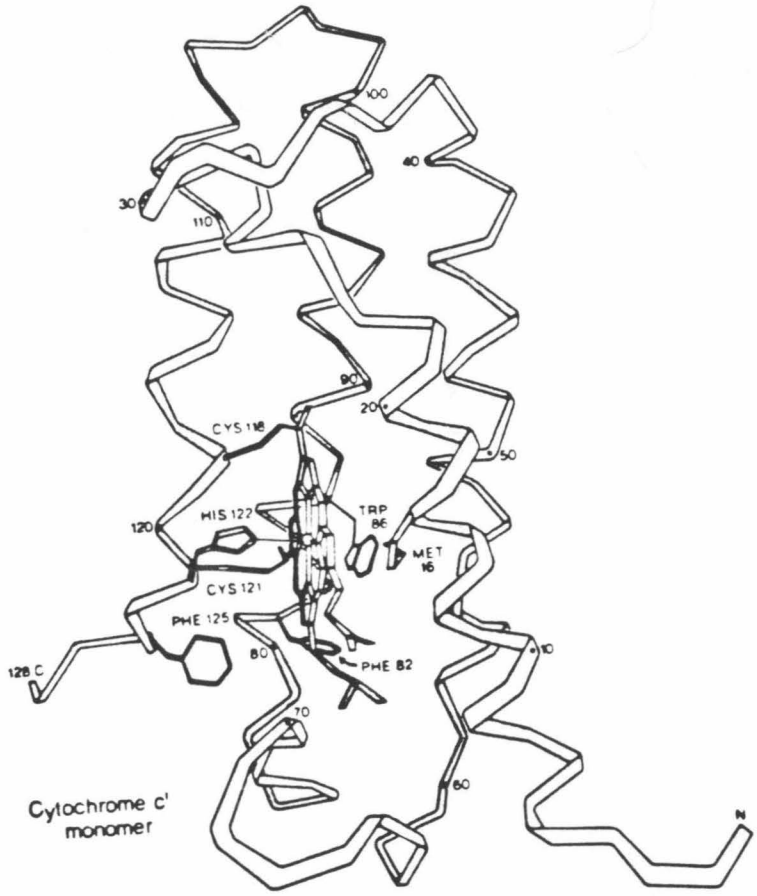
100
40
30
110
90
20
CYS 118
50
HIS 122
TRP 86
120
MET 16
CYS 121
PHE 125
80
PHE 82
10
128 C
70
60
N
Cytochrome c'
monomer

Figure 11. Thin-layer spectroelectrochemistry of R. palustris cytochrome c′ (0.13 mM), ionic strength 0.1 M, pH 7.0 phosphate buffer, 39.5 ^{o}C, 1.5 mM $[Ru(NH_3)_6]Cl_3$. Overlay spectra at different values of the applied potential in mV vs. SCE.

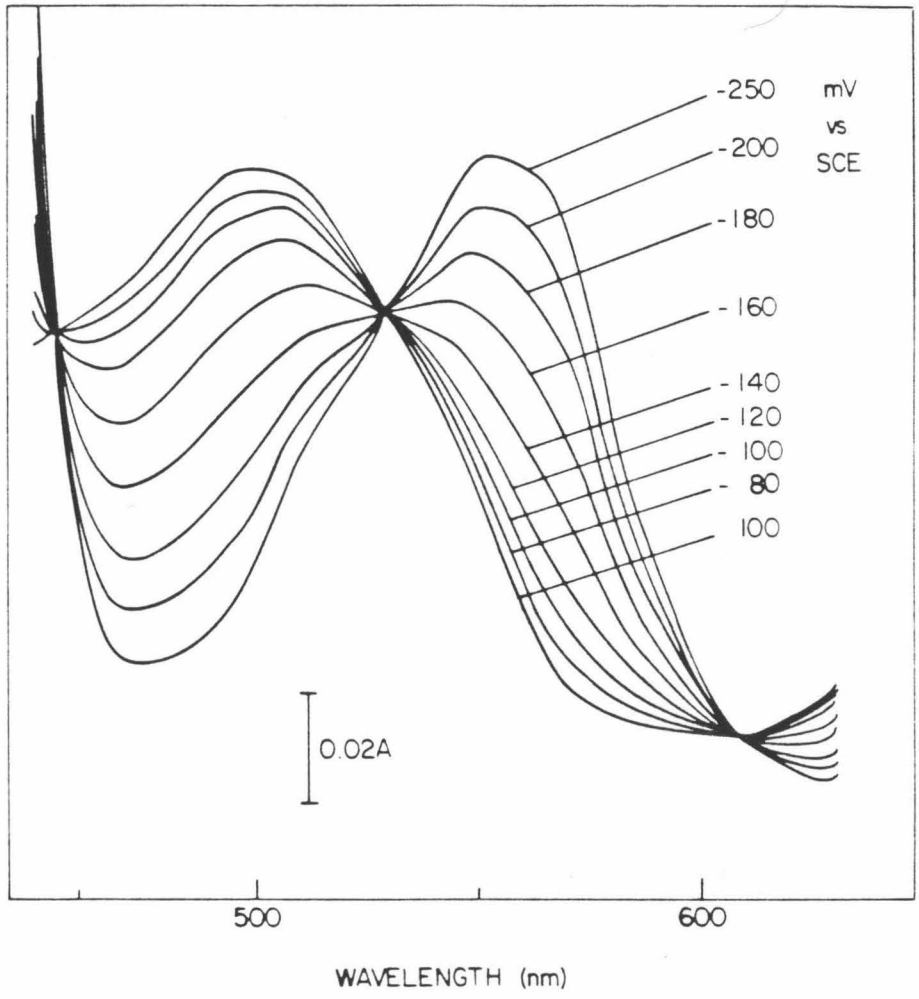
-250
-200
-180
-160
-140
-120
-100
-80
100
mV
vs
SCE
0.02A
500
600
WAVELENGTH (nm)

Figure 12. Nernst plot (59 mV slope) of the data in Figure 11 at 560 nm. $E^{0'}$ = 88 ± 2 mV vs. NHE.

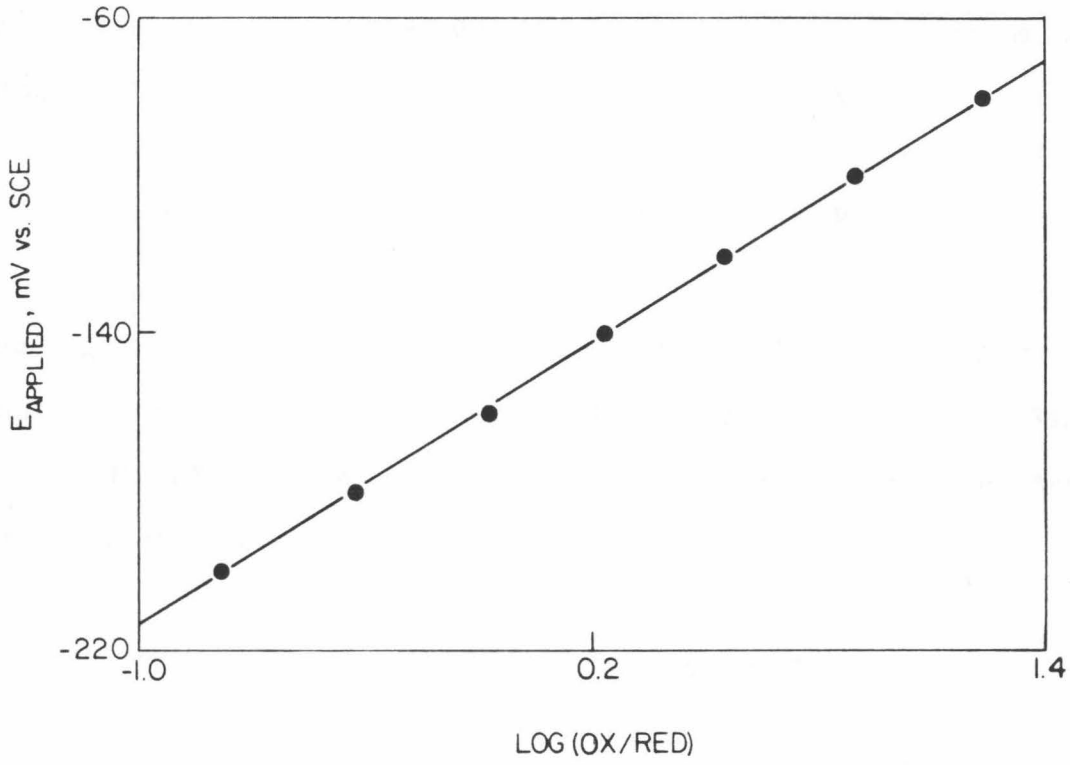
-60
-140
-220
$E_{APPLIED}$, mV vs. SCE
-1.0
0.2
1.4
LOG (OX/RED)

Figure 13. pH dependence of the formal reduction potential of R. palustris cytochrome c′ (I = 0.1 M, 25 °C). The solid line is a least-squares fit to the following equation:

$$E_m = E_o + 59\log\{([H^+]^2 + 10^{-pK_{a_2}^{red}}[H^+])/([H^+] + 10^{-pK_{a_1}^{ox}})\},$$

where E_m is the reduction potential at pH m and E_o is the reduction potential at unit proton concentration. From the best fit, E_o = 382 mV vs. NHE, pK_{a1}^{ox} = 8.2, and pK_{a2}^{red} = 4.8. The half-reactions that correspond to the three regions of the plot are as follows:

$$OxH^+ + H^+ + e^- \rightleftharpoons RedH_2^+$$

$$OxH^+ + e^- \rightleftharpoons RedH$$

$$Ox + H^+ + e^- \rightleftharpoons RedH$$

The pK_as quoted above correspond to different protonations; pK_{a1}^{red} > 11 and pK_{a2}^{ox} < 3.5. The following buffers were used: Na_2CO_3/NaOH (pH 10.65), glycine/NaOH (pH 10.0, 9.16), phosphate (pH 7.65, 7.0, 5.75), and acetate (pH 4.96, 3.97).

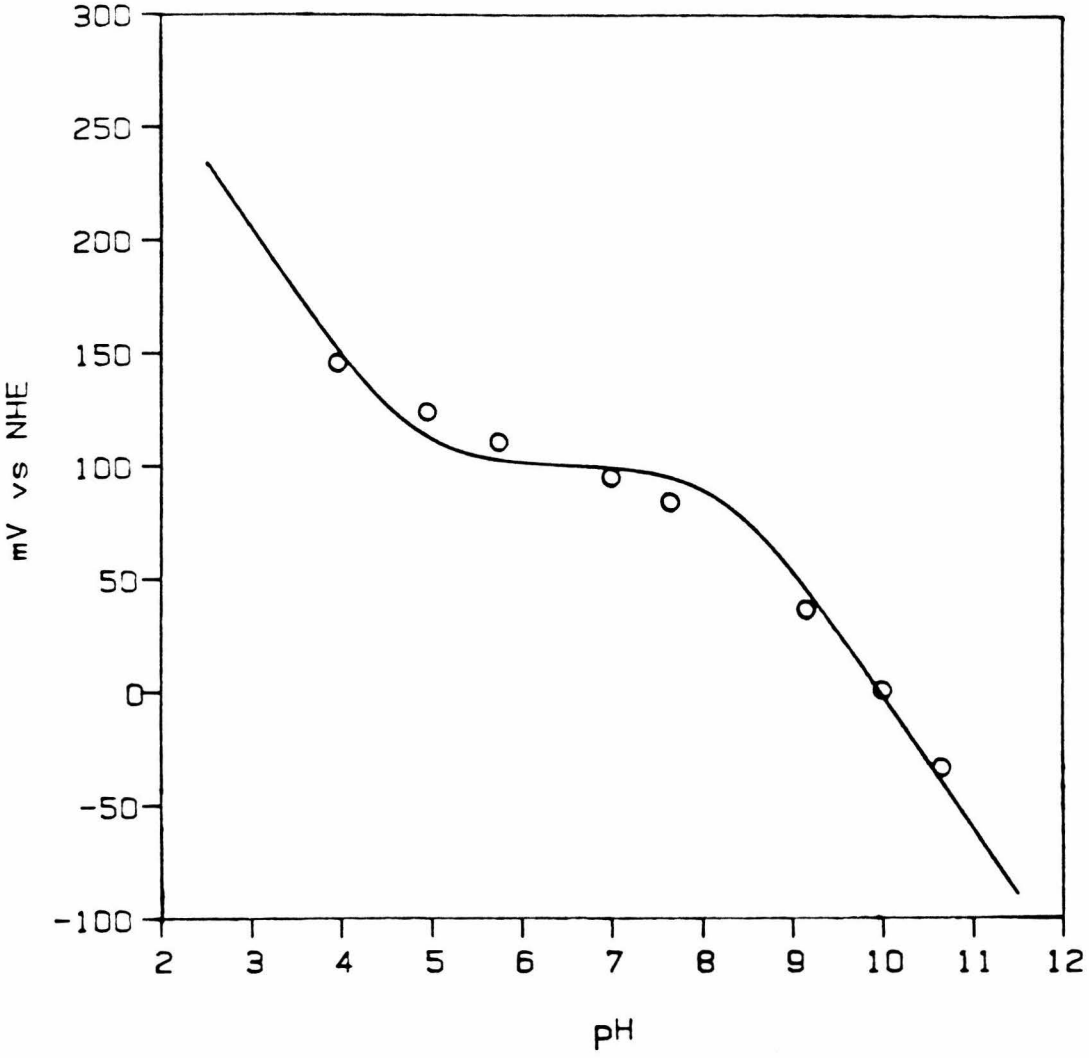
300
250
200
150
100
50
0
-50
-100
mV vs NHE
2
3
4
5
6
7
8
9
10
11
12
pH

spectroscopic data, that this transition involves deprotonation of the axial imidazole ligand, which would slightly strengthen the axial ligand field and result in an S = 5/2 spin state at high pH. More recent proton NMR results (55) confirm this proposal.

The temperature dependence (pH 7.0) of the cytochrome c′ reduction potential is displayed in Figure 14. The thermodynamic parameters (25 ^{o}C) derived from these experiments are as follows: $\Delta G^{o\prime}$ = -2.2 ± 0.5 kcal/mol, $\Delta H^{o\prime}$ = -9.3 ± 0.4 kcal/mol, and $\Delta S^{o\prime}$ = -23.7 ± 2 eu. The reaction entropies observed for the three hemoproteins discussed thus far are: cytochrome c′, -8.1 eu; cytochrome c, -12.9 eu; and myoglobin, -23.5 eu. These results suggest that cytochrome c′ should exhibit faster electron transfer rates than cytochrome c. A recent study (56) of the kinetics of electron transfer between cytochromes c′ and flavin semiquinones concluded that these cytochromes are ca. three times more reactive than mitochondrial cytochrome c. This reactivity difference was attributed to a greater solvent exposure of the heme in the c′-type cytochromes. Another interpretation of the data is that the cytochromes c′ exhibit somewhat lower reorganization energies. Verification of this suggestion must await structural details for ferrocytochrome c′ at high resolution.

Alcaligenes azurins. Azurins are small (14,000 dalton) water-soluble bacterial electron carriers that have been the subject of intensive structural and spectroscopic studies because of their distinctive properties (57-62). Particularly noteworthy are the intense absorption band (λ ~ 625 nm) responsible for the blue color of these proteins, an axial EPR spectrum with a very low hyperfine splitting

Figure 14. Temperature dependence of the formal potential of R. palustris cytochrome c′ using nonisothermal thin-layer spectroelectrochemistry (pH 7.0, I = 0.1 M phosphate buffer).

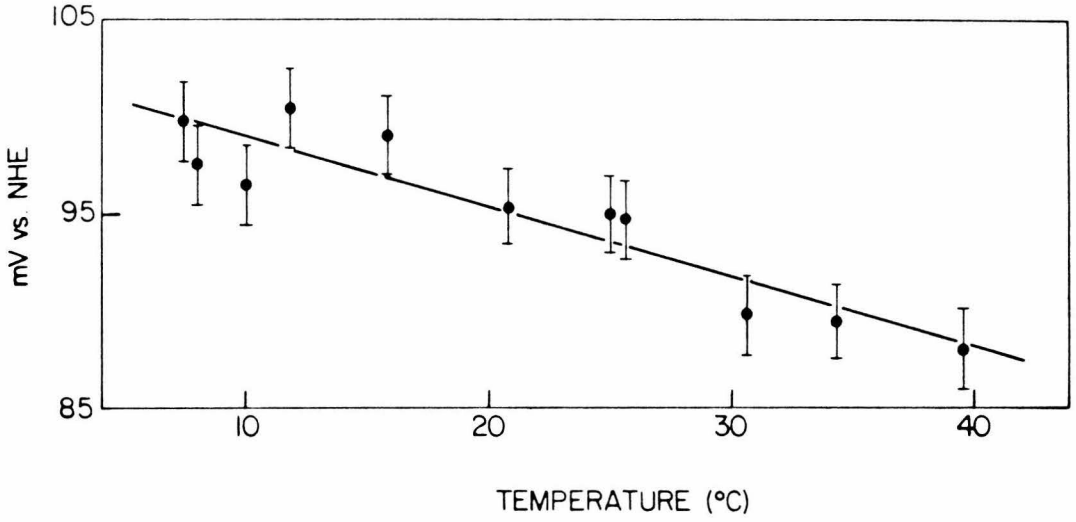
105
95
85
mV vs. NHE
10
20
30
40
TEMPERATURE (°C)

(A_{11} ~ 0.006 cm^{-1}), and a relatively high formal potential. Proper interpretation of spectral data has been hampered by the lack of low molecular weight models, and by the relative lack of structural information on the proteins themselves.

Medium-resolution crystallographic analyses (2.7Å and 2.5Å respectively) have been reported for P. aeruginosa (63) and A. denitrificans azurins (64). There are important sequence differences between the azurins (65). Differences are found in the resonance Raman spectra (66) of different azurins and there is also evidence for subtle functional differences. For example, a conformational transition proposed for P. aeruginosa azurin apparently does not occur for A. faecalis azurin (67), and sequence comparisons suggest that it may not occur in A. denitrificans azurin either (58).

The X-ray structure of Alcaligenes denitrificans azurin has been recently refined to 1.8Å resolution (68). The copper site in this azurin is best described in terms of a three-coordinate, distorted trigonal planar geometry, with two additional, much more weakly interacting groups in axial positions, completing an axially-elongated trigonal bipyramid. The three in-plane, strongly-bound ligands are the thiolate sulfur of Cys-112 (2.12Å bond length), and the imidazole nitrogens of His-117 and His-46 (1.98Å and 2.04Å bond lengths). The copper atom lies very close to the N_2S plane. These bond distances are consistent with those derived for P. aeruginosa azurin. Much longer approaches are made to the thioether sulfur of Met-121 on one side of the trigonal plane (3.11Å Cu-S distance) and to the main chain carbonyl oxygen of Gly-45 on the other side (3.12Å Cu-O distance). At

best these can only be described as weak interactions.

The copper site in azurin differs from that determined crystallographically for poplar plastocyanin (69) in that although the three strong bonds, to the Cys and two His ligands, are essentially the same, the axial interactions are different. The Cu-S(Met) distance is 0.2Å longer in azurin, and plastocyanin has no equivalent Cu-O interaction (the distance in plastocyanin is 3.8Å). These structural differences are of relevance to the reduction potentials of these proteins.

A typical Nernst plot for A. denitrificans azurin is shown in Figure 15. The plot exhibits a 62 mV Nernst slope and yields $E^{0'}$ = 276 mV vs. NHE. The temperature dependence of the formal reduction potential is displayed in Figure 16. The redox thermodynamic quantities resulting from these data are as follows: $\Delta G^{0'}$ = -6.37 ± 0.05 kcal/mol, $\Delta H^{0'}$ = -13.3 ± 0.4 kcal/mol, and $\Delta S^{0'}$ = -23.2 ± 1.2 eu. These values are not unlike those reported for P. aeruginosa azurin (70). The large negative entropy change accompanying the reduction of azurin has been attributed to an increase in the ordering of water molecules in the vicinity of the copper (71). We note, however, that there are no internal water molecules in the azurin structure, and a more likely explanation is an increased interaction of the Cu(I) atom with the thioether sulfur of Met-121, leading to a tightening up of the copper site structure (though this could conceivably also affect water molecules bound to the molecular exterior, more distant from the copper atom). The negative value for $\Delta H^{0'}$ may also signify increased Cu-S(Met) interaction.

Figure 15. Nernst plot of absorbance changes at 625 nm during a spectroelectrochemical titration of A. denitrificans azurin. The best fit to the data (solid line) yields n = 1.05 and $E^{0\prime}$ = 276 mV vs. NHE. Conditions: 25 ^{o}C, pH 7.0, I = 0.1 M phosphate buffer, 1 equivalent $[Ru(NH_3)_5py](ClO_4)_3$.

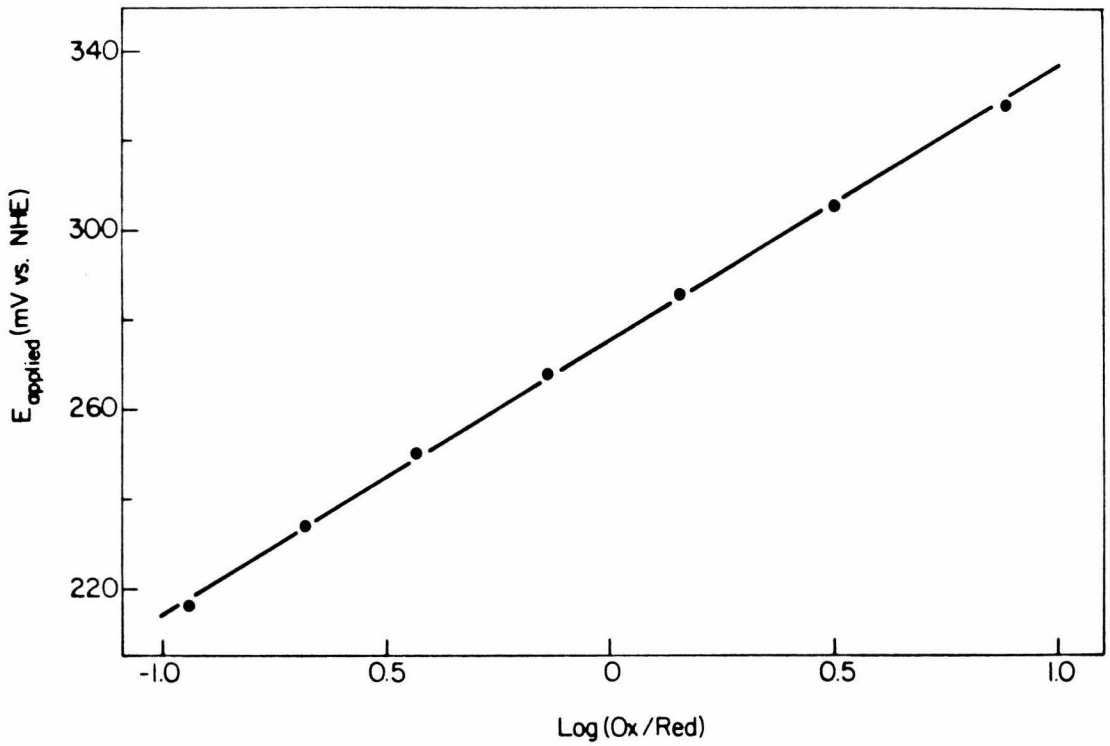
340
300
260
220
$E_{applied}$ (mV vs. NHE)
-1.0
0.5
0
0.5
1.0
Log (Ox / Red)

Figure 16. Temperature dependence of the formal potential of A. denitrificans azurin using nonisothermal thin-layer spectroelectrochemistry. Conditions as in Figure 15.

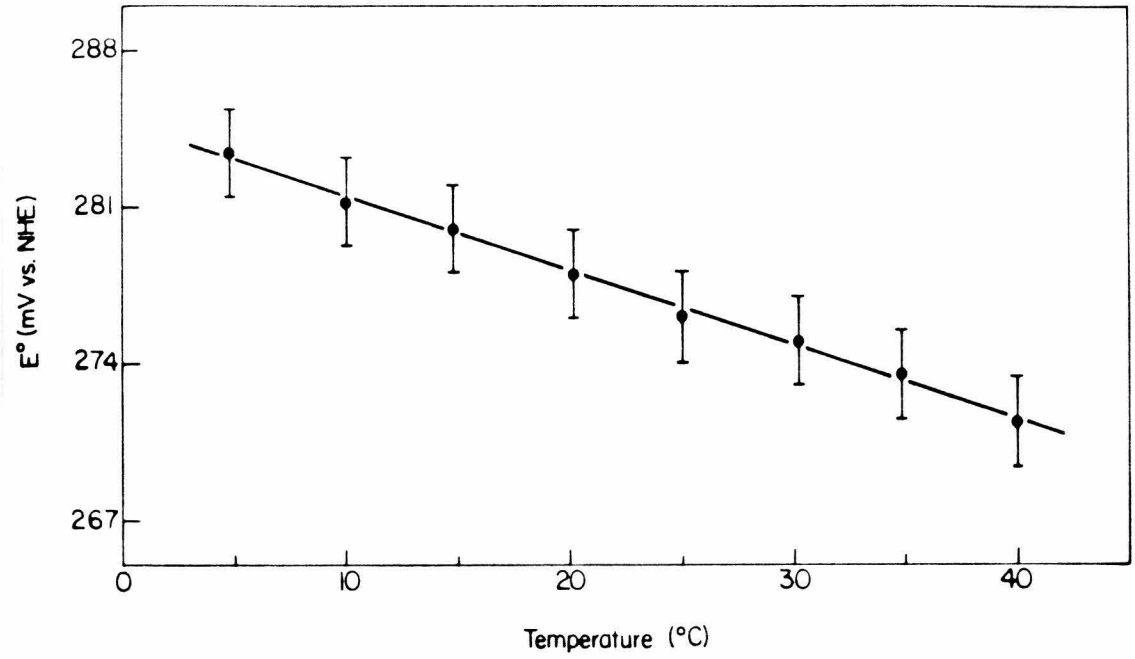
288
281
274
267
E° (mV vs. NHE)
0
10
20
30
40
Temperature (°C)

pH dependences of reduction potentials have been reported for the azurins from P. aeruginosa (72,73) and A. faecalis (73). In both cases a sigmoidal plot is observed (similar in shape to Figure 2 of Chapter I) with pK_a^{ox} ~ 6.0 and pK_a^{red} ~ 7.6. A classical pH titration (74) carried out on the reduced and oxidized forms of both proteins indicates that two protons are released between pH 6 and pH 8; in both cases the potentiometric data indicate that only one of these protonations affects E^o. Figure 17 illustrates a square scheme that accounts for the pH-dependent behavior of azurins. Thus, azurin becomes half protonated upon reduction at pH 7.6.

Due to a lack of protein, a pH study of the A. d. azurin formal potential was not feasible. Instead, ΔS^o for A. faecalis azurin was determined from a series of nonisothermal measurements of E^o at three pH values. The results of these experiments are plotted in Figure 18 and are easily rationalized by noting that proton uptake by reduced azurin should result in a larger (here, 5 eu) entropy decrease at pH 7.0 than at pH 5.0 (where both forms are protonated) or at pH 8.5 (where both forms are deprotonated). All of the present azurin results are collected in Table I, together with previously reported data for other single-site "blue" proteins for comparison. The extent of any structural change at the Cu(I) site upon protonation is not known, since a crystal structure for reduced azurin is not yet available. The pH dependence of ΔS^o for A. faecalis azurin suggests that any structural change upon proton uptake by the reduced protein will be minimal at the copper site. Plastocyanin offers an example of the opposite behavior: the reduction potential increases below ca. pH 5.5

Figure 17. Thermodynamic scheme to account for pH-dependent formal reduction potentials of azurins.

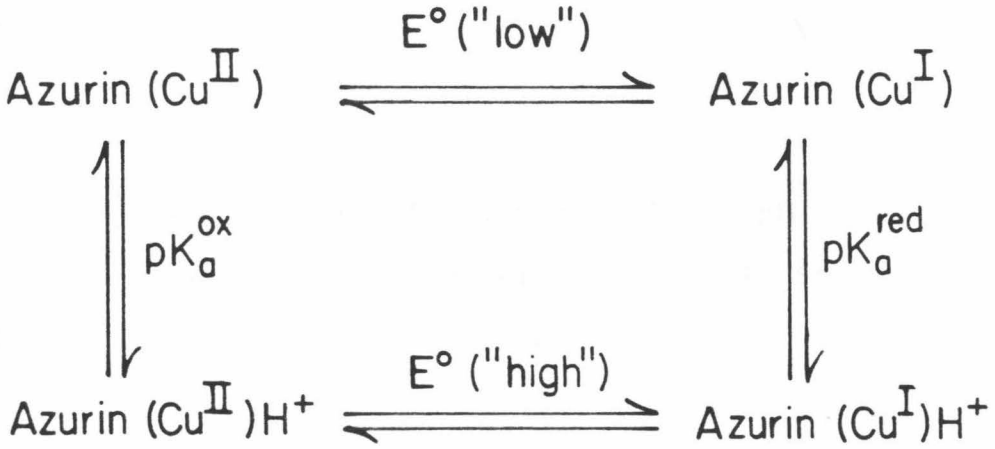
E° ("low")
Azurin (Cu^{II})
Azurin (Cu^{I})
pK_a^{ox}
pK_a^{red}
E° ("high")
Azurin (Cu^{II})H^+
Azurin (Cu^{I})H^+

Figure 18. Temperature dependences of the formal reduction potential of A. faecalis azurin at three pH values selected to span a proton-transfer transition defined by pK_a^{ox} ~ 6.0 and pK_a^{red} ~ 7.6. Proton uptake by reduced azurin at pH 7.0 is observed to contribute to ΔS^o. Solution conditions: I = 0.1 M phosphate (pH 8.5, pH 7.0) or acetate (pH 5.0), 1 equivalent $[Ru(NH_3)_5py](ClO_4)_3$. At pH 5.0, 1 equivalent $[Co(phen)_3](ClO_4)_3$ was also present in solution.

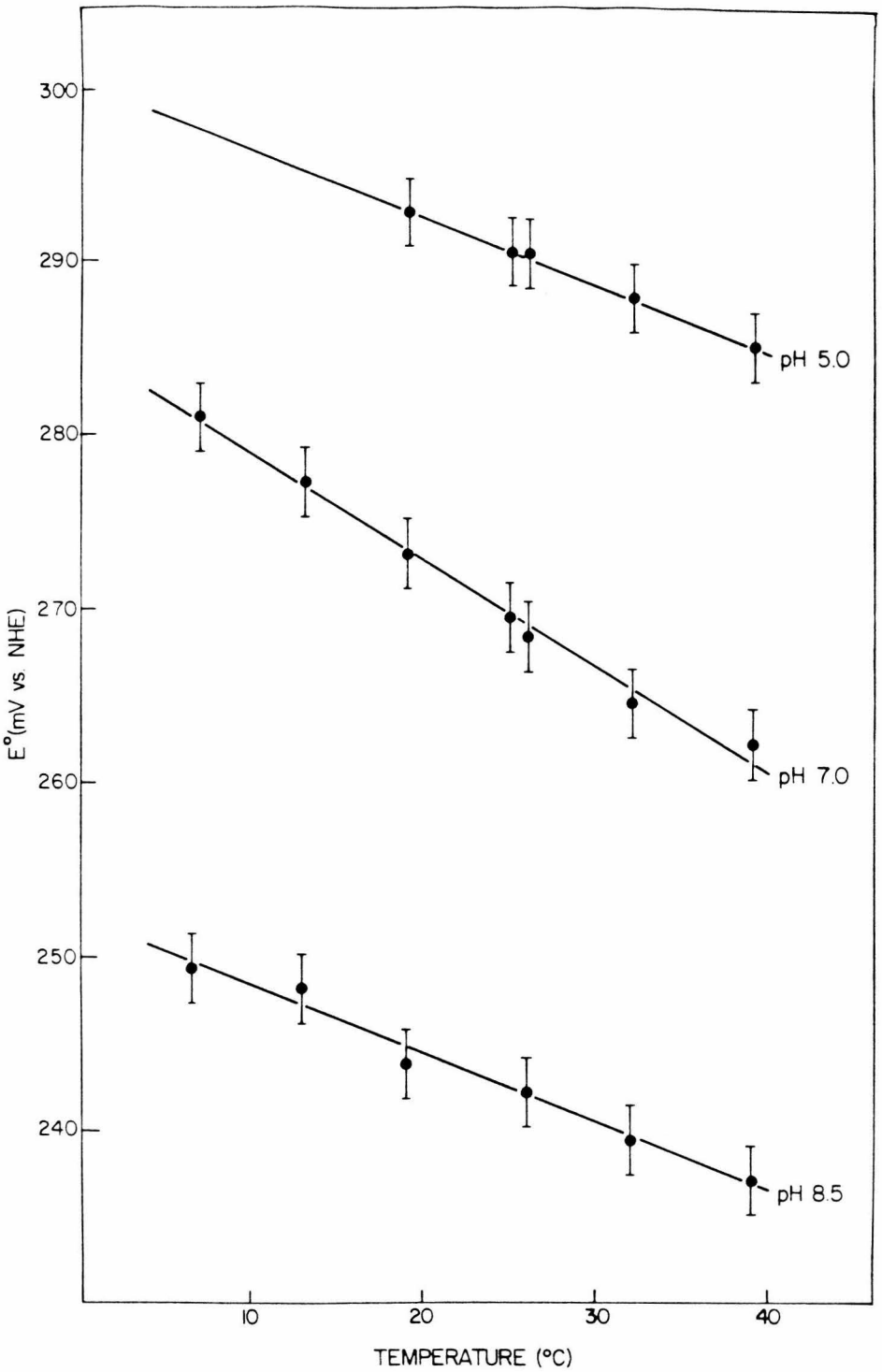
300
290
280
270
260
250
240
E°(mV vs. NHE)
pH 5.0
pH 7.0
pH 8.5
10
20
30
40
TEMPERATURE (°C)

Table I. Thermodynamic parameters for single-site "blue" copper proteins.

Protein	E^o(mV vs. NHE)[a]	ΔS^o(eu)	ΔH^o(kcal/mol)
Azurin (P. aeruginosa)[b,e]	308 ± 2	-31.7 ± 1.2	-16.6 ± 0.4
Azurin (A. denitrificans)[b]	276 ± 2	-23.2 ± 1.2	-13.3 ± 0.4
Azurin (A. faecalis)[b]	270 ± 2	-29.6 ± 1.2	-15.0 ± 0.4
Azurin (A. faecalis)[c]	291 ± 2	-24.6 ± 1.2	-14.0 ± 0.4
Azurin (A. faecalis)[d]	243 ± 2	-24.6 ± 1.2	-12.9 ± 0.4
Plastocyanin (P. vulgaris)[b,e]	360 ± 2	-18.0 ± 1.2	-13.7 ± 0.4
Stellacyanin (R. vernicifera)[b,e]	191 ± 2	-19.8 ± 1.2	-10.3 ± 0.4

[a]At 25 °C. All thermodynamic parameters are referenced to the NHE.

[b]Phosphate buffer, pH 7.0, ionic strength 0.1 M.

[c]Acetate buffer, pH 5.0, ionic strength 0.1 M.

[d]Phosphate buffer, pH 8.5, ionic strength 0.1 M.

[e]Reference 69.

protonation of His-87, which results in dissociation of this ligand from the copper center in the reduced (but not the oxidized) protein (75).

With the exception of the P. aeruginosa protein, azurins have $E^{o'}$ values in the range 230 to 280 mV, with that of A. denitrificans azurin at the upper end of the group. P. a. azurin appears to be atypical in that it has been shown to undergo a pH-dependent conformational change (76), which proton NMR studies suggest is linked to the deprotonation of His-35 (77-79).

Comparison of A. d. azurin with plastocyanin offers an important insight into the relationship between structure and reduction potential. The E^o value for the former is substantially lower than that of plastocyanin (by 80-100 mV). At the same time, the crystal structures show that in azurin the axial Cu-S(Met) bond is 0.2Å longer than in poplar plastocyanin, and there is a carbonyl oxygen 3.1Å from the copper, compared with 3.8Å in plastocyanin. Both these changes should produce a more Cu(II)-like copper site and a lower E^o value, as is observed. Thus, it is likely that variation in these axial groups tunes the redox potential, while the interaction with the copper atom with its three strongly-bound ligands (one Cys and two His) remains essentially constant. Further, stellacyanin (E^o = 184 mV) contains no methionine and appears to possess the same three basic ligands as azurin and plastocyanin (60). There are suggestions (80) that a disulfide sulfur may substitute for methionine. It is a logical extension of the azurin and plastocyanin structures and E^o values to suggest that stellacyanin, like azurin, may have a peptide carbonyl

oxygen making a relatively close axial approach to copper, and the lower E^o value of stellacyanin may arise from slightly stronger Cu-O interaction, and slightly weaker Cu-S(disulfide) interaction in the other axial position. This ultimately should be tested by crystallographic analysis, but it is interesting to note (a) that NMR studies on Cd(II)-substituted proteins indicate that the azurin and stellacyanin spectra are very similar, but different from plastocyanin, in a manner that suggests a higher coordination number in the former two proteins (81), and (b) the resonance Raman spectrum of stellacyanin contains a prominent feature at 1233 cm^{-1} which suggests resonance enhancement of a peptide mode, consistent with backbone peptide carbonyl coordination (66).

REFERENCES

1. Adman, E.T. (1979) *Biochim. Biophys. Acta* **549**, 107.

2. Vallee, B.L., and Williams, R.J.P. (1968) *Proc. Natl. Acad. Sci. U.S.A.* **59**, 498.

3. Gray, H.B., and Malmström, B.G. (1983) *Comments Inorg. Chem.* **2**, 203.

4. Ibers, J.A., and Holm, R.H. (1980) *Science* **209**, 223.

5. Lippard, S.J. (1986) *Chem. Brit.* **22**, 222.

6. Mayo, S.L., Ellis, W.R., Jr., Crutchley, R.J., and Gray, H.B. *Science*, accepted for publication.

7. Brautigan, D.L., Ferguson-Miller, S., and Margoliash, E. (1978) *Meth. Enzymol.* **53**, 128.

8. Cummins, D., and Gray, H.B. (1977) *J. Amer. Chem. Soc.* **99**, 5158.

9. Pladziewicz, J.R., Meyer, T.J., Broomhead, S.A., and Taube, H. (1973) *Inorg. Chem.* **12**, 639.

10. Schilt, A.A., and Taylor, R.C. (1959) *J. Inorg. Nucl. Chem.* **9**, 211.

11. Moore, G.R., Eley, C.G.S., and Williams, R.J.P. (1984) *Adv. Inorg. Bioinorg. Mech.* **3**, 1.

12. Williams, G., Moore, G.R., and Williams, R.J.P. (1985) *Comments Inorg. Chem.* **4**, 55.

13. Timkovich, R. (1979) in *The Porphyrins, Vol. VII*, Dolphin, D., ed., Academic Press, N.Y., p. 241.

14. Ferguson-Miller, S., Brautigan, D.L., and Margoliash, E. (1979) in *The Porphyrins, Vol. VII*, Dolphin, D., ed., Academic Press, N.Y., p. 149.

15. Dickerson, R.E. (1980) *Sci. Amer.* **242**, 99.

16. Takano, T., and Dickerson, R.E. (1981) *J. Mol. Biol.* **153**, 95.

17. Takano, T., and Dickerson, R.E. (1980) *Proc. Natl. Acad. Sci. U.S.A.* 77, 6371.

18. Weber, P.C., and Tollin, G. (1985) *J. Biol. Chem.* **260**, 5568.

19. Salemme, F.R. (1976) *J. Mol. Biol.* **102**, 563.

20. Poulos, T.L., and Kraut, J. (1980) *J. Biol. Chem.* **255**, 10322.

21. Taniguchi, V.T., Ellis, W.R., Jr., Cammarata, V., Webb, J., Anson, F.C., and

Gray, H.B. (1982) in *Electrochemical and Spectrochemical Studies of Biological Redox Components*, Kadish, K.M., ed., Amer. Chem. Soc., Washington, D.C., p. 51.

22. Margalit, R., and Schejter, A. (1970) *FEBS Lett.* **6**, 278.

23. Rodkey, F.K., and Ball, E.G. (1950) *J. Biol. Chem.* **182**, 17.

24. Watt, G.D., and Sturtevant, J.M. (1969) *Biochemistry* **8**, 4567.

25. George, P., Eaton, W.A., and Trachtman, M. (1968) *Fed. Proc.* **27**, 526.

26. Horn, D., and Heuck, C.-C. (1983) *J. Biol. Chem.* **258**, 1665.

27. Smith, H.T., Staudenmayer, N., and Millett, F. (1977) *Biochemistry* **16**, 4971.

28. Margalit, R., and Schejter, A. (1973) *Eur. J. Biochem.* **32**, 492; 500.

29. Anderson, T., Thulin, E., and Forsén, S. (1979) *Biochemistry* **18**, 2487.

30. Osherhoff, N., Brautigan, D.L., and Margoliash, E. (1980) *Proc. Natl. Acad. Sci. U.S.A.* **77**, 4439.

31. Yocom, K.M., Winkler, J.R., Nocera, D.G., Bordignon, E., and Gray, H.B. (1983) *Chem. Scr.* **21**, 29.

32. Wooten, J.B., Cohen, J.S., Vig, I., and Schejter, A. (1981) *Biochemistry* **20**, 5394.

33. Moore, G.R., and Williams, R.J.P. (1980) *Eur. J. Biochem.* **103**, 513.

34. Bosshard, H.R. (1981) *J. Mol. Biol.* **153**, 1125.

35. Sutin, N., Weaver, M.J., and Yee, E.L. (1980) *Inorg. Chem.* **19**, 1098.

36. Crutchley, R.J., Ellis. W.R., Jr., and Gray, H.B. (1986) in *Frontiers in Bioinorganic Chemistry*, Xavier, A.V., ed., VCH Verlagsgesellschaft, Weinheim, F.R.G., p. 679.

37. Scheidt, W.R., and Reed, C.A. (1981) *Chem. Rev.* **81**, 543.

38. Takano, T. (1977) *J. Mol. Biol.* **110**, 537.

39. Takano, T. (1977) *J. Mol. Biol.* **110**, 569.

40. Pauling, L. (1949) in *Haemoglobin*, Roughton, F.J.W., and Kendrew, J.C., eds., Butterworths, London, p. 57.

41. Brunori, M., Saggese, U., Rotilio, G.C., Antonini, E., and Wyman, J. (1971) *Biochemistry* **10**, 1605.

42. George, P., Hanania, G.I.H., and Eaton, W.A. (1966) in *Hemes and Hemoproteins*, Chance, B., ed., Academic Press, N.Y., p. 267.

43. Bowden, E.F., Hawkridge, F.M., and Blount, H.N. (1980) *J. Electroanal. Chem.* **116**, 447.

44. Bancroft, E.E., Blount, H.N., and Hawkridge, F.M. (1982) in *Electrochemical and Spectrochemical Studies of Biological Redox Components*, Kadish, K.M., ed., Amer. Chem. Soc., Washington, D.C., p. 23.

45. Bartsch, R.G. (1978) in *The Photosynthetic Bacteria*, Clayton, R.K., and Sistrom, W.W., eds., Plenum Press, N.Y., p. 249.

46. Meyer, T.E., and Kamen, M.D. (1982) *Adv. Prot. Chem.* **35**, 105.

47. Mathews, F.S. (1985) *Prog. Biophys. Molec. Biol.* **45**, 1.

48. Maltempo, M.M. (1976) *Quart. Revs. Biophys.* **9**, 181.

49. Maltempo. M.M., Moss, T.H., and Spartalian, K. (1980) *J. Chem. Phys.* 73, 2100.

50. Weber, P.C., Howard, A., Xuong, N.H., and Salemme, F.R. (1981) *J. Mol. Biol.* **153**, 399.

51. Weber, P.C., Salemme, F.R., Mathews, F.S., and Bethge, P.H. (1981) *J. Biol. Chem.* **256**, 7702.

52. Finzel, B.C., Weber, P.C., Hardman, K.D., and Salemme, F.R. (1985) *J. Mol. Biol.* **186**, 627.

53. Barakat, R., and Strekas, T.C. (1982) *Biochim. Biophys. Acta* **679**, 393.

54. Weber, P.C. (1982) *Biochemistry* **21**, 5116.

55. Jackson, J.T., LaMar, G.N., and Bartsch, R.G. (1983) *J. Biol. Chem.* **258**, 1799.

56. Meyer, T.E., Cheddar, G., Bartsch, R.G., Getzoff, E.D., Cusanovich, M.A., and Tollin G. (1986) *Biochemistry* **25**, 1383.

57. Fee, J.A. (1975) *Struct. Bonding* **23**, 1.

58. Adman, E.T. (1985) in *Metalloproteins, Part I*, Harrison, P.M., ed., Macmillan Press, London, p.1.

59. Farver, O., and Pecht, I. (1984) in *Copper Proteins and Copper Enzymes, Vol. I*, Lontie, R., ed., CRC Press, Boca Raton, Fla., p. 183.

60. Lappin, A.G. (1981) *Met. Ions Biol. Syst.* **13**, 15.

61. Gray, H.B., and Solomon, E.I. (1981) in *Copper Proteins*, Spiro, T.G., ed., Wiley, N.Y., p. 1.

62. Gray, H.B. (1986) *Chem. Soc. Rev.* **15**, 17.

63. Adman, E.T., and Jensen, L.H. (1981) *Isr. J. Chem.* **21**, 8.

64. Norris, G.E., Anderson, B.F., and Baker, E.N. (1983) *J. Mol. Biol.* **165**, 501.

65. Ambler, R.P. (1971) in *Recent Developments in the Chemical Studies of Protein Structures*, Previero, A., Pechere, J.-F., and Previero, C., eds., Inserm, Paris, p. 289.

66. Blair, D.F., Campbell, G.W., Schoonover, J.R., Chan, S.I., Gray, H.B., Malmström, B.G., Pecht, I., Swanson, B.I., Woodruff, W.H., Cho, W.K., English, A.M., Fry, H.A., Lum. V., and Norton, K.A. (1985) *J. Am. Chem. Soc.* **107**, 5755.

67. Rosen, P., Segal, M., and Pecht, I. (1981) *Eur. J. Biochem.* **120**, 339.

68. Norris, G.E., Anderson, B.F., and Baker, E.N. *J. Am. Chem. Soc.*, in press.

69. Guss, J.M., and Freeman, H.C. (1983) *J. Mol. Biol.* **169**, 521.

70. Taniguchi, V.T., Sailasuta-Scott, N., Anson, F.C., and Gray, H.B. (1980) *Pure & Appl. Chem.* **52**, 2275.

71. Sailasuta, N., Anson, F.C., and Gray, H.B. (1979) *J. Am. Chem. Soc.* **101**, 455.

72. Lappin, A.G., Segal, M.G., Weatherburn, D.C., Henderson, R.A., and Sykes, A.G. (1979) *J. Am. Chem. Soc.* **101**, 2302.

73. Corin, A.F. (1981) Ph.D. Thesis, Columbia University.

74. Corin, A.F., Bersohn, R., and Cole, P.E. (1983) *Biochemistry* **22**, 2032.

75. Guss, J.M., Harrowell, P.R., Murata, M., Norris, V.A., and Freeman H.C. *J. Mol. Biol.*, submitted for publication.

76. Rosen, P., and Pecht, I. (1976) *Biochemistry* **15**, 775.

77. Mitra, S., and Bersohn, R. (1982) *Proc. Natl. Acad. Sci. U.S.A.* **79**, 6807.

78. Adman, E.T., Canters, G.W., Hill, H.A.O., and Kitchen, N.A. (1982) *FEBS Lett.* **143**, 287.

79. Canters, G.W., Hill, H.A.O., Kitchen, N.A., and Adman, E.T. (1984) *Eur. J. Biochem.* **138**, 141.

80. McMillin, D.R., and Morris, M.C. (1981) *Proc. Natl. Acad. Sci. U.S.A.* **78**, 6567.

81. Engeseth, H.R., McMillan, D.R., and Otvos, J.D. (1984) *J. Biol. Chem.* **259**, 4822.

CHAPTER IV

FORMAL REDUCTION POTENTIALS OF COUPLES IN MULTISITE METALLOPROTEINS

INTRODUCTION

An intriguing reason for studying multisite metalloproteins (and polynuclear transition metal complexes) is the posibility that the chemical reactivity associated with a metal center is significantly altered due to the presence of two or more metal ions per molecule. Such a possibility becomes especially interesting if reactivity changes are not simply additive. Most of the presently known redox metalloenzymes (e.g., cytochrome c oxidase, nitrogenase) typically contain, in addition to a substrate binding site consisting of one or more redox-active metal ions, additional redox cofactors that function as intramolecular electron transfer agents. The presence of multiple redox centers in enzymes catalyzing reactions requiring two or more electrons in proceeding from reactants to products may prevent the formation of radical substrate intermediates that would be produced by single electron-transfer. Thus, protein-bound, multi-metal redox centers might be particularly advantageous in the reactions of small molecules such as dioxygen or dinitrogen.

It is therefore important to carefully examine the electrochemical behavior of metalloproteins containing several electroactive sites as a means of determining reactivity differences between mononuclear and polynuclear metalloprotein systems. Molecules containing a number of identical, noninteracting redox centers are expected to exhibit Nernst slopes identical to those for the corresponding molecule containing a single center even though more than one electron is transferred in the overall reaction (1,2). Only the magnitude of the current is enhanced by the presence of more than one electroactive center and hence

coulometry must be used to distinguish between mononuclear and the corresponding polynuclear systems containing identical noninteracting redox centers. The only literature report to date for a redox protein containing identical, noninteracting centers is a potentiometric study (3) of a ferredoxin from Clostridium pasteuranium. Reduction of one $(4Fe\text{-}4S)^{2+}$ cluster in this iron-sulfur protein has no detectable effect on the reduction potential of the second cluster, despite the additional negative charge present approximately 12 Å away.

There is no reason to believe that different redox centers in a multisite system will exhibit the same ΔS^{o} for electron transfer. In metalloproteins containing several different redox centers, the values of the formal potentials for these sites are likely to exhibit different temperature dependences. An example (4) of such behavior is to be found in the 1:1 complex of putidaredoxin and cytochrome P-450. At room temperature the potential of cytochrome P-450 is more positive than that of putidaredoxin and after addition of one electron the hemoprotein is 90% reduced, the iron-sulfur protein 10% reduced. On cooling the reduction potentials change in opposite directions, that of cytochrome P-450 decreasing while the potential of putidaredoxin increases. At -30 ^{o}C (in glycerol), the iron-sulfur protein is now 90% reduced and cytochrome P-450 is only 10% reduced. Changes in reduction potential and electron distribution are clearly an important phenomenon and should be of considerable concern to individuals engaged in the study of multicenter redox proteins.

In this chapter, an analogy between allosteric ligand binding and allosteric electron binding (i.e., reduction) is discussed in order to

provide a formalism for analyzing electrochemical data for multisite redox proteins. Data for a semisynthetic two-site protein, $(NH_3)_5Ru$(His-48)myoglobin, are then presented to illustrate an extreme example of ΔS^o differences for metal sites within a single noninteractive system. Finally, data pertaining to site-site interactions in cytochrome c oxidase are presented and a new interactive model for the equilibrium redox behavior of this enzyme is suggested.

MANIFESTATIONS OF INTERACTIVE BEHAVIOR IN NERNST PLOTS

A significant simplification in redox behavior occurs when the metal centers in a multisite metalloprotein are identical and noninteracting. Unfortunately, available evidence for presently known systems forces one to conclude that such a situation will seldom be encountered. What must now be considered is the manner in which interactive behavior affects thermodynamic parameters derived from redox titration data. It should be noted at the outset that electrochemical data alone are not sufficient to characterize the redox thermodynamic properties intrinsic to the metal centers of an interactive multisite system; spectral data will also be required.

Site-site interactions in equilibrium redox titrations can be dealt with by considering a closely related problem, the association of ligands with macromolecules under equilibrium conditions (5-8). The uptake of dioxygen by hemoglobin, one of the classic problems in biophysical chemistry, is an example of the ligand binding analogue of a redox titration of a four-site metalloprotein whose metal centers display allosteric behavior. Thus, the electron in a redox process

can be considered the equivalent of a ligand and the equations derived for allosteric ligand-binding proteins are relevant to this problem (9,10).

The ligand binding properties of many proteins can be understood using an expression proposed by A.V. Hill (11) as a consequence of the following type of reasoning. Suppose that a protein oligomer of n subunits combines with substrate molecules such that all intermediate states between the bare and fully occupied oligomer can be neglected (due to instability). The reaction is then

$$P_o + nx \underset{k_{n-}}{\overset{k_{n+}}{\rightleftharpoons}} P_n, \qquad (1)$$

where P_n denotes the oligomer with n bound sites. The steady-state and conservation equations for such a system are

$$-k_{n+}P_o x^n + k_{n-}P_n = 0, \quad P_o + P_n = \bar{P} \qquad (2)$$

where $\bar{P}$ is the total oligomer concentration. The degree of saturation is given by

$$Y = (nP_n/n\bar{P}) = [K_n x^n/(1 + K_n x^n)], \qquad (3)$$

where $K_n = k_{n+}/k_{n-}$. Since $Y/(1-Y) = K_n x^n$, we obtain

$$\ln[Y/(1-Y)] = \ln K_n + n\ln x, \qquad (4)$$

and a straight line of slope n is usually obtained if the quantity on the left is plotted as a function of lnx in the region of 50% saturation. It must be noted that the saturation functions depicted in all such Hill plots, at sufficiently low and sufficiently high ligand concentrations, approach asymptotically a straight line with a slope of unity. The quantity

$$n_H = d\ln[Y/(1 - Y)]/d(\ln x), \qquad (5)$$

obtained in the region of 50% saturation, is called the Hill number and is a measure of cooperativity. The higher n_H is, the higher the cooperativity. At the upper limit, n_H is equal to the number of binding sites. If $n_H = 1$, there is no cooperativity; if $n_H > 1$, there is positive cooperativity; and if $n_H < 1$, there is negative cooperativity. Cornish-Bowden and Koshland (9) carefully discussed the shapes of saturation functions expected for all possible permutations of the binding ratios K_2/K_1, K_3/K_2, and K_4/K_3 for a tetrameric protein. Figure 1, taken from Reference 9, illustrates the dependence of the slopes of the Hill plots on the ratios of the binding constants. For each plot the three-part symbol indicates the values of K_2/K_1, K_3/K_2, and K_4/K_3, respectively. The values for these ratios are 10 (positively cooperative), or 1 (noncooperative), or 0.1 (negatively cooperative). Almost all of the simulated plots are noticeably curved. It is important to note, however, that few of the plots are significantly curved between $\log[Y/(1 - Y)] = \pm 0.5$. From this observation it is apparent that ligand binding experiments must be

Figure 1. Hill plots for a tetrameric protein (from Reference 9). Dashed lines indicate asymptotes. The symbol + indicates positive cooperativity; 0 indicates no cooperativity; and - indicates negative cooperativity. Nine new curves may be seen by viewing the figure upside down.

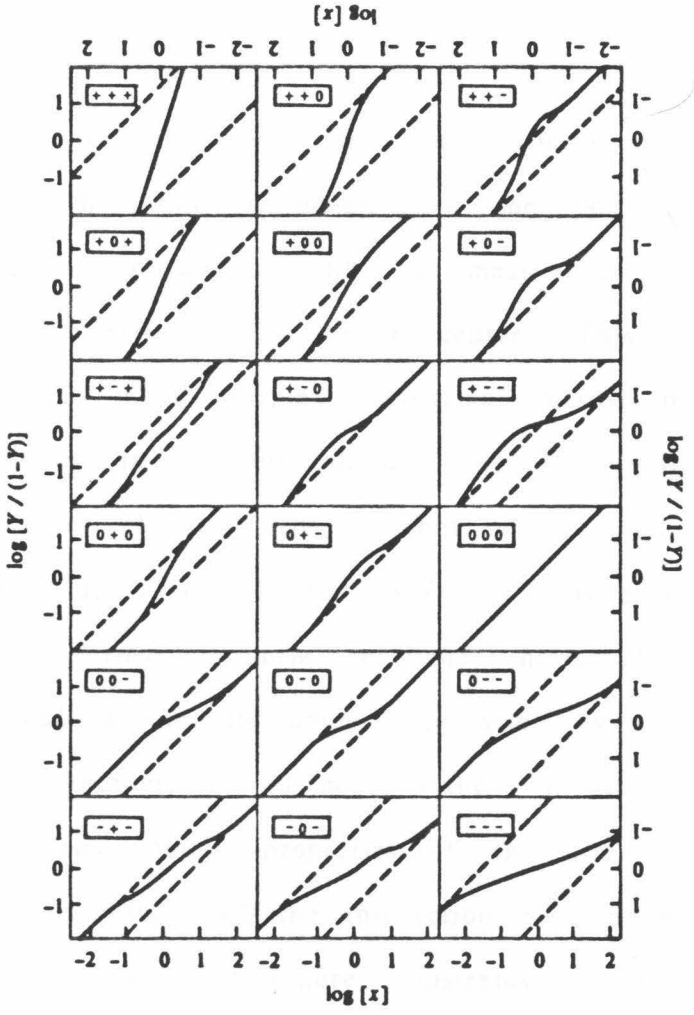
log [x]
log [Y / (1-Y)]
log [Y / (1-Y)]
log [x]
+ + +
+ + 0
+ + -
+ 0 +
+ 0 0
+ 0 -
+ - +
+ - 0
+ - -
0 + +
0 + 0
0 + -
0 0 +
0 0 0
0 0 -
0 - +
0 - 0
0 - -
- + +
- + 0
- + -
- 0 +
- 0 0
- 0 -
- - +
- - 0
- - -

done over a wide range in free ligand concentration.

The Nernst plot of electrochemistry is formally the same as the biochemist's Hill plot, with the axes reversed. We therefore have a ready-made formalism to analyze redox titration data for manifestations of interactive behavior. In particular, a departure from simple Nernstian $n = 1$ behavior is indicative of redox-linked allosteric interactions. In circumstances where such interactions are evident, the formal, or midpoint, potential (i.e., the potential at which a site is one-half reduced) is <u>not</u> a meaningful measure of the thermodynamic properties of a redox center. This is illustrated in Figures 2 and 3, which display theoretical Nernst plots for a site which participates in various thermodynamically manifested interactions with another electron acceptor, but whose intrinsic potential is not varied (12). In Figure 2, for example, it is seen that a 1 mV change in the formal potential of the interactant can shift the midpoint potential of the site under observation by as much as 4 mV (assuming an interaction of 120 mV), without involving <u>any</u> change in the intrinsic thermodynamic properties of the site under observation. Changes in the magnitude of the interaction have a less dramatic, but nevertheless significant effect, as Figure 3 illustrates.

In interactive situations, at least two meaningful thermodynamic quantities may still be defined. These are the reduction potentials which pertain to a given site when its interacting partners are all oxidized, or when its interacting partners are all reduced. Equivalently, one may define the potential when all partners are oxidized, and the "interaction potential," which is equal to the difference

Figure 2. Theoretical Nernst plots for an interactive electron acceptor. In all plots, the potential of the site is +60 mV when its interacting partner is oxidized and -60 mV when its interacting partner is reduced. In the top panel, the potential of the interacting partner is varied between ca. 40 mV and 80 mV while the magnitude of the interaction is fixed at -120 mV (the minus sign indicates that the interaction is anticooperative). The dashed lines indicate the slope expected for a noninteractive one-electron acceptor. In the lower panel, the midpoint potentials (the points at which log(Ox)/(Red) = 0) obtained from the plots in the top panel are plotted as a function of the potential of the interactant. Note that some of the Nernst plots used to obtain the points in the lower panel were omitted from the upper panel for the sake of clarity. The following equation was used to generate these (and succeeding) plots:

$$\log(Ox/Red) = (F/2.303RT)(E - E_1) + \log\{1 + \exp[(F/RT)(E_2-E)]\} - \log\{1 + \exp[(F/RT)(E_2 - E' - E)]\},$$

where E is the applied potential, E_1 is the upper asymptotic potential of the site under observation, E_2 is the upper asymptotic potential of the interacting site (referred to as the interactant), and E' is the potential of interaction between the two sites. This equation reduces to the Nernst equation when $E' = 0$.

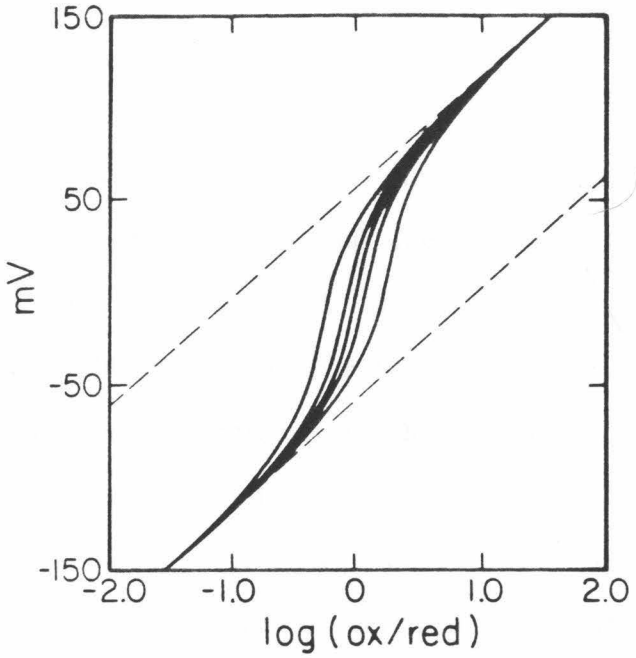
150
50
-50
-150
mV
-2.0
-1.0
0
1.0
2.0
log (ox/red)

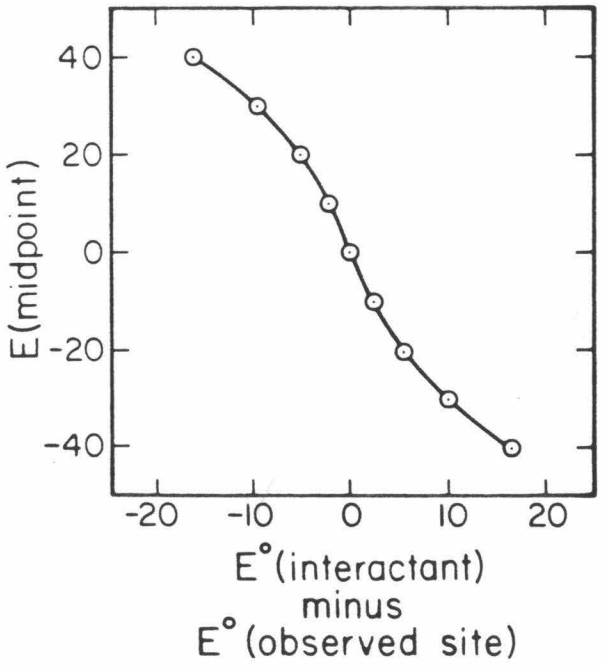
40
20
0
-20
-40
E(midpoint)
-20
-10
0
10
20
E°(interactant)
minus
E° (observed site)

Figure 3. Theoretical Nernst plots for an interactive electron acceptor. In all plots, the potential of the site is +60 mV when its interacting partner is oxidized and -60 mV when its interacting partner is reduced. In the top panel, the interactant potential is fixed at 60 mV while the magnitude of the interaction is varied in 30 mV increments between -30 and -120 mV. The dashed lines indicate the slope expected from a noninteractive one-electron acceptor. In the lower panel, the midpoint potentials obtained from the plots in the upper panel are plotted as a function of the magnitude of the interaction.

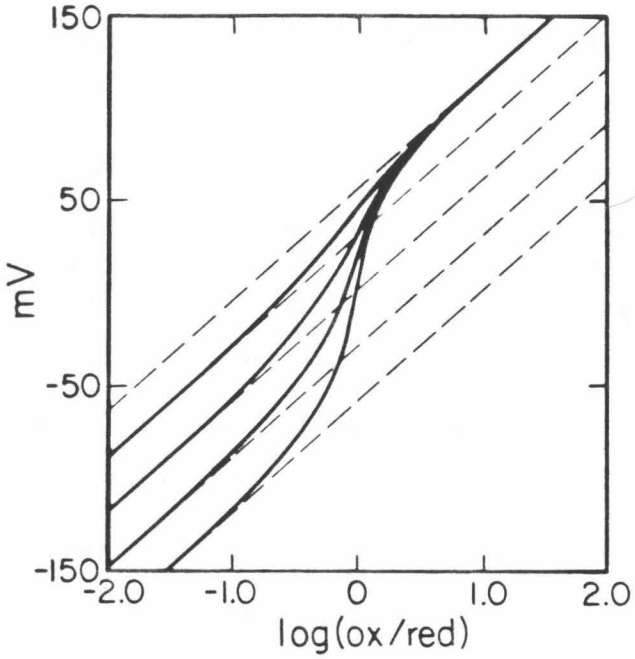
150
50
-50
-150
mV
-2.0
-1.0
0
1.0
2.0
log(ox/red)

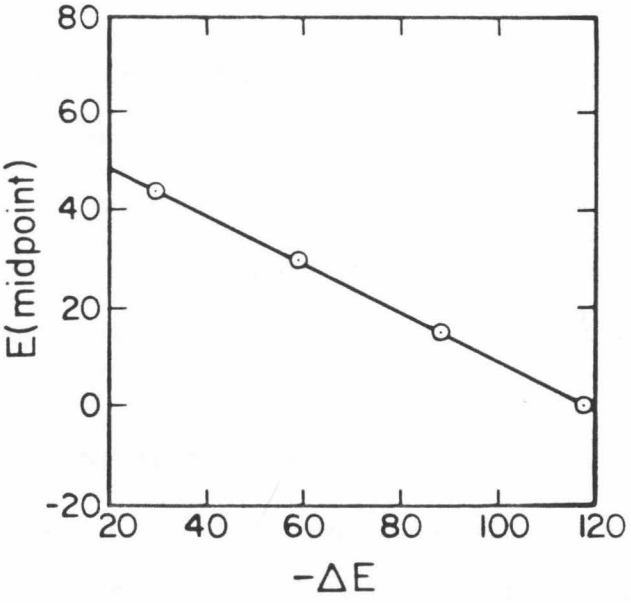
80
60
40
20
0
-20
E(midpoint)
20
40
60
80
100
120
-ΔE

between the all partners oxidized and all partners reduced potentials. As seen in Figures 2 and 3, the Nernst plots of interacting sites approach n = 1 behavior at sufficiently high or low potentials. The n = 1 asymptotes are fixed by the all partners oxidized and all partners reduced potentials, and may therefore be used to estimate these potentials. In the simplest possible (i.e., two-site) interaction model, it is assumed that only one interaction dominates the titration behavior of a given site. In complex situations where more than one interaction is operative, the simplified model may deviate from the observed Nernst plot in the crossover region between the two asymptotes, but it is still able to provide satisfactory estimates of the asymptotic potentials, since in all interaction schemes the asymptotic behavior is the same (i.e., a straight line corresponding to an isolated one-electron acceptor). The determination of asymptotic reduction potentials is more difficult and less precise than the determination of midpoint potentials, because it involves data taken nearer the extremes of a titration. It should be stressed, however, that while plots of midpoint potentials (vs. pH, for example) will thus show less scatter, they cannot be interpreted in terms of well-defined thermodynamic quantities.

PENTAAMMINERUTHENIUM(HIS-48)MYOGLOBIN

Introduction. With few exceptions, multisite redox metalloenzymes have proved resistant to detailed kinetic and thermodynamic analysis, due (in part) to a lack of structural information. The amino acid framework of a structurally characterized metalloprotein may be viewed

from an inorganic standpoint as that of a bridging ligand to which one can attach a substitution-inert transition metal complex in order to "synthesize" a multisite metalloprotein from which one can extract kinetic and thermodynamic information pertaining to electron transfer processes in which the redox site-to-site distance is fixed and known.

Figure 4 displays the sperm whale myoglobin peptide backbone, and illustrates the spatial dispositions of the heme and attachment site of a $(NH_3)_5Ru^{3+/2+}$ label, an imidazole nitrogen of His-48. The two sites in this derivative exhibit similar $E^{o'}$ values, yet their temperature coefficients are very different. When combined with variable-temperature kinetic data, the redox thermodynamic parameters reported herein allow an estimate of the enthalpic reorganizational barrier for myoglobin electron transfer to be made (13,14).

Materials and Methods. Sperm whale myoglobin (Sigma) was subjected to chemical modification with $[(NH_3)_5Ru(OH_2)]^{2+}$ to produce a mixture of protein derivatives, which were then separated by preparative isoelectric focusing and cation-exchange chromatography. One of the singly modified protein derivatives, $(NH_3)_5$Ru(His-48)myoglobin, was supplied by Dr. R.J. Crutchley for electrochemical studies. Details of the preparation and characterization (including peptide mapping) are given in Reference 14.

Anaerobic spectroelectrochemical titrations of the "ruthenated" myoglobin were carried out using the OTTLE cell and shroud described in Chapter II. The solution conditions were identical to those used for native sperm whale myoglobin experiments (pH 7.0, I = 0.1 M) previously described. $[Ru(NH_3)_6]Cl_3$ (Strem Chemicals) was used as a

Figure 4. The main chain of sperm whale myoglobin. The edge-to-edge through-space distance from the imidazole ring of His-48 to the heme is 13.3 Å.

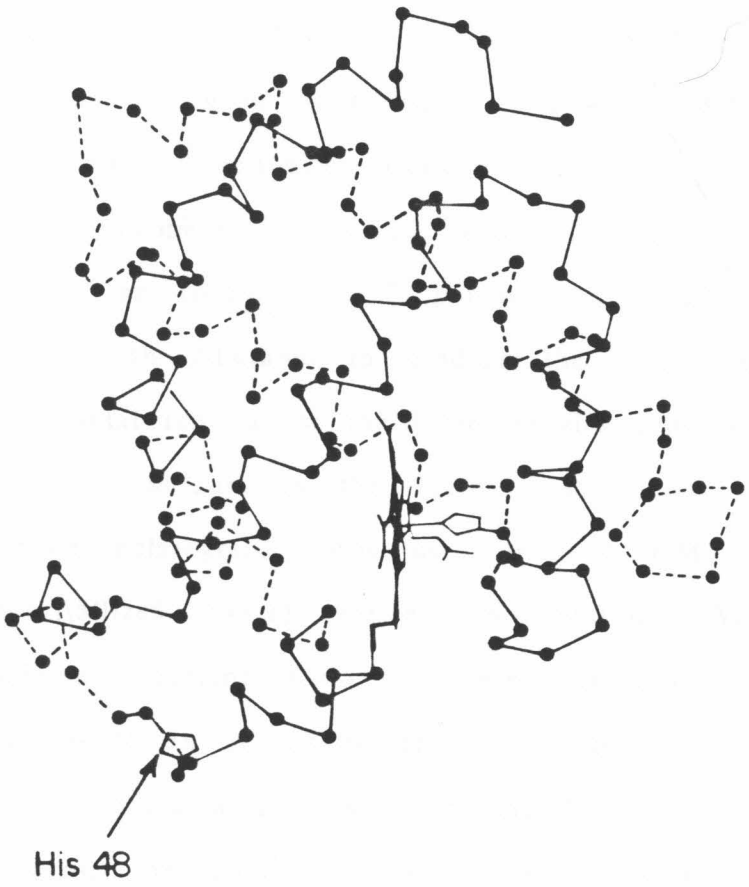
His 48

redox mediator in a 5:1 mediator:protein ratio. Nernst plots were obtained from changes in the absorption spectrum at 556 nm, with at least 7 data points used per plot. Variable-temperature measurements (5-40 ^{o}C) yielded the entropy and enthalpy changes associated with the reduction of the heme(Fe^{3+}) site. All of the Nernst plots were linear (correlation coefficients of 1.000) within experimental error and displayed Nernst slopes in good agreement (± 5%) with those expected for an n = 1 process at each of the temperatures examined.

The heme chromophore interfered with the spectroelectrochemical determination of the $(NH_3)_5Ru^{3+/2+}$ potential; repeated extraction of the labile heme with 2-butanol to produce the derivatized apoprotein did not lead to total removal of the heme, judging from the appearance of the absorption spectrum in the 350-450 nm region. Consequently, differential pulse polarography was used with 2 mM 4,4′-bipyridine (Aldrich, recrystallized twice) present in solution. Variable-temperature anaerobic measurements (5-45 ^{o}C) were carried out using a dual water-jacketed H-cell in a nonisothermal configuration (i.e., the reference electrode compartment was thermostatted at 25 ^{o}C). Prior to each measurement, the gold (2 mm button) working electrode was polished with an alumina slurry, rinsed, and then placed into the protein solution, which was then purged with argon for 15 minutes. No current attributable to the heme iron was observed when native myoglobin was run in a control experiment. $[Co(phen)_3]Cl_3$ was used to calibrate the cell at each temperature used for the modified myoglobin experiments.

Results and Discussion. A typical differential pulse voltammogram

is displayed in Figure 5. Overlay spectroelectrochemical data mirror those for native myoglobin (Chapter III) and are therefore not shown. Figure 6 illustrates the temperature dependences of the heme ($Fe^{3+/2+}$) and $(NH_3)_5Ru^{3+/2+}$ potentials. The redox thermodynamic parameters for both metal sites, together with those for native myoglobin for comparison, are given in Table 1. Since the formal potentials at 25 ^{o}C for the ruthenium and heme sites in the modified protein differ by only 20 mV, one-electron reduction of the fully oxidized protein derivative is expected to produce both mixed-valence intermediates:

$$(NH_3)_5Ru^{2+}\text{--}Mb(Fe^{3+}) \underset{k_{-1}}{\overset{k_1}{\rightleftharpoons}} (NH_3)_5Ru^{3+}\text{--}Mb(Fe^{2+}) \qquad (6)$$

An additional spectroelectrochemical experiment carried out in the absence of a redox mediator confirmed this expectation. The heme center in the modified myoglobin was observed to reduce during a reductive electrolysis, whereas native myoglobin was not found to be electroactive.

Flash photolysis experiments (13,14) on the myoglobin derivative, carried out by Dr. R.J. Crutchley, were used to produce the mixed-valence species and monitor the approach to equilibrium, Equation (6). The observed rate for this process, k_{obs}, is the sum of k_1 and k_{-1}. The forward (k_1) and reverse (k_{-1}) rates were found to be 0.019 $\pm$ 0.002 sec^{-1} and 0.041 $\pm$ 0.003 sec^{-1}, respectively, at 25 ^{o}C. The temperature dependences (5-45 ^{o}C) of these rates yielded values for

Figure 5. Differential pulse voltammogram for the reduction of the ruthenium center in $(NH_3)_5Ru$(His-48)myoglobin. Solution conditions: pH 7.0; ionic strength, 0.1 M; 2 mM 4,4′-bipyridyl; 25 ^{o}C. Electrodes: 2 mm gold working, SCE reference, and Pt wire auxiliary. Scan rate, 2 mV/sec; "drop time," 0.5 sec; pulse amplitude, 25 mV.

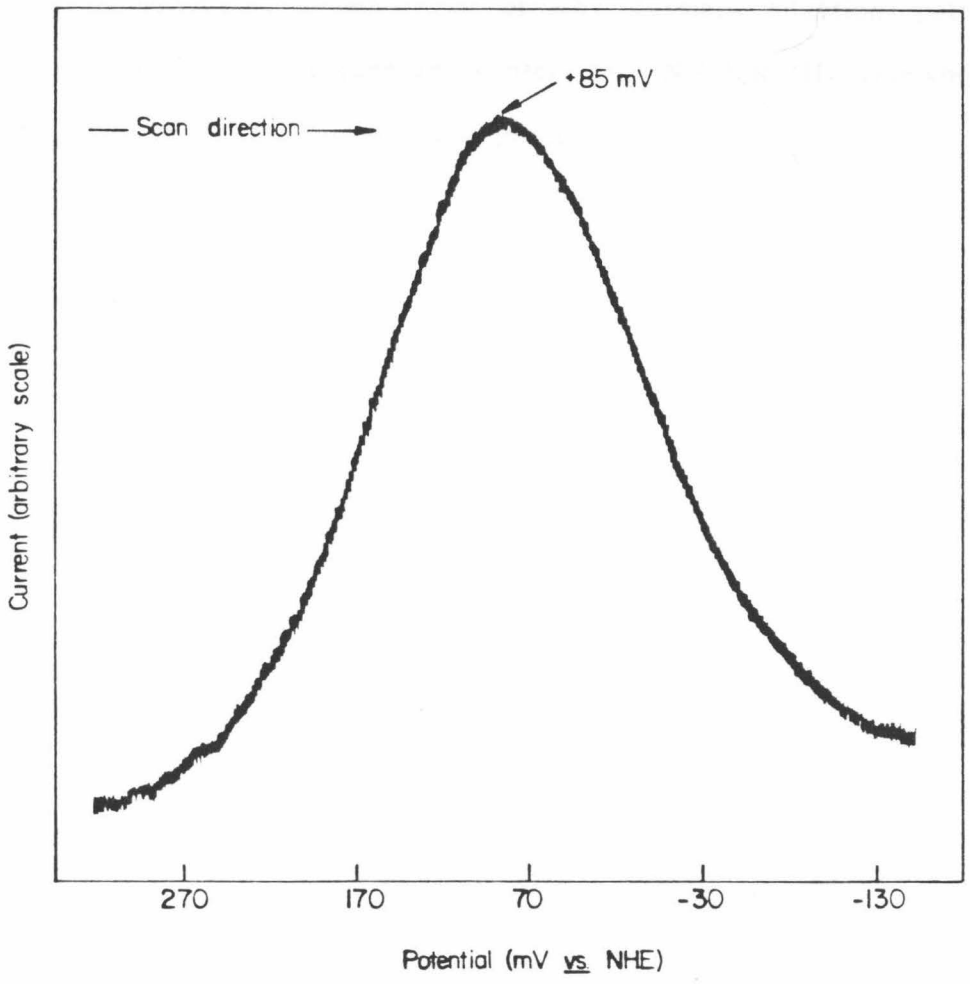
+85 mV
Scan direction
Current (arbitrary scale)
270
170
70
-30
-130
Potential (mV vs. NHE)

Figure 6. Temperature dependences of the formal reduction potentials for the iron (PFe) and ruthenium centers in $(NH_3)_5Ru$(His-48)myoglobin. Conditions: pH 7.0, 0.1 M ionic strength, phosphate buffer.

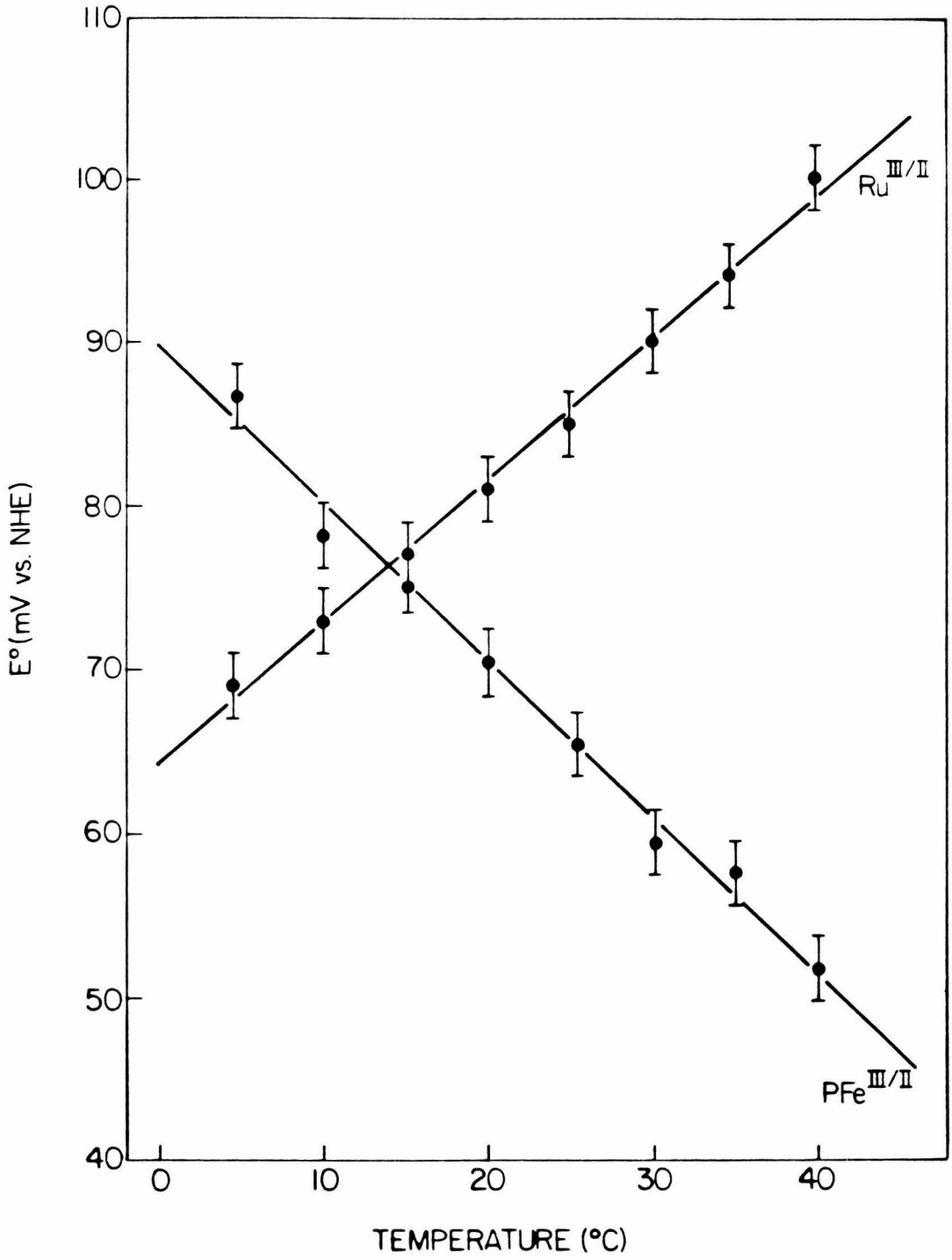
110
100
90
80
70
60
50
40
E°(mV vs. NHE)
0
10
20
30
40
TEMPERATURE (°C)
Ru III/II
PFe III/II

Table I. Thermodynamic parameters (pH 7.0) for the reduction of the ruthenium and heme iron sites in $(NH_3)_5Ru$(His-48)myoglobin. Values for native myoglobin (Mb) are shown for comparison.

	Native Mb	Modified Mb	
	$Fe^{3+/2+}$	$Fe^{3+/2+}$	$Ru^{3+/2+}$
$E^{o'}$, mV vs. NHE (25 ^{o}C)	58.8 ± 2	65.4 ± 2	85.8 ± 2
$\Delta G^{o'}$, kcal/mol (25 ^{o}C)	-1.36 ± 0.05	-1.51 ± 0.05	-1.98 ± 0.05
$\Delta S^{o'}$, eu	-39.2 ± 1.2	-37.6 ± 1.2	4.2 ± 1.2
$\Delta H^{o'}$, kcal/mol (25 ^{o}C)	-13.0 ± 0.4	-12.7 ± 0.4	-0.7 ± 0.4

$\Delta H_1^{\neq}$ (7.4 ± 0.5 kcal/mol) and $\Delta H_{-1}^{\neq}$ (19.5 ± 0.5 kcal/mol).

The reorganizational enthalpy associated with the reduction of the heme site in myoglobin can be estimated using an expression derived by Marcus and Sutin (15):

$$\Delta H_{12}^{*} = 1/2(\Delta H_{11}^{*} + \Delta H_{22}^{*})(1-4\alpha^2) + 1/2\,\Delta H_{12}^{o}(1-2\alpha) \qquad (7)$$

$$\text{where } \alpha = \frac{\Delta G_{12}^{o}}{4(\Delta G_{11}^{*} + \Delta G_{22}^{*})}$$

In the following calculation, we neglect α since ΔG_{12}^{o} is very small. Since the reacting sites are fixed spatially, $\Delta H_{12}^{\neq} = \Delta H_{12}^{*}$. ΔH_{22}^{*} is approximated as 6.9 kcal/mol, the value for the $[(NH_3)_5pyRu]^{3+/2+}$ self-exchange. Using ΔH_{12}^{*} = 7.4 kcal/mol and ΔH_{12}^{o} = -12 kcal/mol (data for the forward reaction), the reorganizational enthalpy (ΔH_{11}^{*}) for the myoglobin($Fe^{3+/2+}$) system is estimated to be 20 kcal/mol.

In contrast, the enthalpic reorganizational barrier for the heme in horse heart cytochrome c is only 7-8 kcal/mol (17). X-ray crystallographic studies (18) indicate that the reduction of metmyoglobin to deoxymyogolbin results in dissociation of the axial water molecule from the iron atom. This change in ligation most likely accounts for the much larger reorganizational enthalpy, because the axial ligands (His and Met) in cytochrome c (19) are retained upon reduction of the iron center.

The contrast in temperature dependences of the iron and ruthenium

centers (Figure 6) is rather striking. The modified myoglobin redox system has a substantial value of $\Delta H_{12}^{o'}$ offset by $\Delta S_{12}^{o'}$ to yield an equilibrium constant K_{eq} near unity at 14 ^{o}C. This type of thermodynamic situation is an ideal one for temperature-jump relaxation studies. While the low values of k_1 and k_{-1} for modified myoglobin are too slow for temperature-jump to be of use, this kinetic technique seems to be worth considering for other multisite redox proteins, subject to thermodynamic constraints.

CHARACTERIZATION OF SITE-SITE INTERACTIONS IN CYTOCHROME C OXIDASE

Introduction. The metal centers of cytochrome c oxidase (Figure 7) catalyze reactions that are of great biological importance and chemical interest, namely the reduction of dioxygen to water, using electrons derived from ferrocytochrome c, and the active transport of protons across the inner mitochondrial membrane. These reactions account for most of the oxygen utilization in the biosphere and for a substantial fraction of all biological energy transduction.

The oxidase contains four redox-active prosthetic groups: cytochrome a, or Fe_a, is a low-spin bis-imidazole heme that rapidly accepts electrons from bound cytochrome c; a copper ion, Cu_A, exhibits unusual spectroscopic properties (23) and also accepts electrons from cytochrome c rapidly; another heme, cytochrome a_3, and another copper ion, Cu_B, are close, ca. 3 Å, to each other (24) and together form the site of dioxygen reduction. In recent years, considerable progress has been made toward elucidating the structures of these prosthetic groups and the mechanisms of electron transfer and dioxygen reduction

Figure 7. A model for cytochrome c oxidase. Adapted, with modifications, from Reference 22.

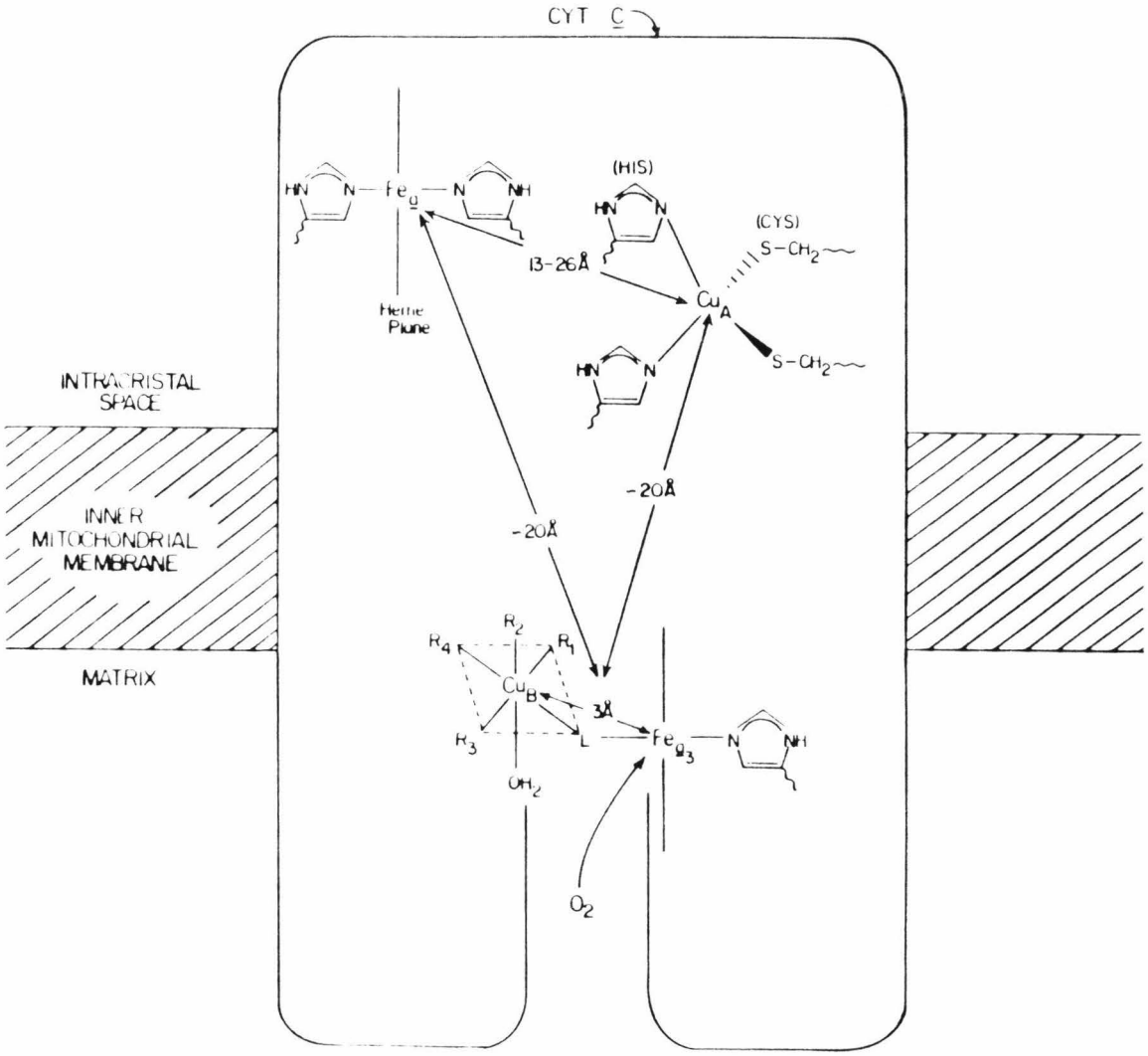
CYT C
(HIS)
(CYS)
S-CH2
13-26Å
CuA
Heme
Plane
INTRACRISTAL
SPACE
INNER
MITOCHONDRIAL
MEMBRANE
MATRIX
~20Å
~20Å
R2
R4
R1
CuB
3Å
R3
L
OH2
FeA3
O2

(for recent reviews, see References 22, 25-29).

Each of the four metal centers of the enzyme is known to function in a redox capacity, as evidenced by optical and EPR measurements at various stages during enzymatic turnover with solution oxidoreductants and dioxygen (30-34). An electrochemical titration has demonstrated that the oxidized enzyme accepts four electrons upon complete reduction (35). In an early spectrophotometrically monitored titration with cytochrome c, Minnaert (36) measured the formal potential of cytochrome a to be 278 mV vs. NHE. However, the titration behavior of cytochrome a was not that expected for a Nernstian $n = 1$ site; the observed Nernst slope was close to $n = 0.5$. Many studies have been subsequently carried out in order to clarify the redox properties of the enzyme.

The present picture of the redox thermodynamics of cytochrome c oxidase is unsatisfactory in several respects. Confusion has arisen primarily from two sources. First, the optical properties of the metal sites (apart from Cu_B, which is essentially spectrally silent) make the interpretation of optically monitored titrations difficult. Cupric Cu_A is associated with a near infrared absorption band centered at 830 nm ($\varepsilon \sim 2000\ M^{-1}cm^{-1}$), which makes monitoring the Cu_A site more difficult and less precise than monitoring the heme sites, which have much stronger absorptions in the visible region. This circumstance probably accounts for the fact that few measurements of the Cu_A potential using optical spectroscopy have been undertaken (37-40), while measurements of the heme potentials have been made repeatedly (38-43). The optical properties of the hemes, and the possibility of

optically manifested interactions between these sites, have been disputed (44-46).

Second, the metal centers of the enzyme evidently interact with each other so that they do not exhibit the electrochemical titration behavior expected of isolated single-electron acceptors. The nature and magnitude of these interactions have been the subject of many recent investigations. In all but one of these studies, the dominant interaction was postulated to be between cytochrome a and cytochrome a_3 (40,42,44,47). However, published optically monitored titrations (36,48) suggest that interaction between cytochrome a and Cu_B is also important. The possibility of other interactions has not been explored.

A consideration of all the possible intersite interactions requires a complex scheme (Figure 8) in which the enzyme may take on any of 16 different states. The redox behavior of the oxidase is simpler in the presence of ligands that bind to cytochrome a_3 and stabilize this site in one redox state (50). For example, cyanide stabilizes cytochrome a_3 in the oxidized state (48), while allowing Cu_B to undergo oxidoreduction (49,51). Carbon monoxide evidently stabilizes both cytochrome a_3 and Cu_B in their reduced states (52). Ligand binding thus decreases the number of overall redox states accessible to the enzyme and simplifies the interaction problem accordingly.

The most widely accepted interaction scheme (44) at present, the "neoclassical" model, incorporates thermodynamic interaction only between cytochrome a and cytochrome a_3 (Figure 9). The results of experiments that further clarify the nature and magnitudes of various

Figure 8. Equilibrium redox states in cytochrome c oxidase. The superscripts o and r denote oxidized and reduced, respectively.

CYTOCHROME C OXIDASE REDOX STATES

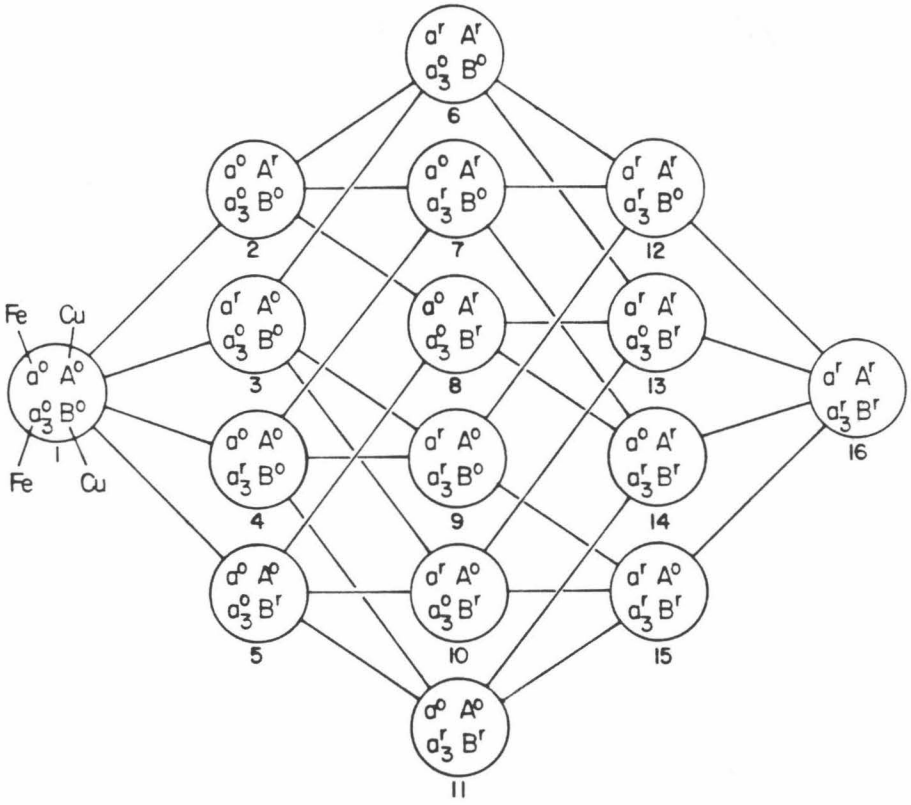

Figure 9. The "neoclassical" redox interaction model of cytochrome c oxidase. The numbers shown represent formal potentials at pH 7.0.

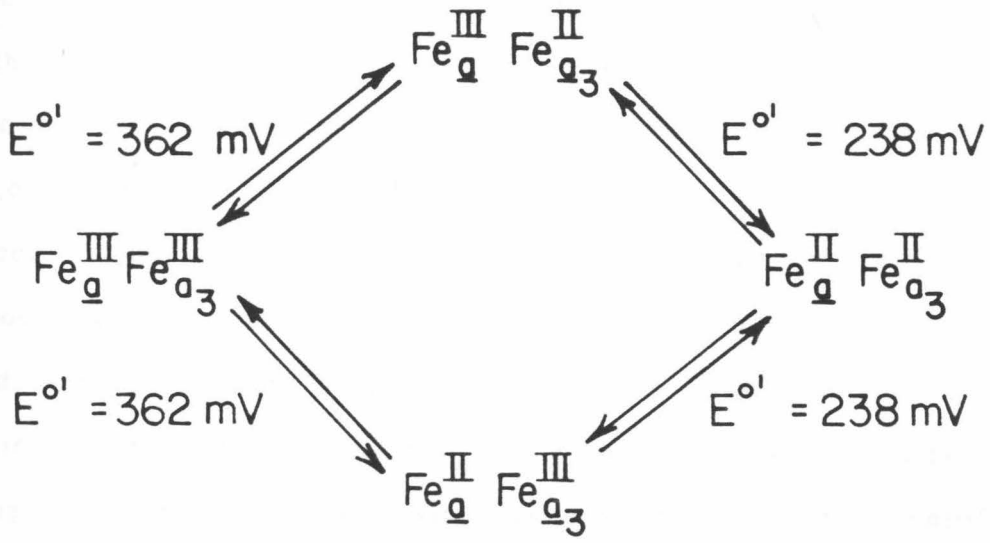
$Fe_a^{III}\ Fe_{a_3}^{II}$
$E^{o'}$ = 362 mV
$E^{o'}$ = 238 mV
$Fe_a^{III}\ Fe_{a_3}^{III}$
$Fe_a^{II}\ Fe_{a_3}^{II}$
$E^{o'}$ = 362 mV
$E^{o'}$ = 238 mV
$Fe_a^{II}\ Fe_{a_3}^{III}$

thermodynamically manifested intersite interactions, and a scheme to account for both the new observations and the earlier data are presented in this section. The "neoclassical" model does not adequately account for the present observations; a scheme that accounts for all of the data must involve interactions of comparable magnitude between cytochrome a and all three other redox centers in the enzyme.

Materials and Methods

Materials. Cytochrome oxidase was purified from beef heart mitochondria by the method of Hartzell and Beinert (53) and was stored frozen at -80 ^{o}C. Protein concentration was determined by the method of Lowry et al. (54) and heme concentration by the reduced-minus-oxidized extinction of the uninhibited enzyme at 604 nm, with an extinction coefficient of 24 $mM^{-1}cm^{-1}$ (55). The purified enzyme contained 8 nmol of heme a per mg. of protein. Just prior to use, the oxidase was thawed and dialyzed into potassium phosphate buffer containing 0.5% Tween-20. Following dialysis, samples were centrifuged at 35000 g for 30 minutes to remove insoluble material. Enzyme concentrations were typically 0.10-0.15 mM for the thin-layer experiments and 40 μM for the long-path spectroelectrochemistry experiments.

All buffer solutions were prepared with glass-distilled water and research grade reagents. $[(NH_3)_6Ru]Cl_3$ was obtained from Alfa and purified by the method of Pladziewicz et al. (56). Hydroxymethylferrocene (Strem) and 1,1′-bis(hydroxymethyl)ferrocene (Research Organic/Inorganic Chemical Corp.) were used as received. $[Ru(NH_3)_5py](ClO_4)_3$ was prepared as described previously (57). The above redox mediators (Table II) were selected because they have a

Table II. Redox mediator titrants employed in cytochrome c oxidase experiments.

Mediator	$E^{o'}$ (mV vs. NHE)	No. of Equiv. A	B
$[Ru(NH_3)_6]Cl_3$	51	1.0	5
$[Ru(NH_3)_5py](ClO_4)_3$	260	1.0	5
(hydroxymethyl)ferrocene	405	0.5	2.5
1,1′-bis(hydroxymethyl)ferrocene	465	0.5	2.5

[A]Thin-layer experiments.

[B]Long-path experiments.

negligible absorbance in the 400-900 nm region at the concentrations used and have formal potentials that allow the solution to be poised from -50 to +550 mV vs. NHE. Equilibrium dialysis control experiments indicate that these mediators do not measurably bind to the enzyme.

Spectroelectrochemistry. Reduction potential measurements were made using OTTLE cells for cytochrome chromophores and 2 mM long-path cells for the Cu_A chromophore. The spectroelectrochemical cell/electrode assemblies were contained in a steel shroud (Chapter II) in order to maintain strict anaerobicity. Absorbance spectra were obtained with a Cary 219 spectrophotometer interfaced to a Spex Industries SCAMP SC-31 data processor.

Methods. After the addition of redox mediators, enzyme and buffer solutions were thoroughly degassed on a high-vacuum apparatus. For CO inhibition experiments, one atmosphere of CO (Matheson, 99.9%) was then added. The solutions, spectroelectrochemical cell, electrodes, and shroud were then transferred into an inert atmosphere box where the cell was then loaded, fitted with the reference and counter electrodes, and placed into the shroud. The loaded shroud was then taken out of the inert atmosphere box and seated into the spectrophotometer sample compartment.

Enzyme/mediator solutions were poised at -50 mV vs. NHE for at least two hours at 10 ^{o}C in order to fully reduce the enzyme. The temperature was then reset in order to begin collecting data. A series of potentials was then applied across the cell; each potential was maintained, typically for between 1 and 3 hours, and was considered complete when no further absorbance change was detectable

for a period of 30-60 minutes. A complete titration (both oxidative and reductive) required up to 48 hours. Care was taken to ensure that oxidations were reversible; rereduction led to data closely superimposable with oxidative data. A slight hysteresis was observed for titrations of the native enzyme; the origin of this is discussed in Chapter 6. Absorption spectra were stored on magnetic disk and difference spectra were obtained by computer subtraction. At least 10 points were included in each Nernst plot.

Data analysis: inhibited enzyme. When CO or cyanide is present in solution, cytochrome $\underline{a}_3$ is not free to titrate; CO stabilizes the Fe(II) state while cyanide stabilizes the Fe(III) state. The spectral changes observed in the visible region are therefore due exclusively to cytochrome $\underline{a}$. The redox state of Cu_A (in the CO-inhibited enzyme) was monitored by the intensity of the absorption band centered at 830 nm. The bulk of the available evidence indicates that this band is due to Cu_A (22,58). The intensity of the absorbance was quantitated as the area under the spectrum and above a straight line connecting the data at 740 nm and 900 nm. This area was taken as a measure of the concentration of oxidized Cu_A in calculating values of log(Ox/Red) at each potential. In the Cu_A experiments, the redox state of Fe_a was monitored simultaneously by the absorbance change at 604 nm, which is due entirely to Fe_a in the CO-inhibited enzyme (59, 60).

To avoid oxidation of the cytochrome $\underline{a}_3/Cu_B$ site with CO bound (which results in consumption of the CO to form CO_2), potentials above 420 mV vs. NHE were not applied across the protein solutions. Oxidation of the Fe_a site was thus not complete at the highest applied

potentials. A correction for this incomplete oxidation was applied in the following manner: the values for $E^{0'}(Fe_a)$ or $E^{0'}(Cu_A)$ that were estimated from the initial computer fits were used to calculate the fraction of Fe_a or Cu_A that remained reduced at the highest applied potentials. The corresponding absorbance difference was then added to the observed absorbance changes, to obtain a corrected fully oxidized endpoint. By the use of the corrected absorbance differences, new values of log(Ox/Red) were calculated, and new estimates of $E^{0'}$ were obtained from computer fits.

The Nernst plots obtained from titrations of Cu_A and Fe_a did not show the behavior expected of single-electron acceptors. The equilibrium equations appropriate to such interacting systems were used in a nonlinear curve fitting program to determine the asymptotic formal potentials and hence the interaction energy.

Data analysis: native enzyme. The absorbance difference spectra of cytochrome oxidase between 700 and 350 nm contain substantial contributions from both cytochromes a and a_3. The contribution of each cytochrome to the strong reduced minus oxidized absorbances at 605 and 443 nm has been estimated by various methods that use exogenous ligands to stabilize cytochrome a_3 (and sometimes Cu_B) in either the oxidized or reduced state while cytochrome a undergoes oxidoreduction (22,46,61,62); the consensus from such studies is that cytochrome a is the primary contributor to the reduced minus oxidized α band at 605 nm, while cytochrome a_3 makes the larger contribution to the reduced minus oxidized Soret band at 443 nm. All of these means of deconvolving the spectra assume that the two cytochrome contributions

to the measured absorbances are not significantly influenced by metal-metal interactions. More recent work (46) has shown that metal-metal interactions can to some degree influence the absorption properties of the oxidase, and that these interactions are most strongly manifested in the absorbance spectrum of cytochrome $\underline{a}_3$. In this interactive situation, the fully reduced minus fully oxidized absorbance difference spectrum of the enzyme can be expressed formally by the following equation:

$$\Delta A(\lambda,\underline{a},\underline{a}_3,A,B) = \Delta A(\lambda,\underline{a}) + \Delta A(\lambda,\underline{a}_3) + \delta A(\lambda,\underline{a},\underline{a}_3,A,B) \qquad (8)$$

The first two terms on the right correspond to the contributions of cytochromes $\underline{a}$ and $\underline{a}_3$ respectively to the reduced minus oxidized absorbance spectra, as deduced by ligand-inhibition methods. The third term contains any contributions from site-site interactions, and thus may depend upon the redox state of any of the oxidase metal centers.

If all of the possible intersite interactions are explicitly taken into consideration, the problem of deconvolving the absorbance difference spectra becomes exceedingly difficult. In view of the weakness of the interactions which have been observed, the interactive term in equation (8) has been neglected in the present analysis of the titration data. The spectra obtained in the titrations were factored into two components which correspond to the reduced minus oxidized difference spectra of cytochromes $\underline{a}$ and $\underline{a}_3$, as measured by the ligand inhibition methods. Since two components are involved, measurements

at a minimum of two wavelengths are required. The reduced minus oxidized peaks at 605 nm and 443 nm were selected for use in the factor analysis because they are the strongest signals in the spectrum and because each reflects one of the cytochromes significantly more strongly than the other. Approximately 72% of the 605 nm band is due to cytochrome a, and approximately 65% of the 443 nm band is due to cytochrome a_3 (as determined in Reference 22 by using CO to stabilize cytochrome a_3 and Cu_B in their reduced states). These individual cytochrome contributions were used in a two-point algebraic deconvolution of the absorbance changes measured at each applied potential. Nernst plots of the deconvoluted spectral data were least-squares fit to a nonlinear curve to obtain the asymptotic reduction potentials of cytochromes a and a_3.

RESULTS AND DISCUSSION

Interaction between Cytochrome a and Cu_A. Overlay difference spectra of cytochrome a in a typical experiment on the CO-inhibited enzyme are displayed in Figure 10. A linear relation between ΔA_{605} and ΔA_{443}, with a slope consistent with measurements of the reduced-minus-oxidized spectrum of cytochrome a (46,62), was observed (plot not shown), indicating that only cytochrome a titrates at the potentials applied.

A Nernst plot of the spectral data is shown in Figure 11. Equilibration at each applied potential was determined from the absorbance change at 443 nm. The plot is not like that expected for a simple n = 1 Nernstian process, i.e., a straight line with a slope of

Figure 10. Representative set of absorbance difference spectra of cytochrome a at different applied potentials in a thin-layer spectroelectrochemical titration of CO-inhibited cytochrome oxidase. Conditions: sample temperature, 9.8 ^{o}C; SCE temperature, 16 ^{o}C; pH 7.0; 0.245 M ionic strength. Applied potentials (mV vs. SCE): (A) -220, (B) -100, (C) -70, (D) -40, (E) -25, (F) -10, (G) 5, (H) 20, (I) 35, (J) 50, (K) 65, (L) 80, (M) 95, (N) 110, and (O) 140. The most oxidized spectrum (measured at 140 mV vs. SCE) has been subtracted from the spectra recorded at each potential to yield the difference spectra shown.

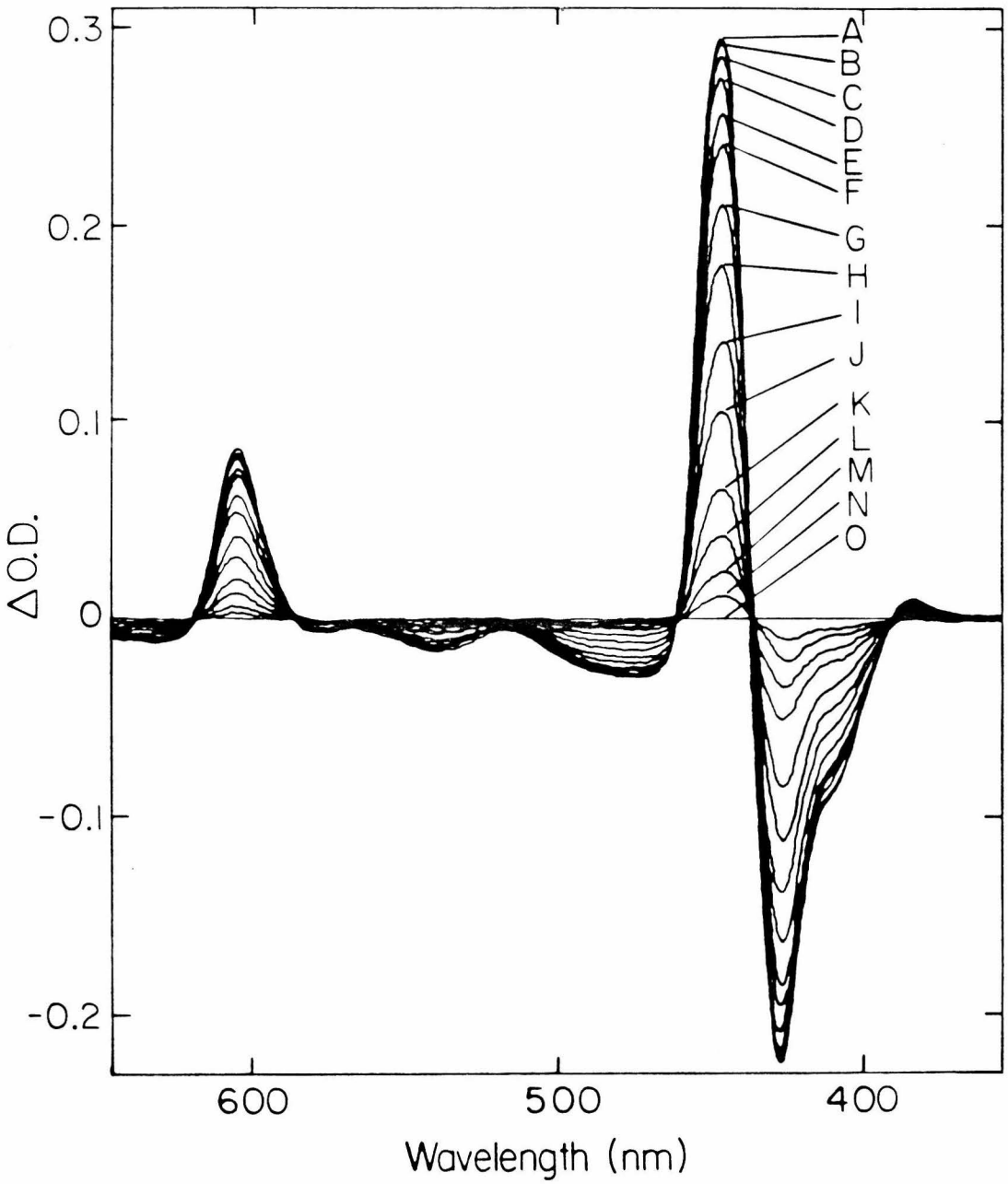
0.3
0.2
0.1
0
-0.1
-0.2
ΔO.D.
600
500
400
Wavelength (nm)
A
B
C
D
E
F
G
H
I
J
K
L
M
N
O

Figure 11. Nernst plot calculated (using ΔA_{443}) from the spectra shown in Figure 10. The solid line is the computer-generated best fit to a model in which the cytochrome a site participates in an anti-cooperative interaction of magnitude 24 mV with another site whose potential is 6 mV vs. SCE. (■ and □) Spectra obtained on oxidation and rereduction, respectively.

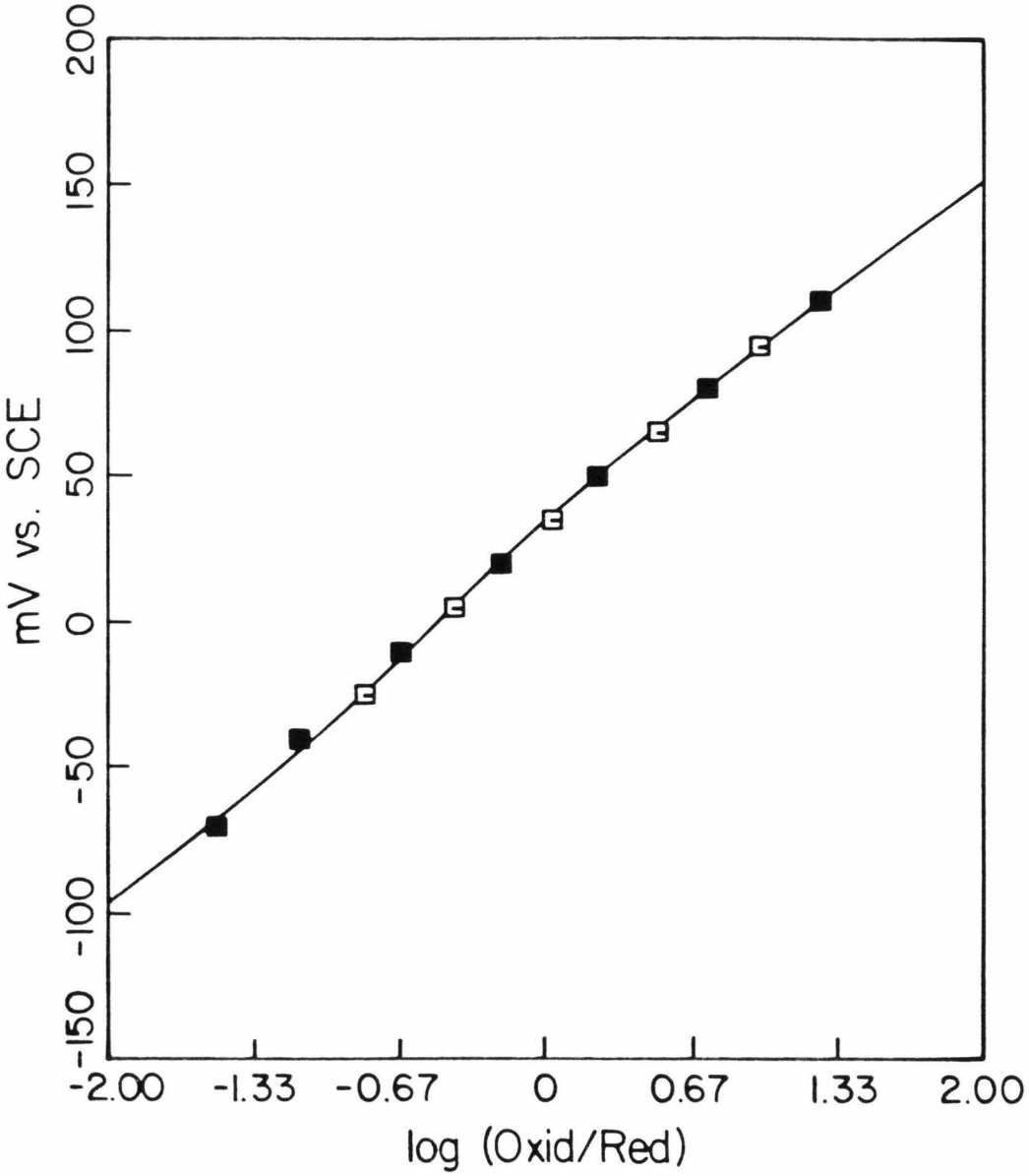
mV vs. SCE
200
150
100
50
0
-50
-100
-150
-2.00
-1.33
-0.67
0
0.67
1.33
2.00
log (Oxid/Red)

56 mV per decade at 9.8 ^{0}C. The line through the data points is the computer-generated best fit to a model in which cytochrome a participates in an anticooperative interaction of magnitude 24 mV with another site whose formal potential is 256 mV vs. NHE.

Unlike previous studies, the present data are of sufficiently high precision to detect deviations from simple Nernstian behavior. Since cytochrome a_3 and Cu_B remain reduced during the course of these experiments, the slightly sigmoidal appearance and nonintegral slopes of the data in Figure 11, if caused by intersite interaction, indicate that there is a previously unsuspected interaction between cytochrome a and Cu_A. The reaction scheme appropriate to this situation is shown in Figure 12. $E^{0\prime}$(Fe) and $E^{0\prime}$(Cu) are the reduction potentials of the iron and copper sites when their respective interaction partners are oxidized, and ΔE is an interaction potential which is a measure of the decrease in reduction potential of the other site. In the course of various experiments on cytochrome a some batch-to-batch variation in the interactive behavior was observed: the interaction energy, which measures the decrease in electron affinity of one site accompanying reduction of the other site, varied between ca. 20 and 40 mV in different enzyme batches.

The correctness of this interpretation was verified by parallel near-infrared spectroelectrochemical experiments monitoring Cu_A. A typical set of overlay Cu_A difference spectra is shown in Figure 13. The spectra indicate that the titration is very nearly reversible except for a minor baseline drift. The absorbance near 830 nm was measured as the area under the curves and above a straight line

Figure 12. Proposed interaction scheme for Cu_A and cytochrome a in redox titrations of CO-inhibited cytochrome c oxidase.

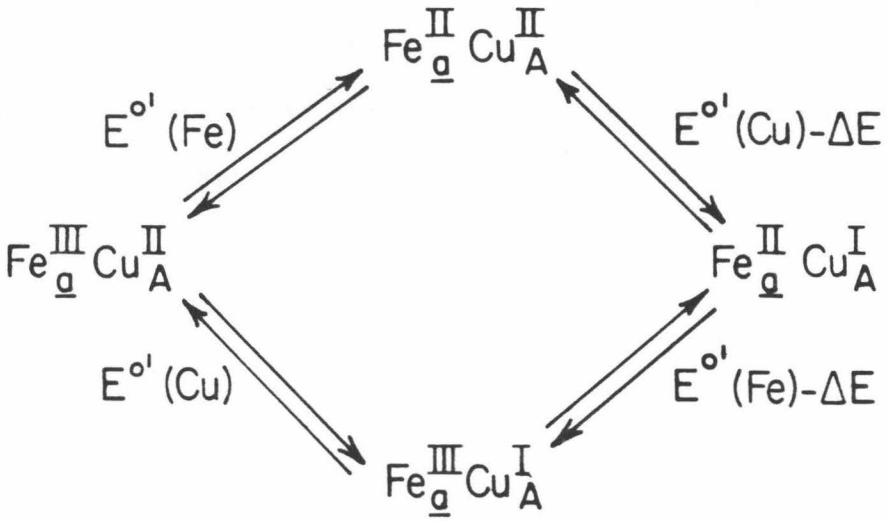
$Fe^{II}_{a}\ Cu^{II}_{A}$
$E^{o'}$ (Fe)
$E^{o'}$ (Cu)-ΔE
$Fe^{III}_{a}\ Cu^{II}_{A}$
$Fe^{II}_{a}\ Cu^{I}_{A}$
$E^{o'}$ (Cu)
$E^{o'}$ (Fe)-ΔE
$Fe^{III}_{a}Cu^{I}_{A}$

Figure 13. Near-infrared absorbance difference spectra obtained during a controlled-potential titration of CO-inhibited cytochrome c oxidase at 6 ^{o}C. The indicated applied potentials are versus the SCE; all spectra are referenced to the spectrum of the fully reduced enzyme obtained at a -200 mV applied potential.

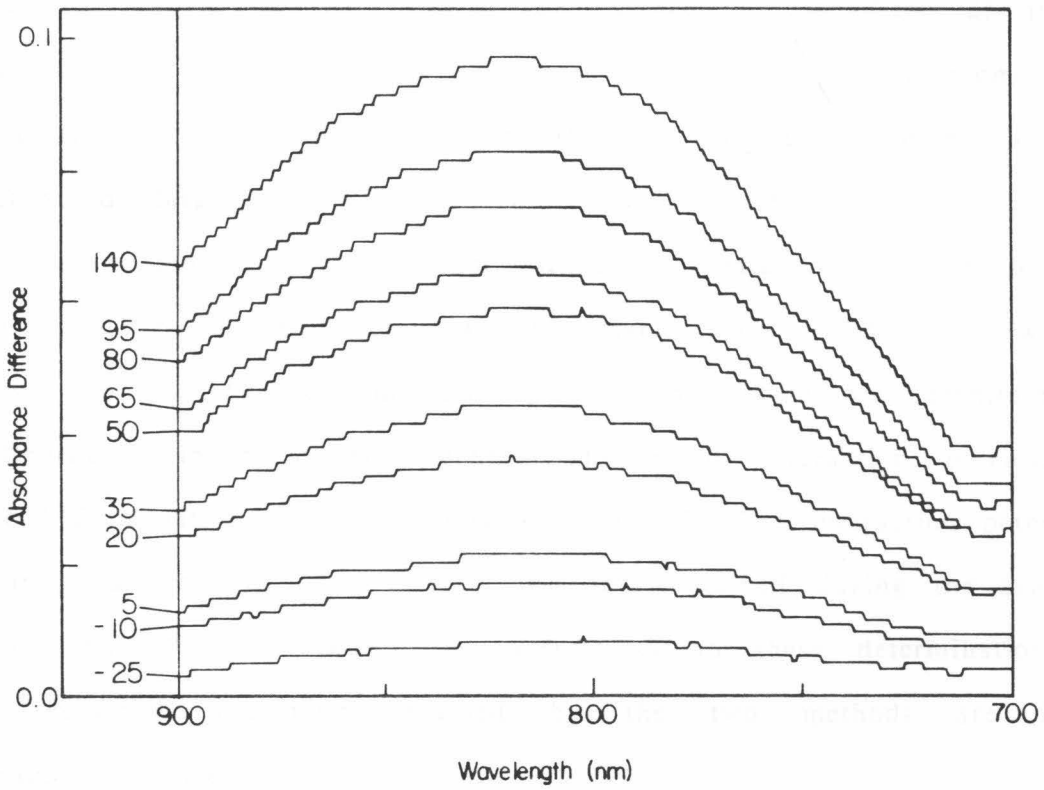
0.1
0.0
Absorbance Difference
140
95
80
65
50
35
20
5
-10
-25
900
800
700
Wavelength (nm)

connecting the data points at 900 and 740 nm; this method compensates for changes in baseline slope and offset. The difference spectrum obtained during the high-potential half of the titration (140 to 35 mV) was not significantly different from that obtained during the low-potential half of the titration (35 to -200 mV, spectra not shown), indicating that the properties of the chromophore did not change during the course of the titration. A change in the shape of the spectrum would be expected, for example, if reduction of cytochrome a (whose reduction potential is close to that of Cu_A under these conditions) caused a large change in the structure of the Cu_A site.

A Nernst plot of the absorbance differences measured in the same titration is shown in Figure 14. The same type of behavior was observed in the Fe_a chromophore at 604 nm, which was monitored simultaneously in these experiments. The mean interaction potential deduced from fits of the Cu_A data was 39 mV. The interaction potential inferred from the fits to the Fe_a data obtained during the same titration was 42 mV. Given the uncertainty in these determinations, the interaction potentials obtained by the two methods are in satisfactory agreement.

The CO-inhibited cytochrome oxidase system is well-suited, because of its simplicity, to the study of interactions between cytochrome a and Cu_A. Various alternatives to intramolecular site-site interactions may be proposed to explain non-Nernstian behavior, including electrostatic effects within a membrane-like aggregate (63) or intradimeric interactions (27). It is therefore important to test a particular interaction model in every way possible and verify that

Figure 14. Nernst plot of the absorbance changes measured during the titration of Figure 13. The line through the data points is the computer-generated best fit appropriate to the interaction model described in the text. (Open circles) Oxidation; (filled circles) re-reduction.

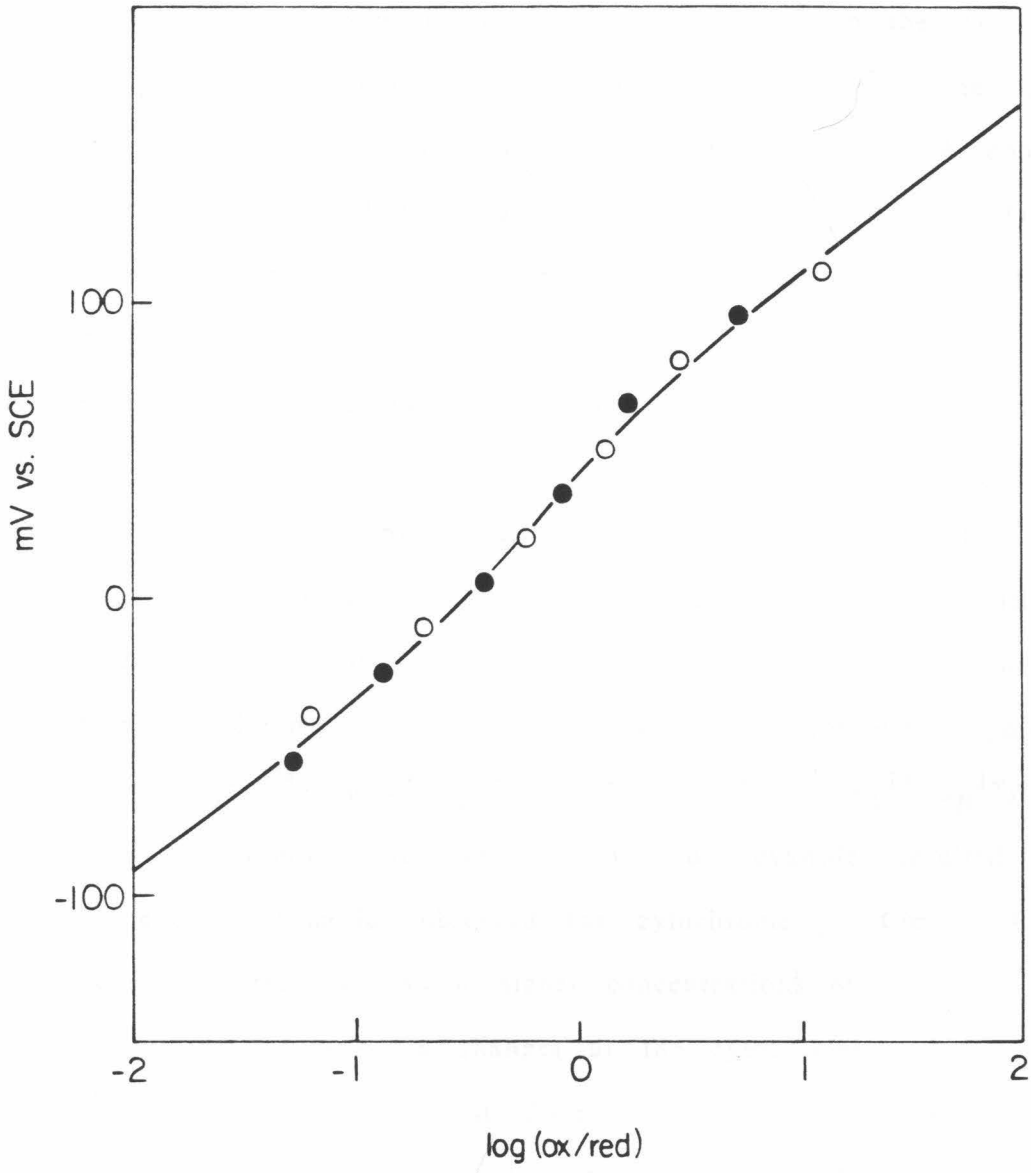
100
0
-100
mV vs. SCE
-2
-1
0
1
2
log (ox/red)

the data are not systematically at variance with the predictions of the model. The data obtained in this study are consistent with the proposed Cu_A/Fe_a interaction model in two key respects: first, the interaction potential ΔE inferred from the data on the iron site is the same, within experimental error, as that inferred from the data on the copper site; and second, the potentials of the copper site that are inferred from the computer fits to the iron data, while poorly determined by the fits and thus subject to considerable variation from one experiment to another, are in agreement with the Cu_A potentials determined directly from the copper data.

Interaction between cytochrome a and Cu_B. In cyanide-inhibited cytochrome oxidase, cytochrome a_3 remains oxidized, while Cu_B can undergo oxidoreduction. Thus, only half (states 1-3,5,6,8,10,13) of the redox states in Figure 8 need be considered in a redox titration. Figure 15 displays a Nernst plot (1.0 mM KCN) for the cytochrome a spectral data at 442 nm (not shown) for which the interaction potential (i.e., $E^{o\prime}(Fe_a{}^{3+/2+})/Cu_A{}^{2+}Cu_B{}^{2+}$ vs. $E^{o\prime}(Fe_a{}^{3+/2+})/Cu_A{}^{1+}Cu_B{}^{1+}$) is 75 ± 3 mV. Submillimolar concentrations of cyanide resulted in decreased interactive behavior observed for cytochrome a. Control EPR experiments showed that the much higher concentrations of cyanide (100 mM) used previously (42) cause changes at the cytochrome a_3/Cu_B site which suggest that copper is lost from this site. The EPR results (obtained at 9-15 ^{o}K) of Goodman (49) also provide evidence that Cu_B interacts with cytochrome a; the magnitude of this interaction was estimated to be 50 mV, in fair agreement with our estimate of 35 mV.

Interaction between cytochrome a and cytochrome a_3. Published

Figure 15. Nernst plot calculated from overlay absorbance spectra (at 442 nm) of cytochrome a in a thin-layer spectroelectrochemical titration of cyanide-inhibited cytochrome c oxidase. Conditions: sample temperature 6.5 ^{o}C, 1.00 mM KCN, pH 7.0, 0.245 M ionic strength. The solid line is a computer-generated best fit to a model in which cytochrome a participates in anticooperative interactions (75 mV) with Cu_A and Cu_B. (Open circles) Oxidation; (filled circles) rereduction. The KCN concentration quoted above is the amount of KCN added to the enzyme solution and hence is greater than the actual concentration of cyanide present during the experiment (due to loss of HCN).

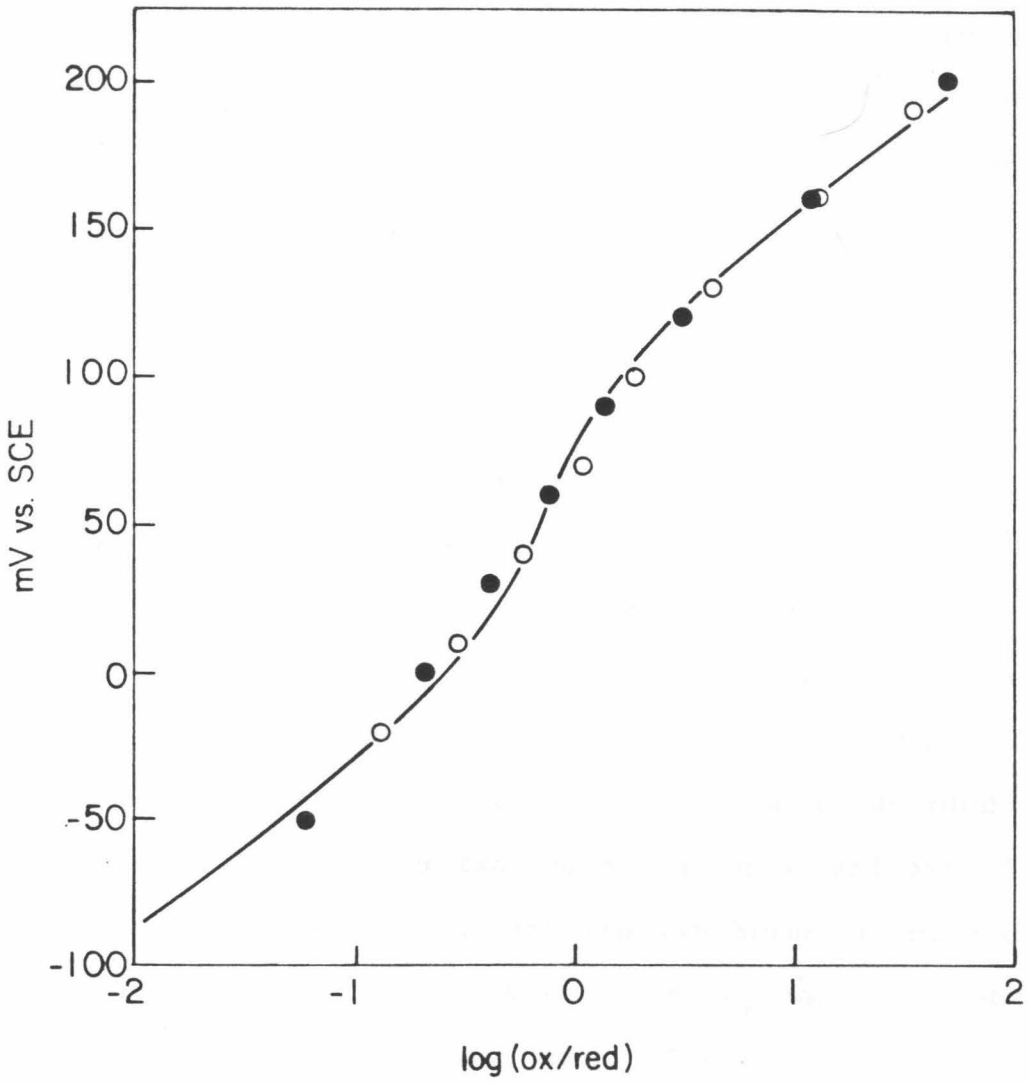
200
150
100
50
0
-50
-100
mV vs. SCE
-2
-1
0
1
2
log (ox/red)

difference spectra for reduced minus oxidized cytochrome a and a_3 (22, 62) were used to estimate the individual contributions of these cytochromes to the absorbance differences measured at each applied potential. The method of deconvolution is described in greater detail in the Materials and Methods section. A significant enzyme batch dependence was observed in several properties of native oxidase in spectroelectrochemical titrations. Absorbance difference spectra obtained during thin-layer experiments (10 ^{o}C, pH 7.66) on two different batches of the enzyme are shown in Figure 16. In the insets to this figure, the absorbance changes at 443 nm and 605 nm are correlated. Since the two cytochromes make very different contributions to the 443 and 605 nm absorptions, a plot of ΔA_{443} vs. ΔA_{605} facilitates characterization of the titration behavior of the individual cytochromes. The dashed lines in the figure insets represent the behavior expected if the two cytochromes titrate at well-resolved potentials (a at a high potential, and a_3 at a lower potential). These lines were obtained by using the spectral assignments described previously, namely, 72% of the α band to cytochrome a, and 65% of the Soret band to cytochrome a_3. If the two cytochromes titrate together at all potentials, the plot of ΔA_{443} vs. ΔA_{605} will be a straight line connecting the extreme data points. Further discussion of the batch dependence is deferred to Chapter V.

Nernst plots for the titration of cytochromes a and a_3 in native cytochrome oxidase are displayed in Figure 17 for both enzyme batches studied. Under all conditions, the titration behavior of both cytochromes was very different from that expected for one-electron

Figure 16. Absorbance difference spectra obtained during spectroelectrochemcal titrations of two different batches of detergent-solubilized cytochrome c oxidase. The indicated potentials are vs. SCE. In the insets, the absorbance changes at 605 nm are plotted as functions of the absorbance changes at 443 nm. The dashed lines in the insets correspond to the behavior anticipated if the cytochromes titrate at well-resolved potentials (cytochrome a at the higher potential). Sample conditions: 10 ^{o}C, pH 7.66, 90 mM phosphate buffer. Panels A and B display data for Batch A and Batch B, respectively.

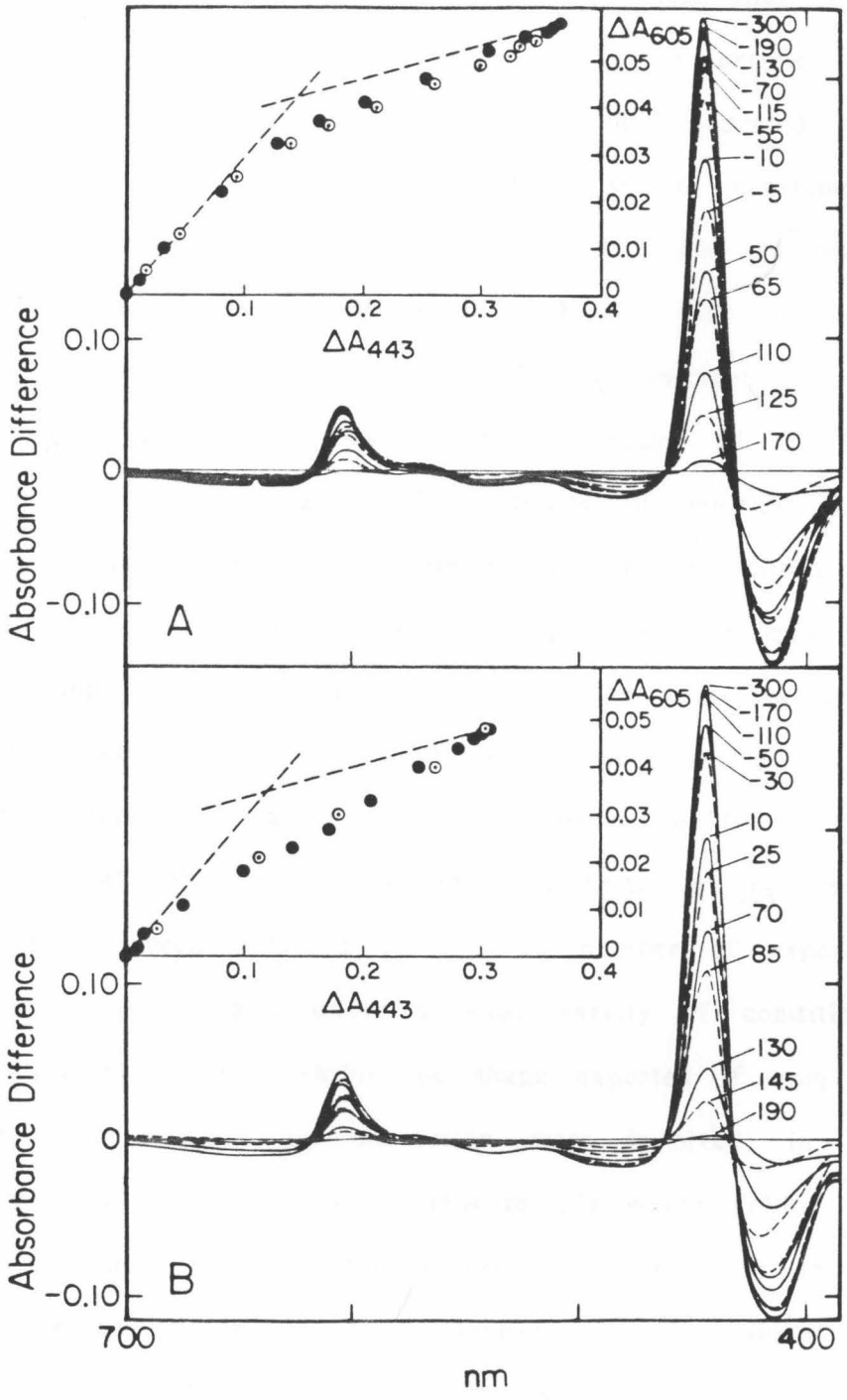
ΔA605
0.05
0.04
0.03
0.02
0.01
0
0.1
0.2
0.3
0.4
ΔA443
-300
-190
-130
-70
-115
-55
-10
-5
50
65
110
125
170
0.10
0
-0.10
Absorbance Difference
A
ΔA605
0.05
0.04
0.03
0.02
0.01
0
0.1
0.2
0.3
0.4
ΔA443
-300
-170
-110
-50
30
10
25
70
85
130
145
190
0.10
0
-0.10
Absorbance Difference
B
700
400
nm

acceptors. The average slope of the observed Nernst plots near the 50% saturation region corresponds to n values less than 1.0, indicating that the interactions are anticooperative. At extreme values of log(Ox/Red), the Nernst plots approach $n = 1$ behavior, as expected.

The data in Figure 17 and data from similar experiments under various conditions were fitted to a simplified interaction model which assumes that the titration behavior of each site may be satisfactorily described in terms of a single effective interaction, cytochrome a/(Cu_A Cu_B cytochrome a_3). This interaction model, while not exact in the present situation owing to the presence of multiple interactions, nevertheless generates acceptable estimates of the asymptotic high and low potentials of the cytochromes, judging from the quality of the fits (as exemplified in Figure 17). This analysis may be used to estimate the magnitude of the total interaction expressed at a given site. The interaction manifested at cytochrome a (ca. 110 mV) is approximately 40 mV greater than that manifested at a_3 (ca. 70 mV). This result has been obtained in a large number of experiments, in both enzyme batches, and under a wide variety of conditions. Also, the Nernst plots do not exhibit the shape expected if only a mutual cytochrome a/cytochrome a_3 interaction were involved; in this case, the Nernst plot for cytochrome a (Figure 17) would follow the upper asymptote for more of the titration before crossing over to the lower asymptote, especially in Batch A (conversely, the Nernst plot for cytochrome a_3 would follow the lower asymptote more closely). These results demonstrate that interaction between cytochromes a and a_3 is not the only source of their unusual titration behavior, implying

Figure 17. Nernst plots for cytochromes $\underline{a}$ (circles) aand $\underline{a}_3$ (squares) obtained by deconvolving spectral changes observed in the spectroelectrochemical titrations shown in Figure 16. The solid points were obtained on oxidation and the open points upon rereduction. The solid lines are computer-generated fits of the data to the interaction model described in the text. Sample conditions as in Figure 16. Left panel: Batch A; right panel: Batch B.

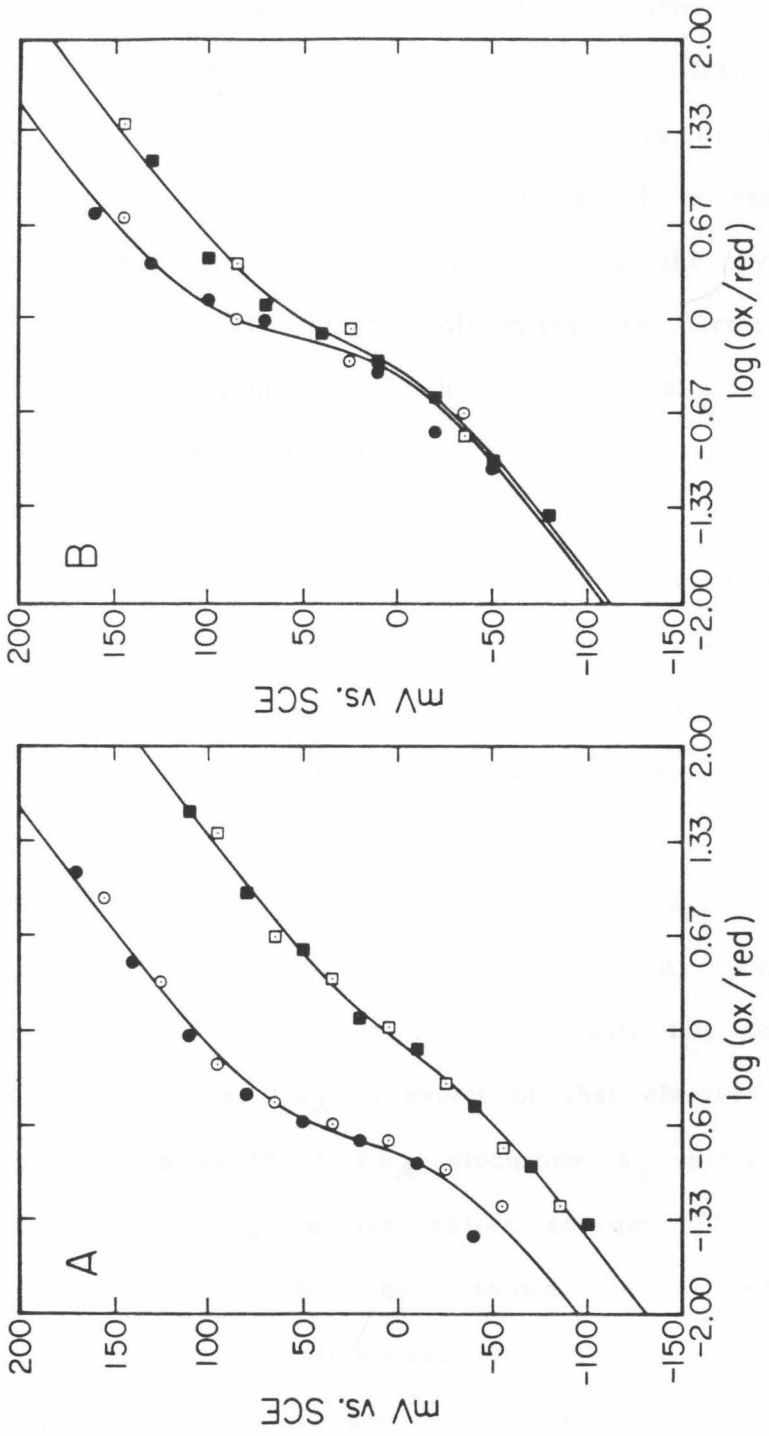
A
B
mV vs. SCE
log (ox/red)
200
150
100
50
0
-50
-100
-150
-2.00
-1.33
-0.67
0
0.67
1.33
2.00

significant interactions which involve copper sites in the enzyme.

Site-site interactions in cytochrome oxidase: résumé. It is clear that the "neoclassical" model cannot explain the titration behavior previously discussed. The computer-generated best fits to the data in Figures 11, 15, and 17 are displayed in Figure 18 to emphasize the observation that the interaction potential seen in the cytochrome a Nernst plots increases as the number of interacting partners increases (see Figure 1 for comparison). From the present results, it cannot be stated with certainty that the anticooperative interactions are simply additive, but this does appear to be a possibility.

Given that only a fraction of the 70 mV of interaction expressed at cytochrome a_3 is due to cytochrome a, a new interaction involving cytochrome a_3 must be proposed. The interaction parameters indicate that cytochrome a_3 interacts with a site whose potential is close to its own, and thus very different from that of cytochrome a. This interaction may in principle involve either Cu_A or Cu_B, but the latter is suggested for reasons of close proximity (3-5 Å). Careful titrations of the Cu_A site in the native enzyme will test this proposal, since interactive behavior at Cu_A in excess of that observed in the CO derivative should be observed if Cu_A/cytochrome a_3 interaction occurs. Published titrations of Cu_A in the native enzyme (37), as well as additional experimental results not shown here, indicate that significant additional interactions are not manifested at Cu_A.

An interaction scheme to account for all of the presently available data is displayed in Figure 19. All of the proposed interactions are anticooperative and will have the effect of buffering the redox state

Figure 18. Nernst plots for cytochrome a illustrating the manifestations of interactions with Cu_A, Cu_B, and cytochrome a_3. The plots shown in the panels are the computer-generated nonlinear best fits to the data presented in Figures 11, 15, and 17 (in descending order). The magnitudes of the interacting potentials are: panel (A), 40 mV; panel (B), 75 mV; and panel (C), 110 mV. The dashed lines are n = 1 asymptotes.

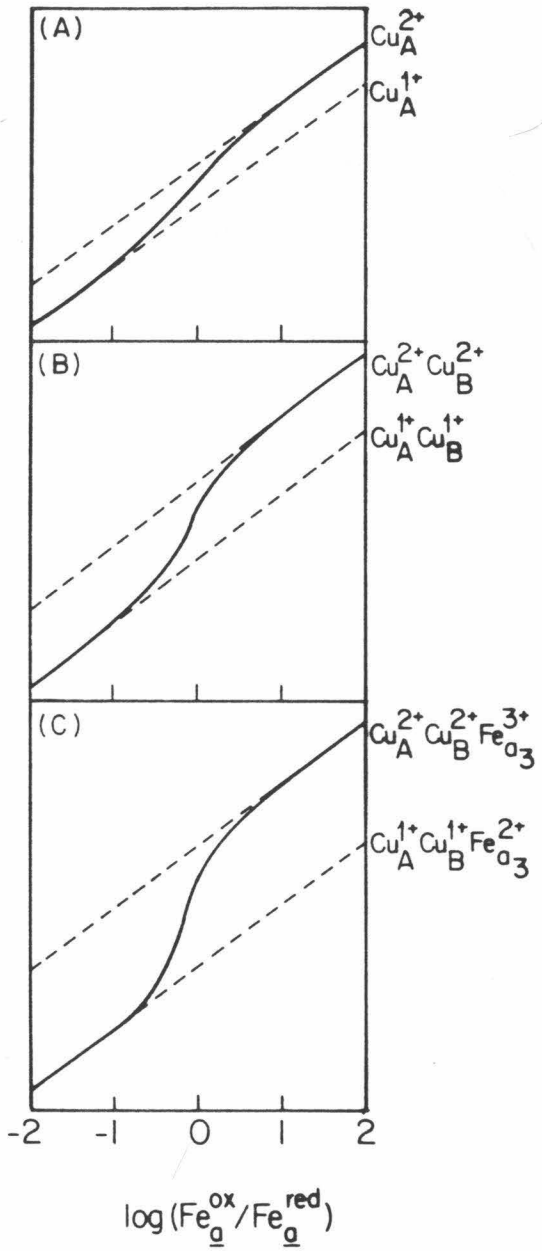
(A)
Cu_A^{2+}
Cu_A^{1+}
(B)
$Cu_A^{2+}Cu_B^{2+}$
$Cu_A^{1+}Cu_B^{1+}$
(C)
$Cu_A^{2+}Cu_B^{2+}Fe_{a_3}^{3+}$
$Cu_A^{1+}Cu_B^{1+}Fe_{a_3}^{2+}$
-2
-1
0
1
2
$\log(Fe_{\underline{a}}^{ox}/Fe_{\underline{a}}^{red})$

Figure 19. Proposed interaction scheme to account for available data on CO-inhibited, cyanide-inhibited, and native cytochrome c oxidase. The negative signs indicate that all of the proposed interactions are anticooperative.

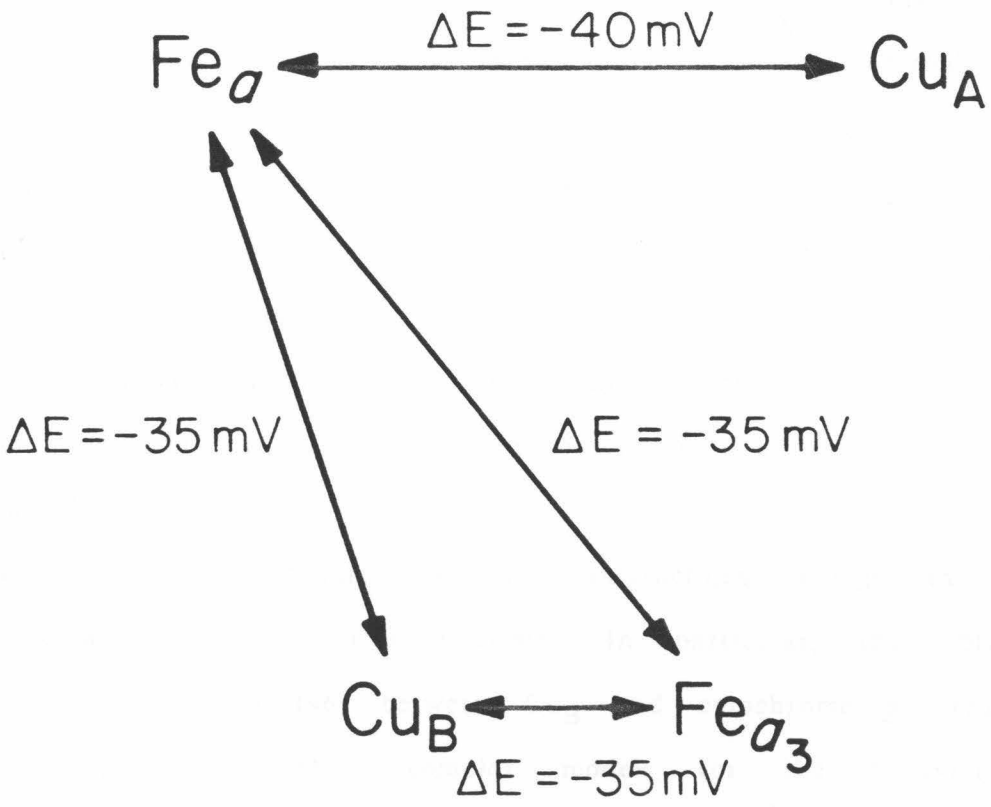
ΔE = -40 mV
Fe$_a$
Cu$_A$
ΔE = -35 mV
ΔE = -35 mV
Cu$_B$
Fe$_{a_3}$
ΔE = -35 mV

of the enzyme, so that the number of electrons which it contains will depend less sensitively on the potential of its environment than would otherwise be the case. The mechanism of the site-site interactions is not clear. It may be electrostatic (64) in nature. However, the long distances indicated in Figure 7, which are inferred from EPR measurements (65), make 40 mV electrostatic interactions seem unlikely. Alternatively, the allosteric interactions may be conformationally linked. Since a conformational change is evidently associated with the reduction of cytochrome a (66,67), it is tempting to associate a cytochrome a-linked conformational change with the changes in the potentials of the other sites. Close examination of the lineshape of the Cu_A EPR resonance shows that one of its g values shifts slightly (by approximately 3G at X-band) upon reduction of Fe_a (65). This indicates that reduction of Fe_a does induce a minor structural change at the Cu_A site.

The effects of optically manifested interactions amongst the sites have been ignored in this analysis. In particular, the optically manifested interaction (46) between Cu_B and cytochrome a_3 requires closer consideration. More complex models for the behavior of cytochrome oxidase in redox titrations that take explicit account of optical interactions would necessarily introduce more adjustable parameters and assumptions into the analysis. Given the evident complexity of the enzyme, such an extended model should probably await support from measurements using other techniques, such as resonance Raman spectroelectrochemistry. In the meantime, the present study furnishes the most detailed and precise information presently

available on the equilibrium redox behavior of any allosteric multi-site metalloenzyme.

REFERENCES

1. Flanagan, J.B., Margel, S., Bard, A.J., and Anson, F.C. (1978) *J. Am. Chem. Soc.* **100**, 4248.

2. Flanagan, J.B., (1978) Ph.D. Thesis, California Institute of Technology.

3. Sweeney, W.V., and McIntosh, B.A. (1979) *J. Biol. Chem.* **254**, 4499.

4. Debey, P., and Balny, C. (1978) *Biochem. Soc. Trans.* **6**, 1289.

5. Hill, T.L. (1985) *Cooperativity Theory in Biochemistry*, Springer-Verlag, New York.

6. Kurganov, B.I. (1982) *Allosteric Enzymes*, Wiley, Chichester, U.K.

7. Perlmutter-Hayman, B. (1986) *Accts. Chem. Res.* **19**, 90.

8. Edsall, J.T., and Gutfreund, H. (1983) *Biothermodynamics*, Wiley, Chichester, U.K.

9. Cornish-Bowden, A., and Koshland, D.E., Jr. (1975) *J. Mol. Biol.* **95**, 201.

10. Malmström, B.G. (1974) *Quart. Rev. Biophys.* **6**, 389.

11. Hill, A.V. (1910) *J. Physiol.* **40**, iv.

12. Blair, D.F., Ellis, W.R., J.R., Wang, H., Gray, H.B., and Chan, S.I. *J. Biol. Chem.*, accepted for publication.

13. Crutchley, R.J., Ellis, W.R., Jr., and Gray, H.B. (1985) *J. Am. Chem. Soc.* **107**, 5002.

14. Crutchley, R.J., Ellis, W.R., Jr., and Gray, H.B. (1986) in *Frontiers in Bioinorganic Chemistry*, Xavier, A.V., ed., VCH Verlagsgesellschaft, Weinheim, F.R.G., p. 679.

15. Marcus, R.A., and Sutin, N. (1975) *Inorg. Chem.* **14**, 213.

16. Brown, G.M., and Sutin, N. (1979) *J. Am. Chem. Soc.* **101**, 883.

17. Nocera, D.G., Winkler, J.R., Yocom, K.M., Bordignon, E., and Gray, H.B. (1984) *J. Am. Chem. Soc.* **106**, 5145.

18. Takano, T. (1977) *J. Mol. Biol.* **110**, 537; 569.

19. Takano, T., and Dickerson, R.E. (1981) *J. Mol. Biol.* **153**, 79; 95.

20. Ellis, W.R., Jr., Wang, H., Blair, D.F., Gray, H.B., and Chan, S.I. (1986) *Biochemistry* **25**, 161.

21. Wang, H., Blair, D.F., Ellis, W.R., Jr., Gray, H.B., and Chan, S.I. (1986)

Biochemistry **25**, 167.

22. Blair, D.F., Martin, C.T., Gelles, J., Wang, H., Brudvig, G.W., Stevens, T.H, and Chan, S.I. (1983) *Chem. Scr.* **21**, 43.

23. Stevens, T.H., Martin, C.T., Wang, H., Brudvig, G.W., Scholes, C.P., and Chan, S.I. (1982) *J. Biol. Chem.* **257**, 12106.

24. Scott, R.A., Schwartz, J.R., and Cramer, S.P. (1984) in *EXAFS and Near Edge Structure III*, Hodgson, K.O., Hedman B., and Penner-Hahn, J.O., eds., Springer-Verlag, Berlin, 1984, p. 111.

25. Malmström, B.G. (1980) in *Metal Ion Activation of Dioxygen*, Spiro, T.G., ed., Wiley, New York, p. 181.

26. Brunori, M., Antonini, E., and Wilson, M.T. (1981) *Met. Ions Biol. Syst.* **13**, 187.

27. Wikström, M., Krab, K., and Saraste, M. (1981) *Cytochrome Oxidase: A Synthesis*, Academic Press, London.

28. Wainio, W.W. (1983) *Biol. Rev.* **58**, 131.

29. Freedman, J.A., and Chan, S.H.P. (1984) *J. Bioenerg. Biomembr.* **16**, 75.

30. Gibson, Q.H., and Greenwood, C. (1965) *J. Biol. Chem.* **240**, 2694.

31. Greenwood, C., and Gibson, Q.H. (1967) *J. Biol. Chem.* **242**, 1782.

32. Chance, B., Saronio, C., and Leigh, J.S., Jr. (1975) *J. Biol. Chem.* **250**, 9226.

33. Clore, G.M., Andréasson, L.-E., Karlsson, B., Aasa, R., and Malmström, B.G. (1980) *Biochem. J.* **185**, 139.

34. Antalis, T.M., and Palmer, G. (1982) *J. Biol. Chem.* **257**, 6194.

35. Heineman, W.R., Kuwana, T., and Hartzell, C.R. (1972) *Biochem. Biophys. Res. Commun.* **49**, 1

36. Minnaert, K. (1965) *Biochim. Biophys. Acta* **110**, 42.

37. van Gelder, B.F., van Rijn, J.L.M.L., Schilder, G.J.A., and Wilms, J. (1977) in *Structure and Function of Energy-Transducing Membranes*, van Dam, K., and van Gelder, B.F., eds., Elsevier/North Holland, Amsterdam, p. 61.

38. Tiesjema, R.H., Muijsers, A.O., and van Gelder, B.F. (1973) *Biochim. Biophys. Acta* **305**, 19.

39. Schroedl, N.A., and Hartzell, C.R. (1977) *Biochemstry* **16**, 4961.

40. Babcock, G.T., Vickery, L.E., and Palmer, G. (1978) *J. Biol. Chem.* **253**, 2400.

41. Schroedl, N.A., and Hartzell, C.R. (1977) *Biochemistry* **16**, 4966.

42. Kojima, N., and Palmer, G. (1983) *J. Biol. Chem.* **258**, 14908.

43. Wilson, D.F., Lindsay, J.G., and Brocklehurst, E.S. (1972) *Biochim. Biophys. Acta* **256**, 277.

44. Wikström, M.K.F., Harmon, H.J., Ingledew, W.J., and Chance, B. (1976) *FEBS Lett.* **65**, 259.

45. Wilson, D.F., and Leigh, J.S. (1974) *Ann. N.Y. Acad. Sci.* **227**, 630.

46. Blair, D.F., Bocian, D.F., Babcock, G.T., and Chan, S.I. (1982) *Biochemistry* **21**, 6928.

47. Carithers, R.P., and Palmer, G. (1981) *J. Biol. Chem.* **256**, 7967.

48. Artzatbanov, V.Y., Konstantinov, A.A., and Skulachev, V.P. (1978) *FEBS Lett.* **87**, 180.

49. Goodman, G. (1984) *J. Biol. Chem.* **259**, 15094.

50. Erecińska, M., and Wilson, D.F. (1980) *Pharmac. Ther.* **8**, 1.

51. Jensen, P., Wilson, M.T., Aasa, R., and Malmström, B.G. (1984) *Biochem. J.* **224**, 829.

52. Wilson, D.F., and Nelson, D. (1982) *Biochim. Biophys. Acta* **680**, 233.

53. Hartzell, C.R., and Beinert, H. (1974) *Biochim. Biophys. Acta* **368**, 318.

54. Lowry, O.H., Rosebrough, N.J., Farr, A.L., and Randall, R.J. (1951) *J. Biol. Chem.* **193**, 265.

55. van Gelder, B.F. (1966) *Biochim. Biophys. Acta* **118**, 36.

56. Pladziewicz, J.R., Meyer, T.J., Broomhead, S.A., and Taube, H. (1973) *Inorg. Chem.* **12**, 639.

57. Cummins, D., and Gray, H.B. (1977) *J. Am. Chem. Soc.* **99**, 5158.

58. Beinert, H., Shaw, R.W., Hansen, R.E., and Hartzell, C.R. (1980) *Biochim. Biophys. Acta* **591**, 458.

59. Greenwood, C., Wilson, M.T., and Brunori, M. (1974) *Biochem. J.* **137**, 205.

60. Anderson, J.L., Kuwana, T., and Hartzell, C.R. (1976) *Biochemstry* **15**, 3847.

61. Horie, S., and Morrison, M. (1963) *J. Biol. Chem.* **238**, 2859.

62. Vanneste, W.H., and Vanneste, M.-T. (1965) *Biochem. Biophys. Res. Commun.* **19**, 182.

63. Walz, D. (1979) *Biochim. Biophys. Acta* **505**, 279.

64. Krishtalik, L.I. (1975) *Arch. Biochem. Biophys.* **243**, 701.

65. Brudvig, G.W., Blair, D.F., and Chan, S.I. (1984) *J. Biol. Chem.* **259**, 11001.

66. Cabral, F., and Love, B. (1972) *Biochim. Biophys. Acta* **283**, 181.

67. Urry, D.W., Wainio, W.W., and Grebner, D. (1972) *Biochem. Biophys. Res. Commun.* **27**, 625.

CHAPTER V

FURTHER SPECTROELECTROCHEMICAL STUDIES OF CYTOCHROME C OXIDASE

INTRODUCTION

In the previous chapter, two important consequences of the juxtaposition of two or more redox centers within a protein were illustrated: temperature, possibly leading to different entropies of reduction for different sites; and allosteric behavior in some instances, leading to Nernst plots exhibiting unusual slopes. The data presented in Chapter four clearly indicate that the equilibrium redox behavior of cytochrome oxidase is considerably more complex than that suggested by the "neoclassical" model.

In order to more completely characterize the thermodynamic properties of the spectrally visible metal centers of cytochrome oxidase, a series of spectroelectrochemical experiments, employing a variety of conditions of temperature, pH, and ionic strength, are reported here. These results, taken from References 1-3, are discussed with respect to the mechanisms of electron transfer and proton pumping by the enzyme.

MATERIALS AND METHODS

Spectroelectrochemical experiments were carried out as described in Chapter IV. Phosphate buffer was used because the pH of phosphate, unlike that of Tris (which is more commonly used), is relatively insensitive to temperature (4). The pH dependences of the cytochrome potentials were determined in phosphate buffer with the concentration adjusted to maintain a constant ionic strength. For measurements of the effect of ionic strength, the ionic strength was adjusted by changing the phosphate concentration, except where noted. Horse heart

cytochrome c (Sigma Type VI) was chromatographically purified on Whatman CM-52 cellulose prior to use.

Standard entropies of reduction were obtained from the slopes of plots of reduction potential vs. temperature, as described earlier. The reported error estimates in $\Delta G^{0\prime}$, $\Delta H^{0\prime}$, and $\Delta S^{0\prime}$ are derived from the standard errors of determination of the relevant parameters in linear least-squares fits.

The equilibrium equations appropriate to a two-site interactive system were used in a nonlinear curve-fitting program to obtain estimates of the asymptotic potentials of the metal centers, and hence estimates of the total interaction potential influencing each site. The equilibration times required (ca. two hours for each potential) were significantly longer for the experiments on Cu_A and the cytochromes in the native enzyme than for cytochrome a in CO-inhibited cytochrome oxidase; a complete (oxidative and reductive) titration required up to 48 hours. Hence some degree of irreversibility was noted in the titrations above 22 ^{o}C, probably owing to aggregation and/or denaturation of the enzyme. The total absorbance change accompanying oxidation was used in calculating log(Ox/Red) for an oxidative titration, and the total absorbance change accompanying rereduction was used in calculating log(Ox/Red) for the rereduction, thus partially compensating for irreversibility in the absorbance changes. Because of the way in which the titrations were carried out (oxidation followed by rereduction), the higher asymptotic potentials were more accurately determined. The time elapsing between the oxidative and corresponding reductive titrations, and the observed discrepancy between them, was

greater at the lower applied potentials. In most cases, both of the asymptotic potentials, and thus the total interaction potential, could be satisfactorily estimated.

The potentials reported herein are those that pertain when the interacting partners are oxidized; in the present situation, where the proposed interactions are anticooperative, these are the higher of the two asymptotic potentials which may be taken on by a metal site in the enzyme. The potentials defined in this manner are meaningful measures of the intrinsic thermodynamic properties of the redox centers, because they refer to a single, specific set of conditions with regard to the interactions that influence the reduction potential of a center. The redox steps in Figure 8 of Chapter IV to which the asymptotic potentials for each of the sites discussed herein correspond are given in Table I.

RESULTS AND DISCUSSION

Cu_A in CO-Inhibited Cytochrome Oxidase. The values of $E^{0\prime}(Cu_A)$ measured at various temperatures between 1 and 29 ^{o}C are plotted in Figure 1. The thermodynamic quantities deduced from a linear least-squares fit to the data are (relative to the NHE): $\Delta G^{0\prime}(25\ ^{o}C)$ = -6.64 ± 0.08 kcal/mol, $\Delta H^{0\prime}$ = -21.1 ± 0.7 kcal/mol, and $\Delta S^{0\prime}$ = -48.7 ± 2.3 eu. The mean interaction potential deduced from the fits to the Cu_A data is 39 mV and is independent of temperature within the standard error of the determinations.

The standard entropy of reduction of the Cu_A site is compared with those of several other metalloprotein copper sites in Table II. All

Table I. Correlation of asymptotic potentials in Nernst plots for cytochrome a with intramolecular electron transfer steps. See Figure 8 of Chapter IV for a correlation of the numbered cytochrome c oxidase redox states with the oxidation states of the metal centers within the enzyme.

Observed Metal Center	Nernstian Asymptote	Redox States in Enzyme Half-Reaction
Cyt $\underline{a}$ (CO deriv.)	Upper	11 → 15
"	Lower	14 → 16
Cu_A (CO deriv.)	Upper	11 → 14
"	Lower	15 → 16
Cyt $\underline{a}$ (native)	Upper	1 → 3
"	Lower	14 → 16
Cyt $\underline{a}_3$ (native)	Upper	1 → 4
"	Lower	13 → 16

Figure 1. Temperature dependence of the reduction potential of Cu_A. The quantity plotted is $E^{0'}(Cu_A)$, the reduction potential of the Cu_A site when Fe_a is oxidized. The straight line through the data points is the computer-generated best fit and leads to the following estimates of the thermodynamic parameters for the reduction of Cu_A (after correction for the isothermal condition under which the experiments were performed): $\Delta G^{0'}(25\ ^{o}C)$ = -6.64 ± 0.08 kcal/mol, $\Delta S^{0'}$ = -48.7 ± 2.3 eu, $\Delta H^{0'}$ = -21.1 ± 0.7 kcal/mol, and $\Delta S_{rc}{}^{0'}$ = -33.1 ± 2.3 eu.

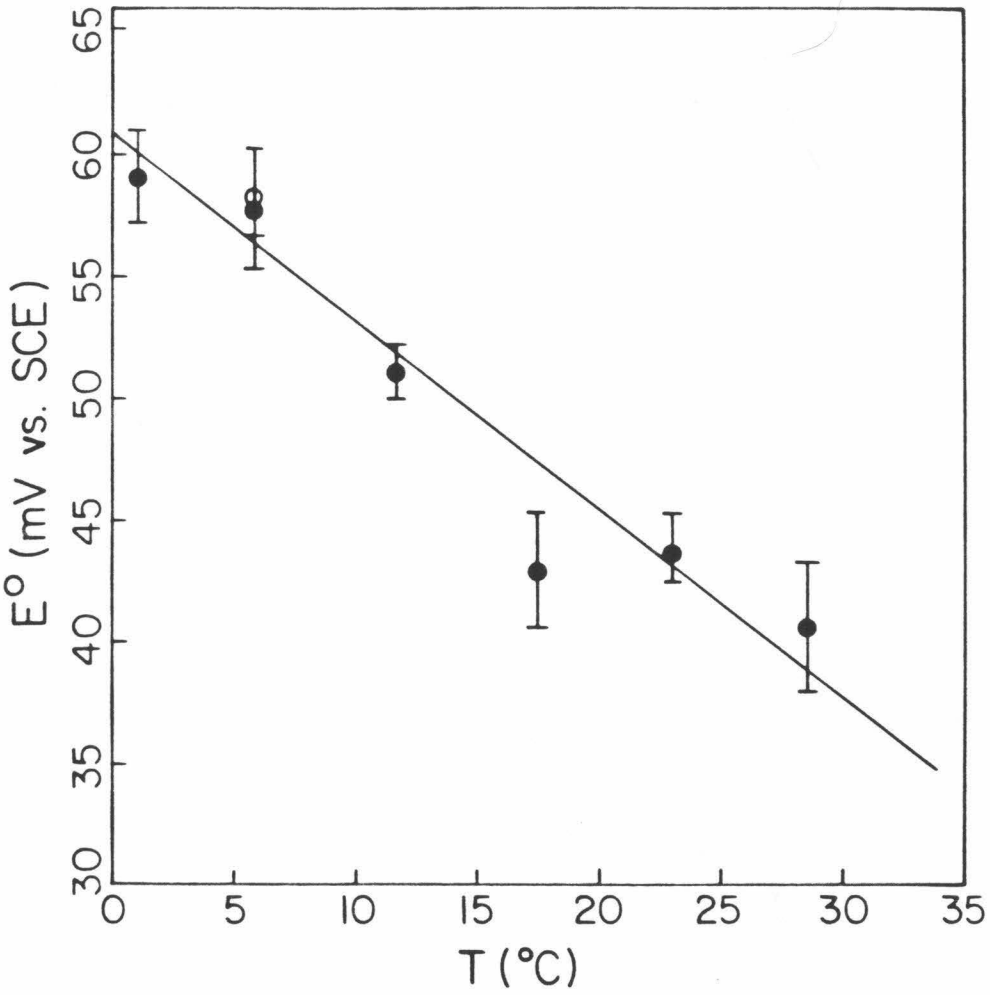
E° (mV vs. SCE)
65
60
55
50
45
40
35
30
0
5
10
15
20
25
30
35
T (°C)

Table II. Thermodynamic parameters for the reduction of metalloprotein copper sites.

Protein	$\Delta G^{o'}$ (kcal/mol)[a]	$\Delta S^{o'}$ (eu)	$\Delta H^{o'}$ (kcal/mol)
Azurin (*P. aeruginosa*)[b,e]	-7.10	-31.7	-16.6
Azurin (*A. denitrificans*)[b,f]	-6.37	-23.2	-13.3
Azurin (*A. faecalis*)[b,f]	-6.22	-29.6	-15.0
Plastocyanin (*P. vulgaris*)[b,e]	-8.30	-18.0	-13.7
Stellacyanin (*R.vernicifera*)[b,e]	-4.41	-19.8	-10.3
Laccase Type I (*P. versicolor*)[c]	-17.99	-13.9	-22.1
Cytochrome c Oxidase (*Bos taurus* heart)[d]	-6.64	-48.7	-21.1

[a]At 25 °C. All thermodynamic parameters are referenced to the NHE.

[b]Phosphate buffer, ionic strength 0.1 M, pH 7.0.

[c]In 0.2 M phosphate buffer, pH 5.4. Reference 6.

[d]In 0.1 M phosphate buffer, pH 7.0.

[e]Reference 5.

[f]This work (Chapter III).

of the thermodynamic data available for comparison are for the Type 1, or "blue," copper centers (for a review, see Ref. 7). These sites are known to function as electron transfer agents, but they are not involved in energy transduction or conservation. Compared to the Type 1 coppers, the Cu_A site has a relatively large and negative entropy of reduction, 17 eu more negative than that of P. aeruginosa azurin (5), with which it is most nearly comparable. At the pH employed for the azurin study, pH 7.0, it is expected that reduction is partially linked to protonation of an ionizable group in the protein, perhaps His-35 (8,9), so that a component of the observed $\Delta S^{o'}$ may be due to protonation rather than to reduction per se. The reduction potential of Cu_A is weakly if at all pH dependent near pH 7.0 (10), so proteolysis is not expected to contribute to its measured entropy of reduction.

The relatively large entropy change that occurs upon reduction of Cu_A may reflect a substantial protein conformational change, possibly related to a role of the copper site in energy transduction (i.e., proton pumping). Further spectroscopic studies are needed to test this suggestion.

It is not known whether Cu_A is reduced by cytochrome c directly or only via cytochrome a during enzymatic turnover. The standard entropy change that accompanies electron transfer from cytochrome c ($\Delta S^{o'}$ = -28.5 eu) to Cu_A is approximately -20.2 eu, and that accompanying electron transfer from cytochrome a to Cu_A is approximately +2.1 eu (assuming that the entropy of reduction of Cu_A is not greatly changed upon binding of cytochrome c to the oxidase). The standard free

energy change accompanying electron transfer from cytochrome c to Cu_A at physiological temperature, predicted by extrapolation of the present measurements, is -0.40 ± 0.09 kcal/mol.

The Cu_A/cytochrome a interaction is likely to have implications for the behavior of the enzyme during turnover. Because of this interaction, Cu_A and Fe_a will tend to accept only one electron between them, and it will be thermodynamically less likely for both sites to be reduced simultaneously. The reduction potential of Fe_a is substantially increased upon oxidation of the cytochrome a_3/Cu_B site (compare Figures 11 and 17 of Chapter IV), so the effective reduction potential of Fe_a will probably be significantly greater than that of Cu_A under turnover conditions (where the cytochrome a_3/Cu_B site is mostly oxidized). If electron transfer between Cu_A and Fe_a is very rapid, so that these sites are at redox equilibrium with each other, this would mean that the Cu_A/Fe_a redox interaction will not be manifested as a splitting of their reduction potentials as is observed in the present experiments. The first electron into these sites would transfer rapidly to Fe_a and reside on this site most of the time. The Cu_A site would not be substantially reduced until the transfer of a second electron into these sites; in this case, the pertinent reduction potential of the Cu_A site will be the lower of the two measured here. However, the electron transfer between Cu_A and Fe_a is not necessarily as rapid as is sometimes suggested (11,12). The available kinetic data may be interpreted as well if it is postulated instead that Cu_A can accept electrons directly from cytochrome c. The presence of two different functional cytochrome c binding sites on the oxidase (13,14)

and the proximity of Cu_A to residues that are involved in binding cytochrome c (15) are consistent with this proposal. If electron transfer between Fe_a and Cu_A is relatively slow, the Fe_a and Cu_A sites could each take on one of two different effective reduction potentials, depending upon the redox states of their respective interaction partners. Since Fe_a is mostly oxidized in the mitochondrial steady state, the higher of the two potentials measured here will most often be the pertinent potential for Cu_A.

Cytochrome a in CO-Inhibited Cytochrome Oxidase. Although several measurements of the Fe_a reduction potential have been reported (16-18) for the CO derivative of cytochrome oxidase, none has carefully evaluated the effects of pH, temperature, and ionic strength. The available measurements ($E^{o'}$ = 250-255 mV vs. NHE at 24-25 ^{o}C) are in close agreement with the values determined here.

The effect of pH on the reduction potential of Fe_a is shown in Figure 2. A linear least-squares fit to the data yields a slope of -9 mV/pH unit. Significant degradation of the enzyme took place at pH values outside the extremes shown. The observed pH dependence is similar to that observed by Hinkle and Mitchell (19). Cytochrome oxidase is known to function as a proton pump (20,21). The site of redox-linked proton translocation is still unclear, although either cytochrome a or Cu_A is implicated on energetic grounds. Babcock and Callahan (22) suggest, on the basis of resonance Raman data, that the heme *a* formyl group of cytochrome a is involved in a redox-coupled hydrogen-bonding interaction with a proton donor supplied by the enzyme. Such interactions are commonplace among hemoproteins

Figure 2. pH dependence of the cytochrome a reduction potential in CO-inhibited cytochrome oxidase (9.8 ^{o}C, ionic strength 0.245 M). The solid line is a linear least-squares fit to the data, with a slope of -9 mV/pH unit.

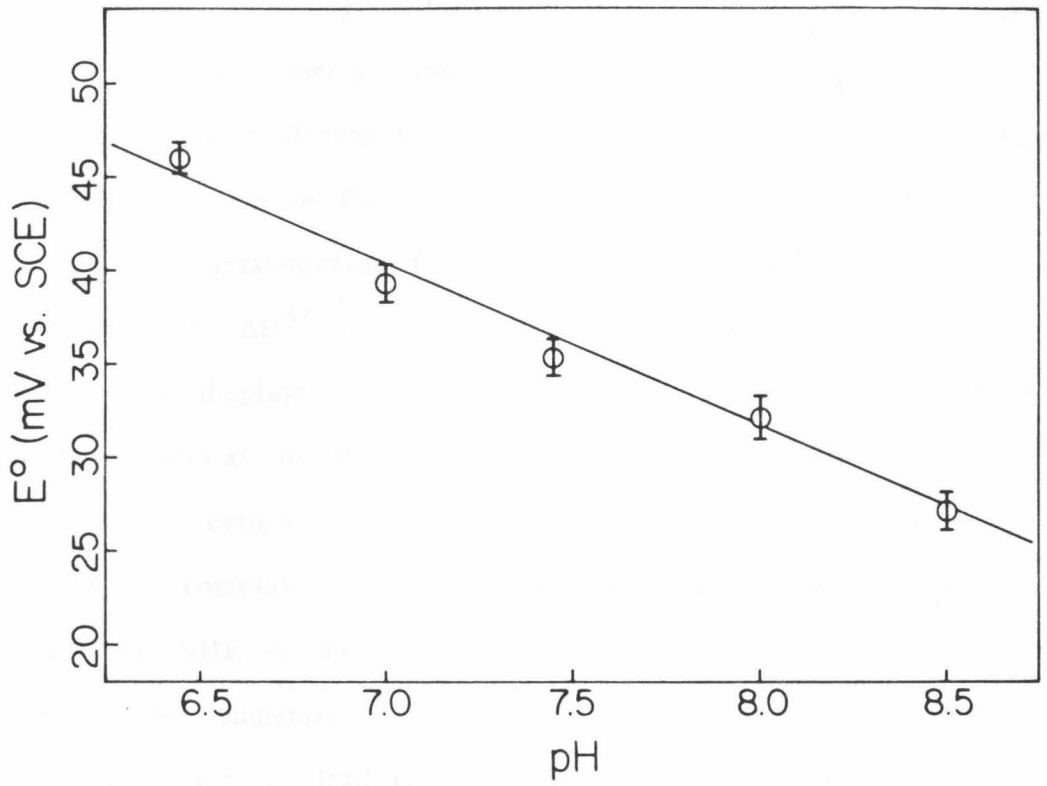
E° (mV vs. SCE)
20
25
30
35
40
45
50
6.5
7.0
7.5
8.0
8.5
pH

containing propionate groups. However, if a strongly redox-linked protonation were occurring at pH 7.4 (the pH where the redox-linked hydrogen-bonding interaction is inferred from the Raman data), one would expect a ca. 56 mV/pH unit change (at 10 ^{o}C) in E^{o}. The data shown in Figure 2 show only a very shallow pH dependence. It should be noted, however, that the lack of a pronounced pH dependence in E^{o}, and hence of a strong redox Bohr effect, does not rule out the possibility that cytochrome a is involved in proton pumping (23).

The temperature dependence of the cytochrome a reduction potential at pH 7.0 is shown in Figure 3. The thermodynamic parameters deduced from a linear least-squares fit to the data are: $\Delta G^{o'}$(25 ^{o}C) = -6.37 ± 0.05 kcal/mol, $\Delta H^{o'}$ = -21.5 ± 0.8 kcal/mol, and $\Delta S^{o'}$ = -50.8 ± 2.8 eu. Figure 4 displays the temperature dependence of the cytochrome a reduction potential in the cytochrome oxidase/cytochrome c complex (2 equivalents of cytochrome c). At 25 ^{o}C, $E^{o'}$ is not significantly different in the complex with cytochrome c than in the uncomplexed enzyme (274 mV vs. NHE in the complex; 276 mV vs. NHE in the uncomplexed enzyme). The temperature dependence is also the same within experimental uncertainty, leading to the following estimates for the thermodynamic parameters: $\Delta G^{o'}$(25 ^{o}C) = -6.32 ± 0.05 kcal/mol, $\Delta H^{o'}$ = -20.3 ± 1.2 kcal/mol, and $\Delta S^{o'}$ = -46.9 ± 3.9 eu.

The large, negative values of $\Delta S^{o'}$ obtained from analyses of the $E^{o'}$ vs. temperature data suggest that reduction of cytochrome a is accompanied by a significant conformational change. Close inspection of Figure 3 reveals that the plot is slightly nonlinear within the estimated experimental error. This nonlinearity indicates that ΔCp^{o} is

Figure 3. Temperature dependence of the cytochrome a reduction potential in CO-inhibited cytochrome oxidase (pH 7.0, ionic strength 0.245 M). The solid line is a linear least-squares fit to the data, corresponding to the following thermodynamic parameters (after correction for partial thermostatting of the reference electrode): $E^{o'}(25\ ^{o}C)$ = 276 ± 3 mV vs. NHE, $\Delta G^{o'}(25\ ^{o}C)$ - -6.37 ± 0.08 kcal/mol, $\Delta H^{o'}$ = -21.5 ± 0.8 kcal/mol, $\Delta S^{o'}$ = -50.8 ± 2.8 eu, and $\Delta S_{rc}^{o'}$ = -35.2 ± 2.8 eu.

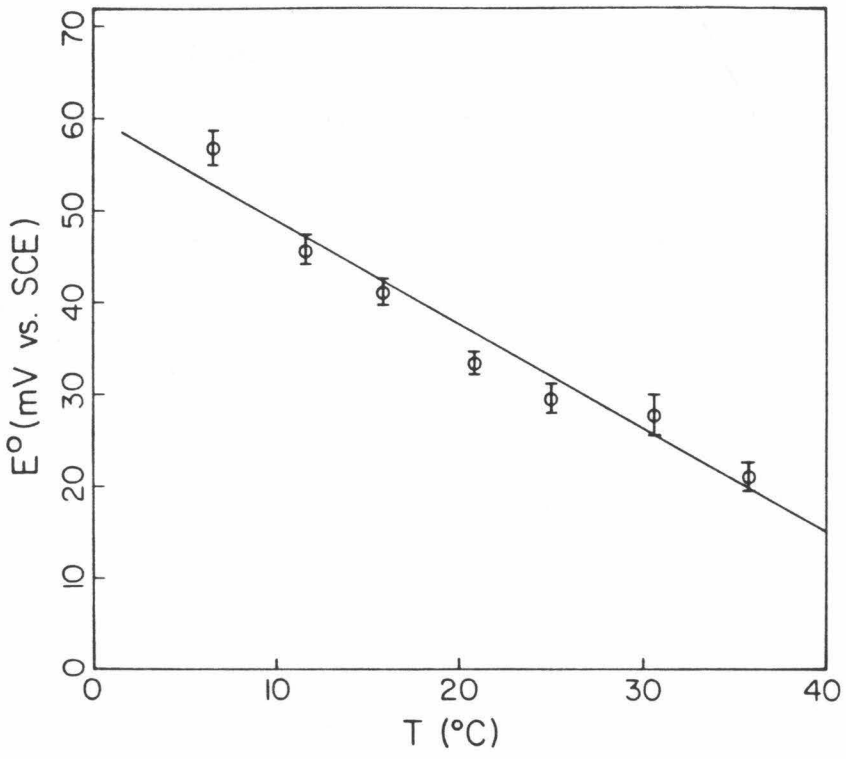
E°(mV vs. SCE)
0
10
20
30
40
50
60
70
0
10
20
30
40
T (°C)

Figure 4. Temperature dependence of the cytochrome a reduction potential in CO-inhibited cytochrome oxidase and in the presence of 2 equivalents of horse heart cytochrome c. The solid line is a linear least-squares fit to the data, corresponding to the following thermodynamic parameters (after correction for partial thermostatting of the reference electrode): $E^{o\prime}(25\ ^{o}C)$ = 274 ± 3 mV vs. NHE, $\Delta G^{o\prime}(25\ ^{o}C)$ = -6.32 ± 0.08 kcal/mol, $\Delta H^{o\prime}$ = -20.3 ± 1.2 kcal/mol, and $\Delta S^{o\prime}$ = -46.9 ± 3.9 eu. Solution conditions as in Figure 3.

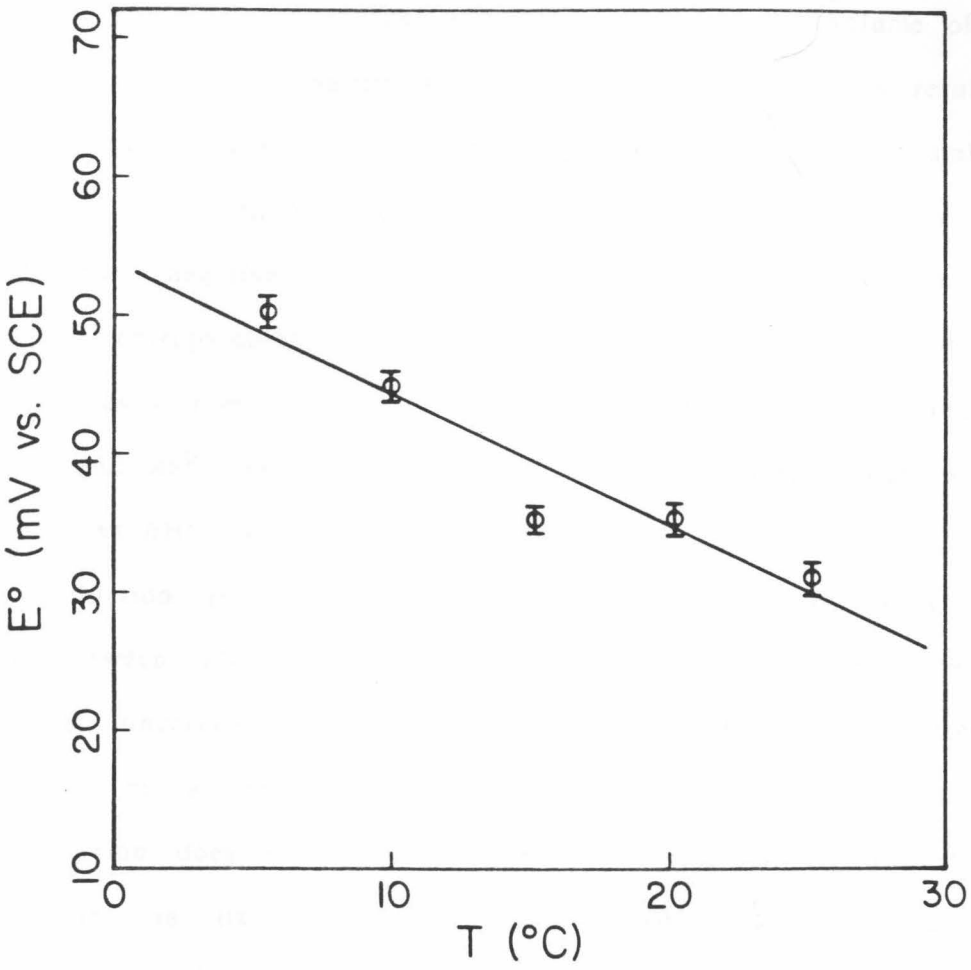
E° (mV vs. SCE)
70
60
50
40
30
20
10
0
10
20
30
T (°C)

not negligible. A value for the standard heat capacity change is not reported here since this quantity can only be reliably estimated from calorimetric reaction heats obtained at several temperatures. Note, however, that a non-negligible ΔCp^{o} is consistent with a conformational change (25). It is known that reduction of cytochrome oxidase causes ORD spectral changes (24) and an increase in the volume of the enzyme (26). The $\Delta H^{o'}$ values are negative, most likely as a result of favorable metal-to-ligand π back-bonding, which tends to stabilize Fe(II). The redox thermodynamic parameters reported here are substantially more negative than those for small low-spin cytochromes (5, 27-29). An entropy-enthalpy compensation effect has been noted (30) for c-type cytochromes. This situation also holds for cytochrome a; the $\Delta H^{o'}$ and $\Delta S^{o'}$ values deduced from Figure 3 correlate well with a plot of $\Delta S^{o'}$ vs. $\Delta H^{o'}$ for c-type cytochromes.

The reduction potential of Fe_a was measured at different ionic strengths between 0.05 and 0.42 M, as illustrated in Figure 5. Within experimental uncertainty, no ionic strength dependence was observed. The absence of a measurable ionic strength dependence suggests that charge solvation does not play a large direct role (as opposed to an indirect role via its effect upon the overall conformation of the enzyme) in determining the reduction potential of cytochrome a. Spin label-spin probe studies employing dysprosium compounds (31) suggest that the heme of cytochrome a is less accessible to the solvent than the heme of cytochrome c. The absence of any significant effect of complex formation upon the reduction potential of cytochrome a is consistent with the suggestion that the aqueous solvent plays a

Figure 5. Ionic strength dependence of the cytochrome a reduction potential in CO-inhibited cytochrome oxidase (9.8 ^{o}C, pH 7.0). The ionic strength was raised with phosphate buffer, supplemented with KCl for the 0.42 M point.

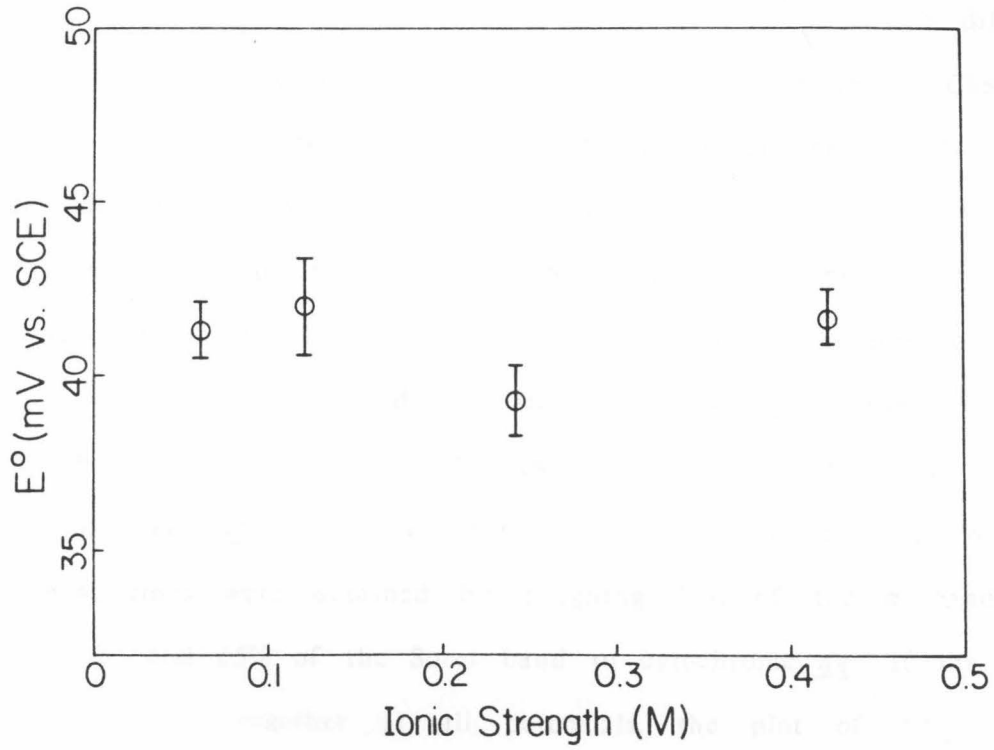
E° (mV vs. SCE)
50
45
40
35
0
0.1
0.2
0.3
0.4
0.5
Ionic Strength (M)

relatively small direct role in tuning the cytochrome a potential, and may in fact be the physiologically desirable consequence of "designing" the enzyme so that the cytochrome a reduction potential is not very sensitive to the immediate solvent environment.

Cytochromes a and a_3 in the Native Enzyme. A significant enzyme batch dependence was observed in several properties of the oxidase in spectroelectrochemical titrations. Absorbance difference spectra obtained during thin-layer experiments (10 ^{o}C, pH 7.66) on two different batches of cytochrome oxidase are shown in Figure 16 of Chapter IV. In the insets to this figure, the absorbance changes at 443 nm and 605 nm are correlated. Since the two cytochromes make very different contributions to the 443 and 605 nm absorptions, a plot of ΔA_{443} vs. ΔA_{605} facilitates characterization of the behaviors of the individual cytochromes. The dashed lines in the figure insets represent the behavior expected if the two cytochromes titrate at well-resolved potentials (a at a high potential, and a_3 at a lower potential). These lines were obtained by assigning 72% of the α band to cytochrome a, and 65% of the Soret band to cytochrome a_3. If the two cytochromes titrate together at all potentials, the plot of ΔA_{443} vs. ΔA_{605} will be a straight line connecting the extreme data points.

For one of the enzyme batches, designated batch A, the titration follows the dashed line closely for much of the high-potential portion of the experiment. This implies that in Batch A, cytochrome a is the primary contributor to the spectral changes which occur at the highest potentials, while the spectral changes at lower potentials are caused by both cytochromes, with cytochrome a_3 making a substantially larger

contribution. For the other enzyme batch, designated Batch B, the plot follows the dashed line for only a small portion of the titration at the highest applied potentials, and then closely follows a straight line connecting the extreme data points. This behavior indicates that in Batch B the two cytochromes titrate together throughout most of the range of applied potentials.

A comparison of selected absorbance difference spectra of the two enzyme batches titrated under similar conditions (pH 7.66, 10 ^{o}C) is presented in Figure 6. While the fully reduced minus fully oxidized difference spectra are similar in the two batches, as is evident in Figure 16 of Chapter IV, the spectra obtained during the low-potential half of the titration, as well as the spectra obtained during the high-potential half of the titration, are significantly different in the two batches. Much of the difference can be explained in terms of the different apportioning of oxidoreduction of the two cytochromes between the high and low potential parts of the titration, as was noted in the insets to Figure 16 of Chapter IV. However, the spectral differences near 415-420 nm are not as readily explained. In both enzyme batches, the absorbance changes in this region which occur at low applied potential do not resemble those expected for cytochrome _a_, cytochrome $\underline{a}_3$, or any linear combination of the two. Specifically, the trough at 415 nm is not as deep as expected, relative to the peak near 443 nm, for either cytochrome _a_ or cytochrome $\underline{a}_3$.

The Nernst plots (Figure 17 of Chapter IV) for enzyme batches A and B are very different. The largest difference involves cytochrome $\underline{a}_3$, whose upper asymptotic potential is significantly (ca. 50 mV) lower in

Figure 6. Absorbance difference spectra which describe the low (solid lines) and high (dashed lines) potential portions of spectroelectrochemical titrations (pH 7.66, 10 ^{o}C) of two batches of cytochrome oxidase. Panel A (corresponding to Batch A): solid line, sample poised at -300 mV (vs. SCE) minus sample poised at -50 mV; dashed line, sample poised at -50 mV minus sample poised at +300 mV. Panel B (corresponding to Batch B): solid line, sample poised at -300 mV minus sample poised at -70 mV; dashed line, sample poised at -70 mV minus sample poised at +300 mV.

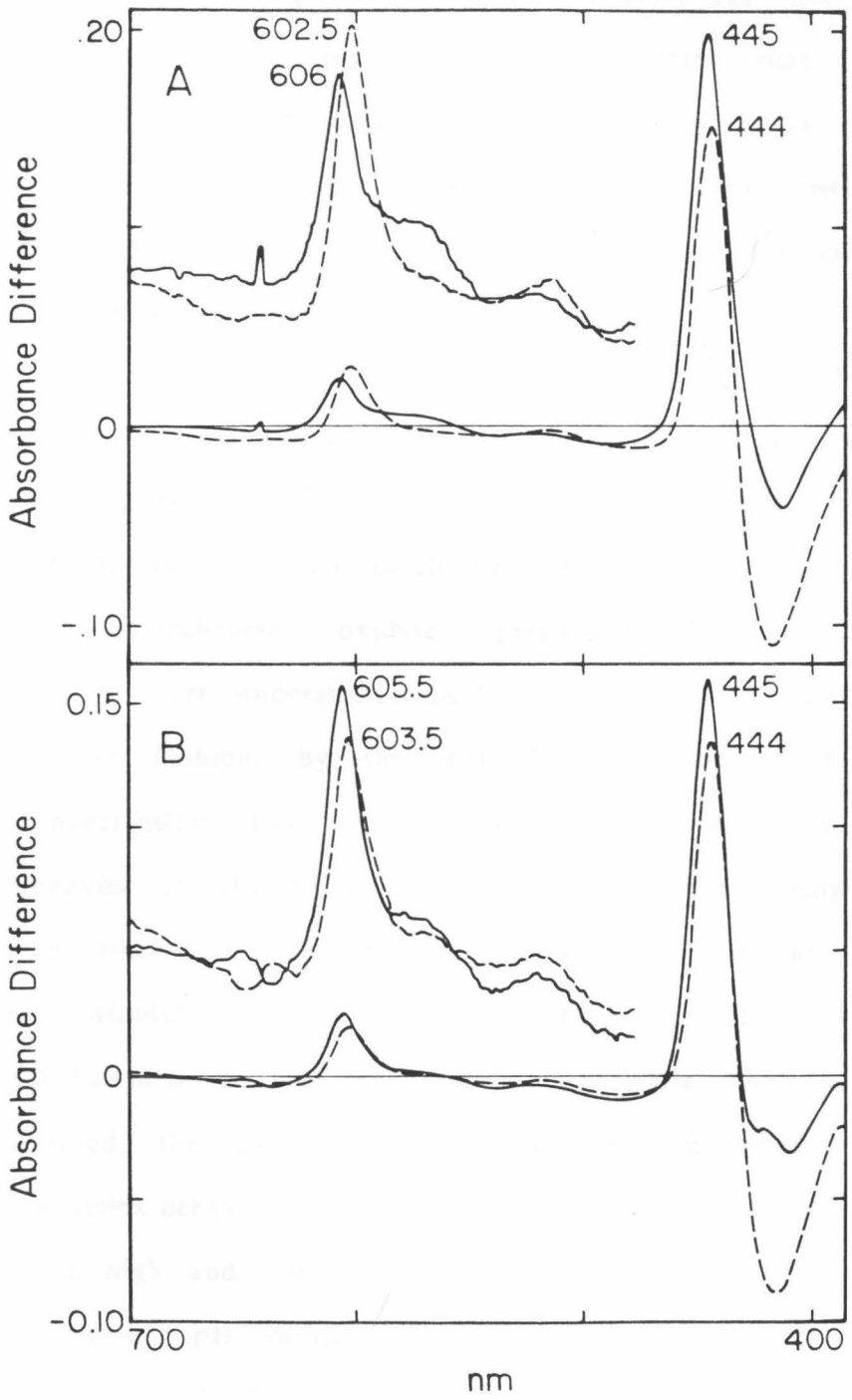
.20
602.5
606
A
445
444
0
-.10
Absorbance Difference
0.15
605.5
603.5
B
445
444
0
-0.10
Absorbance Difference
700
400
nm

Batch A. Cytochrome a exhibits differences also: in Batch A, the Nernst plot for cytochrome a follows $n = 1$ behavior for much of the high-potential half of the titration, which indicates that the site (or sites) with which it interacts has a substantially lower reduction potential than itself. In this batch, the chromophore titrating at high applied potentials appears to be almost purely cytochrome a. In Batch B, the upper asymptotic potential of cytochrome a is approximately the same as that in Batch A, but its Nernst plot follows the upper asymptote for less of the titration, crossing over to the lower asymptote nearer log(Ox/Red) = 0.

The origin of the observed batch dependence (which is commonly observed for cytochrome oxidase preparations from different laboratories) is not yet understood. Both batches were prepared in an essentially similar fashion, by the method of Hartzell and Beinert. They may nevertheless have been delipidated to different extents, since the behavior of the lipid/protein/detergent system during enzyme purification is likely to be complex, and subtile variations in composition or absolute concentration could conceivably lead to significant differences in the final product. While their origin is poorly understood, the batch variations have proven helpful in understanding the redox behavior of the enzyme.

The limiting high and low potentials of cytochromes a and a_3 were measured at various pH values between ca. 6.5 and 8.5. The results are plotted in Figure 7 (Batch A) and Figures 8 and 9 (Batch B). In both enzyme batches, the upper asymptotic potential of cytochrome a exhibits a moderate (ca. 30 mV/pH unit, on the average) dependence

Figure 7. pH dependences of the reduction potentials of cytochrome a (●) and cytochrome a_3 (□) in enzyme Batch A. The potentials plotted are the upper asymptotic potentials obatined from the fitting protocol described in the text, and pertain when the other sites in the enzyme are oxidized. The line drawn through the data for cytochrome a describes the behavior predicted for coupling to a protolyzable group whose pK_a is 7.5 when cytochrome a is reduced and significantly lower when it is oxidized. The line drawn through the data points for cytochrome a_3 has a slope of -56 mV/pH unit, corresponding to a protolyzable group whose pK_as flank the middle of the pH range examined, i.e., $pK_a^{ox} < 6.7$ and $pK_a^{red} > 8.0$.

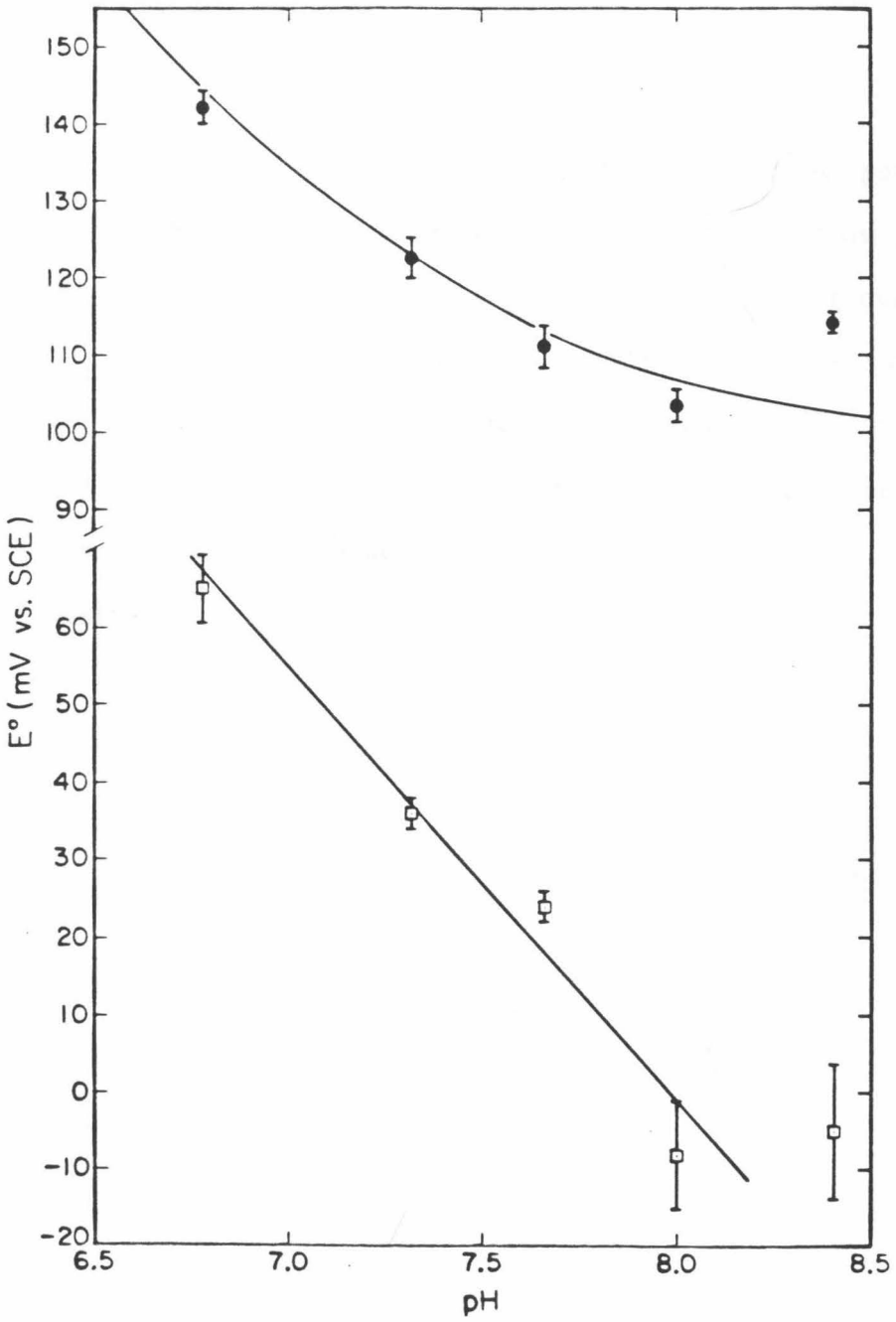
150
140
130
120
110
100
90
60
50
40
30
20
10
0
-10
-20
E° (mV vs. SCE)
6.5
7.0
7.5
8.0
8.5
pH

Figure 8. pH dependences of the upper asymptotic reduction potentials of cytochromes <u>a</u> (●) and <u>a_3</u> (□) in Batch B. These potentials pertain when the other sites in the enzyme are oxidized. The line through the cytochrome <u>a</u> data points refers to the same model used to describe the cytochrome <u>a</u> data from Batch A (cf. legend to Figure 7), except that pK_a^{red} is 7.4. The line through the cytochrome <u>a_3</u> data corresponds to coupling to a protolyzable group with pK_a^{ox} = 7.8, and pK_a^{red} significantly higher.

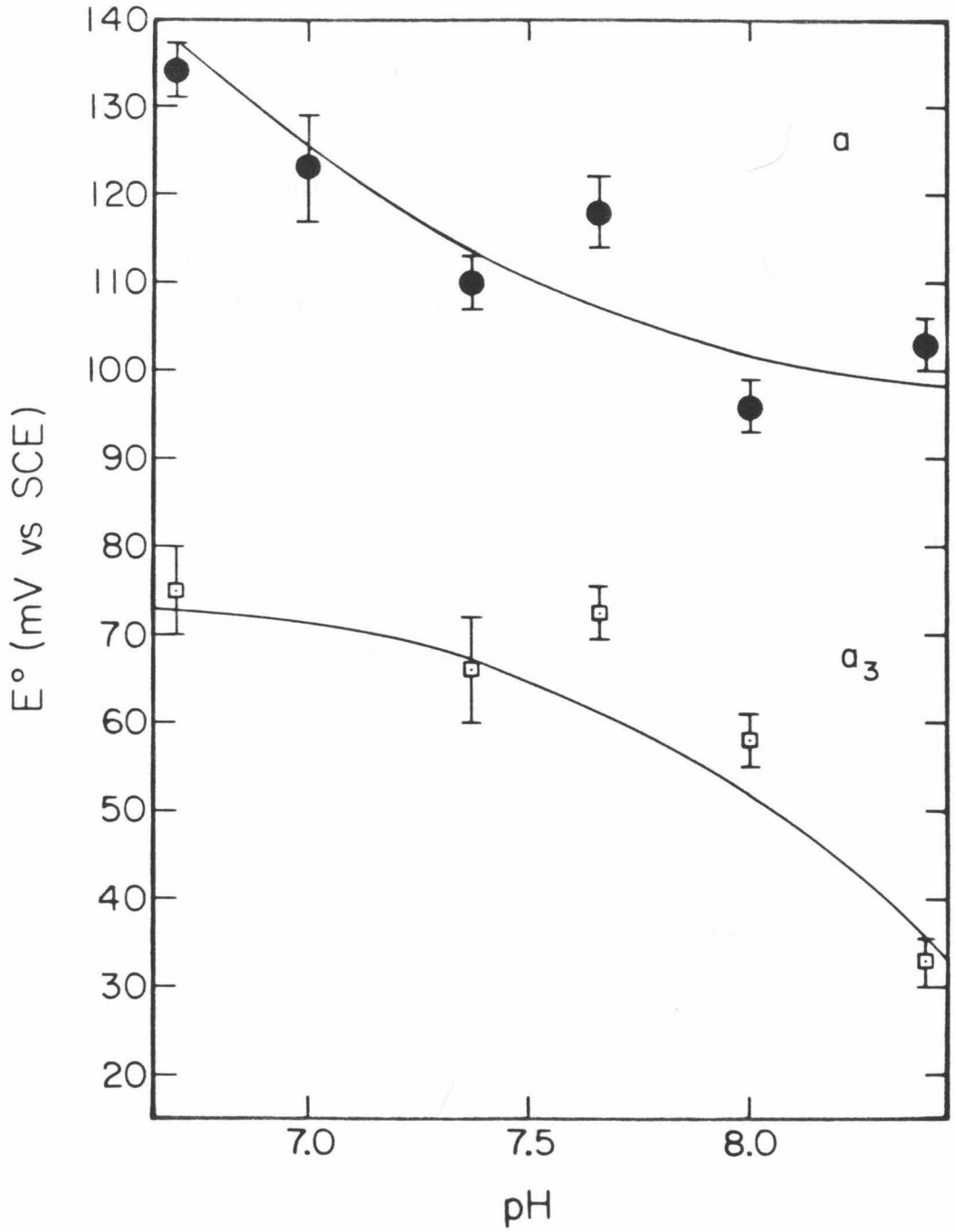
140
130
120
110
100
90
80
70
60
50
40
30
20
E° (mV vs SCE)
7.0
7.5
8.0
pH
a
a_3

Figure 9. pH dependences of the lower asymptotic reduction potentials of cytochromes $\underline{a}$ (●) and $\underline{a}_3$ (□) in Batch B. These potentials pertain when the other sites in the protein are reduced. Error bars are not shown for the points in this figure, since the lower asymptotic potentials are determined by the upper asymptotic potentials and the corresponding interaction potentials. Computer-generated fits to Nernst plot data yield only the latter two quantities. Errors in the lower asymptotic potentials are expected to be comparable to those for the corresponding upper asymptotic potentials (see Figure 8).

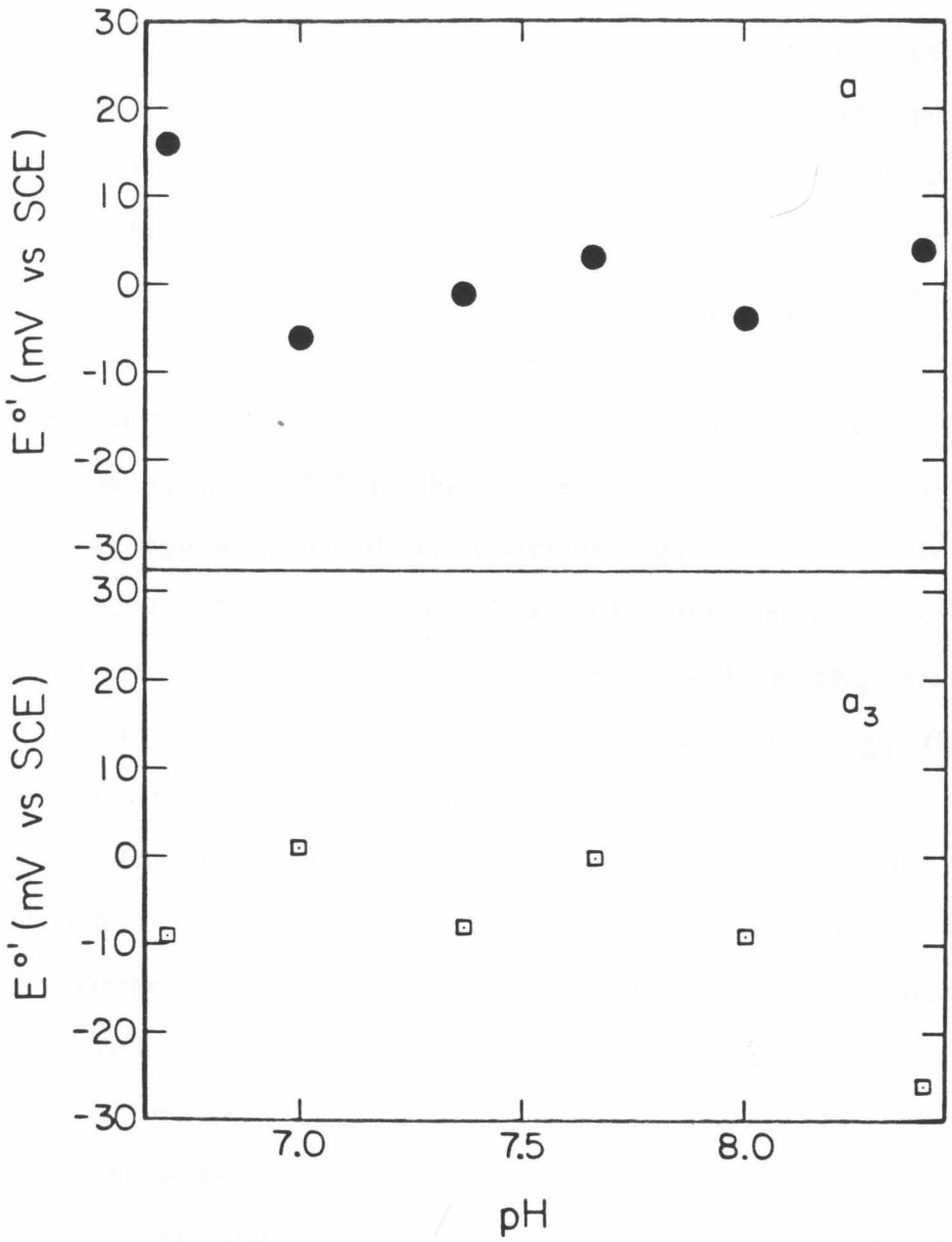
30
20
10
0
-10
-20
-30
E°' (mV vs SCE)
a
30
20
10
0
-10
-20
-30
E°' (mV vs SCE)
a3
7.0
7.5
8.0
pH

upon pH, consistent with (but not restricted to) coupling to an ionizable group whose pK_a is near 7.4 when cytochrome *a* is reduced and significantly lower when this site is oxidized. The lower asymptotic potential of cytochrome *a* could be satisfactorily estimated only in Batch B (Figure 9); this potential is less steeply dependent upon pH than the upper asymptotic potential (Figure 8). It should be stressed that neither the low nor the high potential transition of cytochrome *a* is stoichiometrically ($1H^+/1e^-$) linked to proton uptake. The behavior of cytochrome a_3 is more batch-dependent. In Batch A, a steep (ca. -56 mV/pH unit) pH dependence was observed, indicating that reduction of cytochrome a_3 is coupled to the uptake of one proton. In Batch B, the upper asymptotic potential of cytochrome a_3 is not sensitive to pH below pH 7.5, but it drops at higher pH values in a manner that suggests the involvement of an ionizable group with a pK_a near 7.8 (Figure 8). The lower asymptotic potential of cytochrome a_3 (Figure 9) behaved similarly, but with an apparent pK_a of ca. 8.2.

The pH dependences of the cytochrome potentials have previously been inferred from models, proven incorrect in Chapter four, in which the two cytochromes are both assumed to titrate as $n = 1$ acceptors (10,32), or from models in which the cytochromes are constrained to interact with one another (20). In a recent study (33), only one wavelength (the α band maximum) was monitored, and the resulting data were deconvoluted using the central assumption of the "neoclassical" model, i.e., interaction only between the two cytochromes, to place a necessary additional constraint upon the factor analysis. More reliable estimates of the pH dependence of the Fe_a reduction potential

have been obtained from studies of the enzyme inhibited with cyanide (34) or with carbon monoxide, as discussed previously; in these experiments cytochrome $\underline{a}_3$ does not titrate and thus does not complicate the observed spectral changes. Since the reduction potential of Fe_a itself depends sensitively upon the ligation and/or redox state of the cytochrome $\underline{a}_3/Cu_B$ binuclear site, it is important to obtain reliable measurements of pH dependences in the native enzyme. The present work represents the first attempt to deduce pH dependences from systematic deconvolution of the cytochrome spectra (at two wavelengths) observed in titrations of the native enzyme in conjunction with fitting the Nernst plots obtained to an interaction model in which both the intrinsic potentials and the total interaction potentials are treated as independent variables.

The present results for cytochrome $\underline{a}$ are in accord with the results from the inhibited enzyme derivatives: the upper asymptotic potential of cytochrome $\underline{a}$, which pertains when the other sites in the enzyme are oxidized, displays a ca. -30 mV/pH unit dependence in the vicinity of pH 7. This is very close to the result obtained with the cyanide-inhibited enzyme (34), in which cytochrome $\underline{a}_3$ is stabilized in its oxidized state. The lower asymptotic potential of cytochrome $\underline{a}$ (Figure 9), which pertains when the other enzyme sites are reduced, is more weakly dependent upon pH (less than -10 mV/pH unit, on average). This is similar to the weak pH dependence of the Fe_a potential measured in the carbon monoxide adduct (-9 mV/pH unit) in which cytochrome $\underline{a}_3$ and Cu_B are maintained in their reduced states. Hence the oxidation state of the cytochrome $\underline{a}_3/Cu_B$ binuclear site, rather

than its ligation, is important in determining the pH dependence of the Fe_a potential. The pronounced effect of the cytochrome $\underline{a}_3/Cu_B$ binuclear site raises the possibility that the proton taken up upon Fe_a reduction does not bind close to this center but to a site in the vicinity of the cytochrome $\underline{a}_3/Cu_B$ binuclear site. Regardless of the location of proton binding, it is clear that proton uptake is not stoichiometrically linked to reduction of cytochrome $\underline{a}$. At pH values relevant to the mitochondrial matrix (21), i.e., well over 7, the H^+/e^- quotient is less than 0.5. This result has important implications for the mechanism of proton pumping by the oxidase, which has been suggested to involve cytochrome $\underline{a}$ (21,22), as noted earlier.

The pH dependence of the cytochrome $\underline{a}_3$ potential in Batch A indicates that the pK_a of a protolyzable group is quite strongly coupled to oxidoreduction of this site. This coupling, defined as pK_a^{red} minus pK_a^{ox}, must be at least 1.5 pH units, since the data in Figure 7 indicate that the relevant pK_as nearly flank the pH range examined. It has previously been suggested (35) that the axial ligand to cytochrome $\underline{a}_3$ is derived from water (when other dioxygen reduction intermediates are not bound). If this is true, then the observed pH dependence may involve the conversion between cytochrome $\underline{a}_3$-coordinated hydroxide and a water molecule (which may either be bound or free). In Batch B, the pH dependence is less pronounced, but it becomes steeper at high pH in a manner that suggests an ionization with a pK_a near 7.8. At higher pH values, which are not experimentally accessible because of enzyme denaturation, this curve may continue to drop until it parallels that observed in Batch A at lower

pH values. EPR experiments suggest that water coordinated to ferricytochrome $\underline{a}_3$ deprotonates to produce hydroxide at approximately pH 8, in agreement with the pK_a inferred from the reduction potential measurements on Batch B. It is interesting to note that all of the batch-dependent differences in cytochrome $\underline{a}_3$ may be explained if it is postulated that the pK_a^{ox} of the protolyzable group coupled to cytochrome $\underline{a}_3$ has shifted from ca. 6.7 in Batch A to ca. 7.8 in Batch B while the reduction potential of protonated cytochrome $\underline{a}_3$ remains the same. Such a pK_a shift would cause both the increase in the cytochrome $\underline{a}_3$ reduction potential in Batch B at pH 7.66 and the observed change in pH dependence.

The temperature dependence of the cytochrome $\underline{a}$ potential in both enzyme batches is displayed in Figures 10 (Batch A) and 11 (Batch B). Owing to the complexities associated with deconvolving the spectra and analyzing this strongly interactive multisite system, the scatter in the data is greater than that obtained from single-site metalloproteins or from CO-inhibited cytochrome oxidase. An apparent batch dependence was observed. In Batch A, the reduction potential of cytochrome $\underline{a}$ varies with temperature by ca. -0.81 mV/^{o}C, with a corresponding standard entropy of reduction of -43.4 ± 7 eu. In Batch B, the reduction potential of cytochrome $\underline{a}$ is more steeply temperature-dependent, with a corresponding standard entropy of reduction of -56.4 ± 6 eu. For comparison, the standard entropy of reduction of cytochrome $\underline{a}$ in the CO adduct of the enzyme was measured to be -50.8 ± 2.8 eu. The standard free energy of reduction of cytochrome $\underline{a}$ is similar in the two batches: $\Delta G^{o'}$ = -8.1 ± 0.2 kcal/mol in Batch A,

Figure 10. Temperature dependences of the upper asymptotic reduction potentials of cytochromes $\underline{a}$ (●) and $\underline{a}_3$ (□) in enzyme Batch A. The linear least-squares fits to the data yield standard entropies of reduction (after correction for partial thermostatting of the SCE) of -43.4 ± 7 and -19.4 ± 10 eu for cytochromes $\underline{a}$ and $\underline{a}_3$, respectively. Solution conditions: 0.245 M ionic strength, pH 7.66, phosphate buffer.

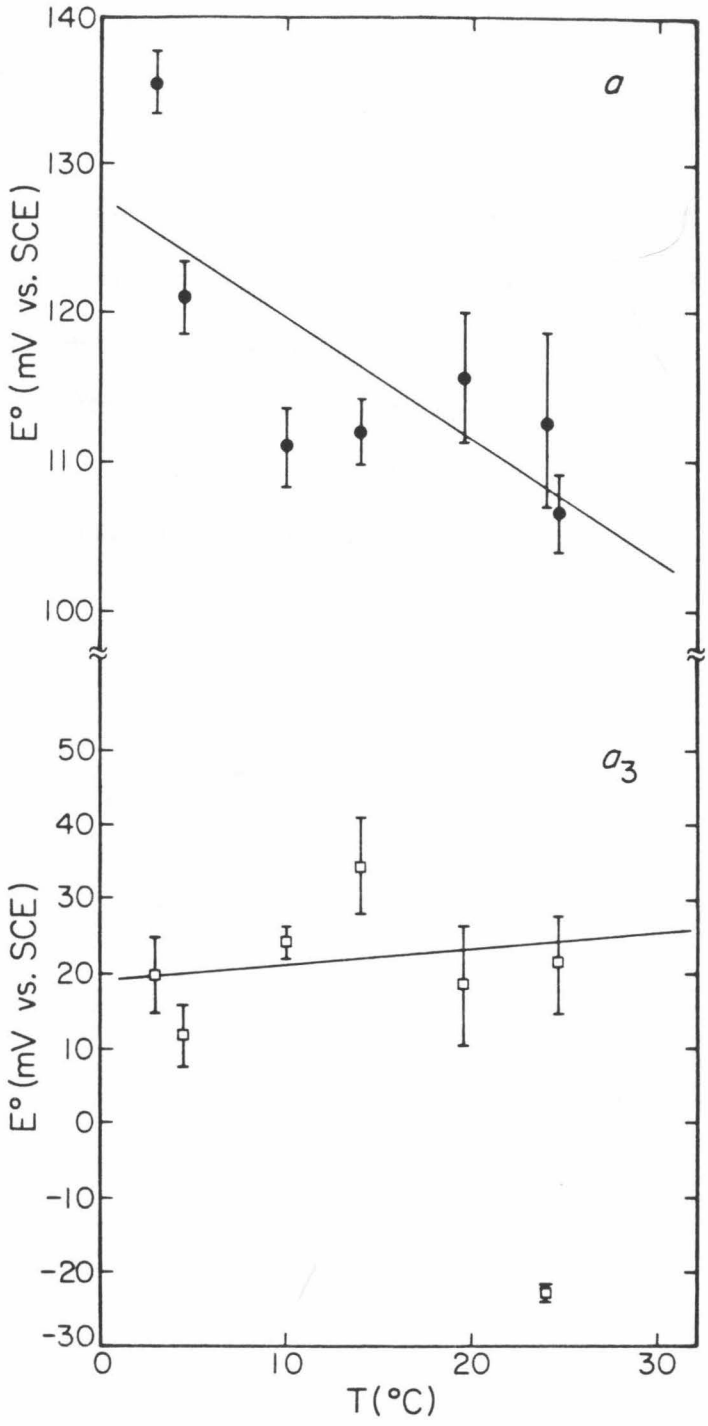
a
a_3
E° (mV vs. SCE)
E° (mV vs. SCE)
T(°C)
140
130
120
110
100
50
40
30
20
10
0
-10
-20
-30
0
10
20
30

Figure 11. Temperature dependences of the upper asymptotic reduction potentials of cytochromes $\underline{a}$ (●) and $\underline{a}_3$ (□) in enzyme Batch B. The solid lines are linear least-squares fits that correspond to standard entropies of reduction (after correction for partial thermostatting of the SCE) of -56.4 ± 6 and -37.4 ± 7 eu for cytochromes $\underline{a}$ and $\underline{a}_3$, respectively. Solution conditions as in Figure 10.

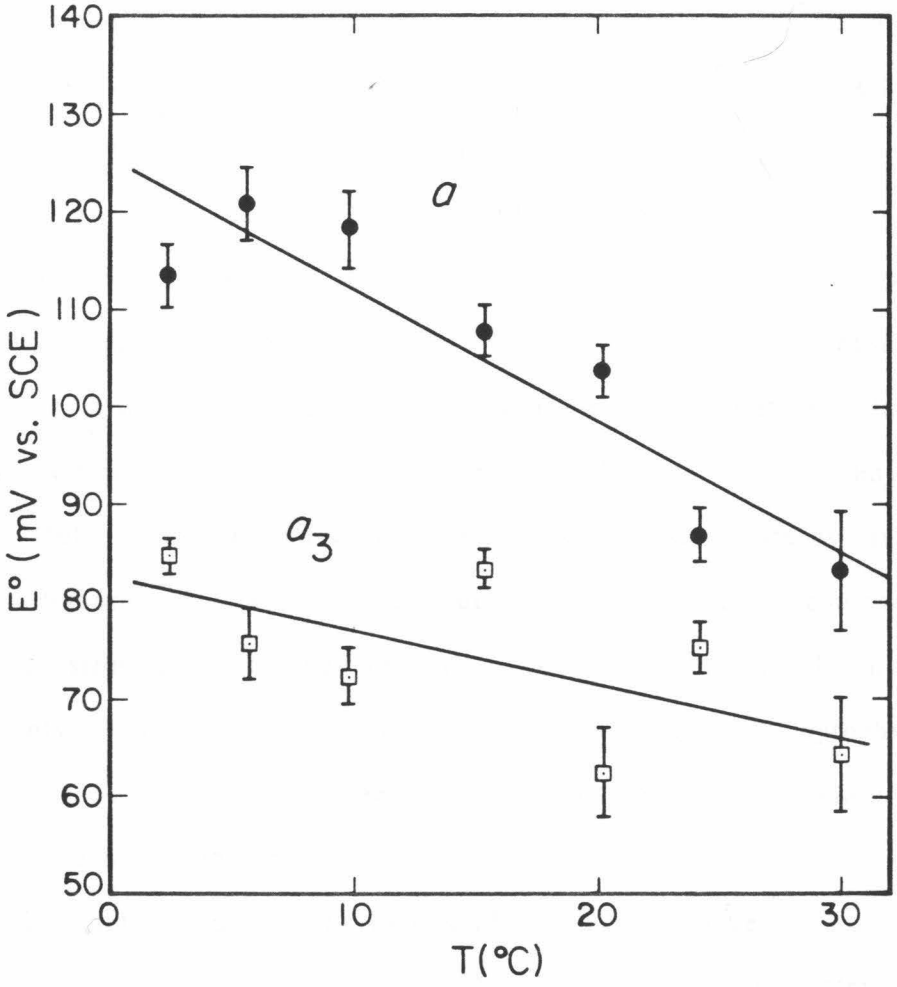
140
130
120
110
100
90
80
70
60
50
E° (mV vs. SCE)
a
a3
0
10
20
30
T(°C)

and -7.7 ± 0.1 kcal/mol in Batch B.

The temperature dependence of the reduction potential of cytochrome $\underline{a}_3$ in the two enzyme batches is also displayed in Figures 10 and 11. In both batches, the standard entropy of reduction of cytochrome $\underline{a}_3$ is significantly more positive than that of cytochrome $\underline{a}$. The measured values are -19.4 ± 10 eu in Batch A, and -37.4 ± 7 eu in Batch B. The standard free energy of reduction of cytochrome $\underline{a}_3$ is -6.2 ± 0.2 kcal/mol in Batch A, and -7.2 ± 0.2 kcal/mol in Batch B.

Thermodynamic parameters for the reduction of cytochromes $\underline{a}$ and $\underline{a}_3$ are compiled in Table III. For comparison, results obtained with the CO-inhibited enzyme and measured values for several other heme proteins are also shown. $\Delta S^{o\prime}$ of cytochrome $\underline{a}$ is relatively large and negative compared to other low-spin cytochromes which have been studied. Only that of cytochrome $\underline{b}_5$, which also contains two axial histidine ligands, is comparable, but in making this comparison it should be stressed that the reduction potential of cytochrome $\underline{b}_5$ is also steeply ionic strength-dependent, unlike that of cytochrome $\underline{a}$. $\Delta S^{o\prime}$ of cytochrome $\underline{a}_3$ is more positive than that of myoglobin, which also contains a high-spin heme.

The interaction potential expressed at cytochrome $\underline{a}$ at various temperatures is plotted in Figure 12. The interaction potential does not change significantly with temperature between 5 and 30 ^{o}C. Thus, the standard entropy of reduction of cytochrome $\underline{a}$ does not depend upon the redox states of the other metal sites in the enzyme. Stated another way, this means that the interaction term itself has no measurable entropic component.

Table III. Redox thermodynamic parameters for selected hemoproteins.

Heme Site	$\Delta G^{o'}$(kcal/mol)[a]	$\Delta S^{o'}$(eu)	$\Delta H^{o'}$(kcal/mol)
Cytochrome *a* (Batch A)	-8.1 ± 0.2	-43.4 ± 7	-21.0 ± 2.1
Cytochrome *a* (Batch B)	-7.7 ± 0.1	-56.4 ± 6	-24.5 ± 1.8
Cytochrome *a* (CO adduct)	-6.37 ± 0.08	-50.8 ± 2.8	-21.5 ± 0.8
Cytochrome a_3 (Batch A)	-6.2 ± 0.2	-19.4 ± 10	-12.0 ± 3.0
Cytochrome a_3 (Batch B)	-7.2 ± 0.2	-37.4 ± 7	-18.3 ± 2.1
Cytochrome *c*	-6.00 ± 0.05	-28.5 ± 1.2	-14.5 ± 0.4
Cytochrome b_5[b]	-0.12 ± 0.01	-37 ± 2.0	-11.0 ± 1.0
Cytochrome *c*′	-2.2 ± 0.5	-23.7 ± 1.2	-9.3 ± 0.4
Myoglobin	-1.36 ± 0.05	-39.2 ± 1.2	-13.0 ± 0.4

[a]At 25 °C. All thermodynamic parameters are referenced to the NHE.

[b]Reference 28.

Figure 12. Temperature dependence of the interaction potential expressed at cytochrome a in Batch B. This interaction potential is equal to the difference in the upper and lower asymptotic potentials derived from fits to a minimal interaction (i.e., effective two-site) model in which cytochrome a interacts with (Cu_A, Cu_B, cytochrome a_3).

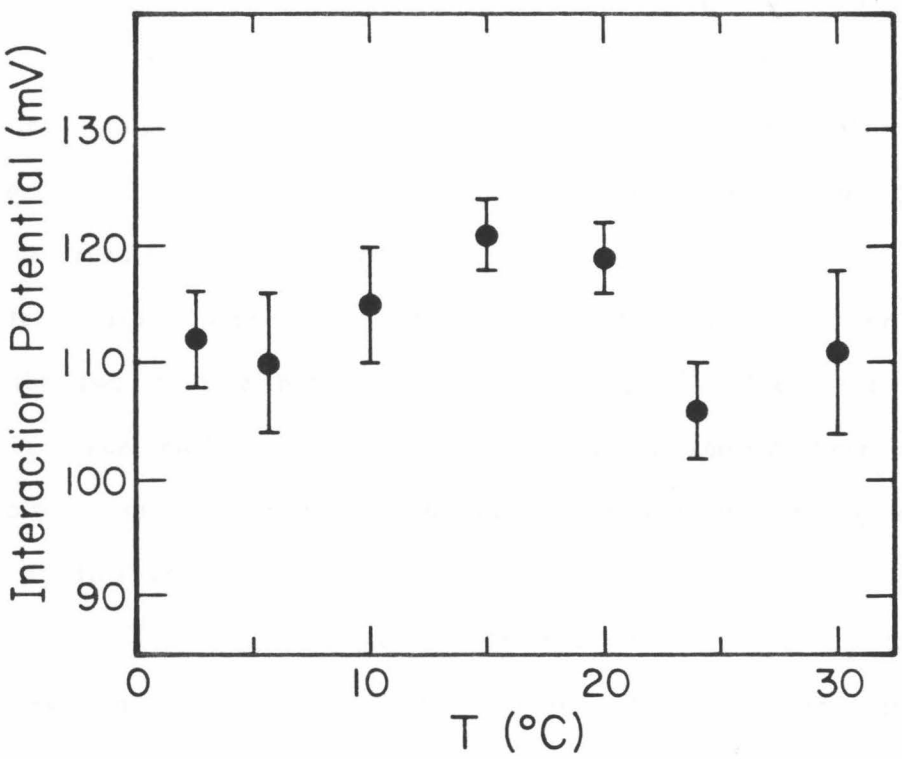
Interaction Potential (mV)
130
120
110
100
90
0
10
20
30
T (°C)

The temperature dependence of the Fe_a reduction potential appears to be different in the two enzyme batches, but this cannot be stated with certainty, given the considerable uncertainty in the determinations. The corresponding measurements on the CO-inhibited enzyme yield a temperature dependence midway between the two reported here. In all cases, the observed temperature dependence is unusually steep and coresponds to a standard entropy of reduction more negative than those of other low-spin cytochromes. As pointed out earlier, this indicates that a substantial protein-ordering conformational change accompanies reduction of cytochrome a. Further, such a conformational change may be responsible for the accompanying changes in reduction potential observed for the other sites in the enzyme.

The temperature dependences of the cytochrome a_3 reduction potentials in the two enzyme batches correspond to $\Delta S^{o\prime}$ values that are not remarkable. The enthalpy and entropy values determined here indicate that electron transfer from cytochrome a to cytochrome a_3 (in the absence of dioxygen) is endoenthalpic by 5-10 kcal/mol. Most of this is compensated by entropic factors, so that the equilibrium constant for the reaction is not very different from unity. The enthalpic cost of this electron transfer is expected to make it a relatively activated process, and the rate of electron transfer from cytochrome a to cytochrome a_3 has been shown to be steeply temperature dependent (37).

The effect of ionic strength on the cytochrome potentials was measured only in Batch B. The results are displayed in Figure 13. The reduction potential of cytochrome a is not significantly affected by variations in ionic strength between 0.06 and 0.50 M, in agreement

Figure 13. Ionic strength dependence of the cytochrome $\underline{a}$ and $\underline{a}_3$ reduction potentials in enzyme Batch B. Solution conditions: 10 ^{o}C, pH 7.66, phosphate buffer. The left panel pertains to the upper asymptotic potentials, and the right panel to the lower asymptotic potentials. Circles denote cytochrome $\underline{a}$ and squares, cytochrome $\underline{a}_3$. As in other figures, the error bars shown refer to the standard error of determination of the potentials in the computer fits. Since the lower potential was not treated as an independent variable in these fits (the interaction potential was used instead), error bars are not shown for them, but are comparable to those of the upper asymptotic potentials. The triangles refer to an experiment in which 0.25 M KCl was added to increase the ionic strength; the Nernst plots from this experiment are shown in Figure 14.

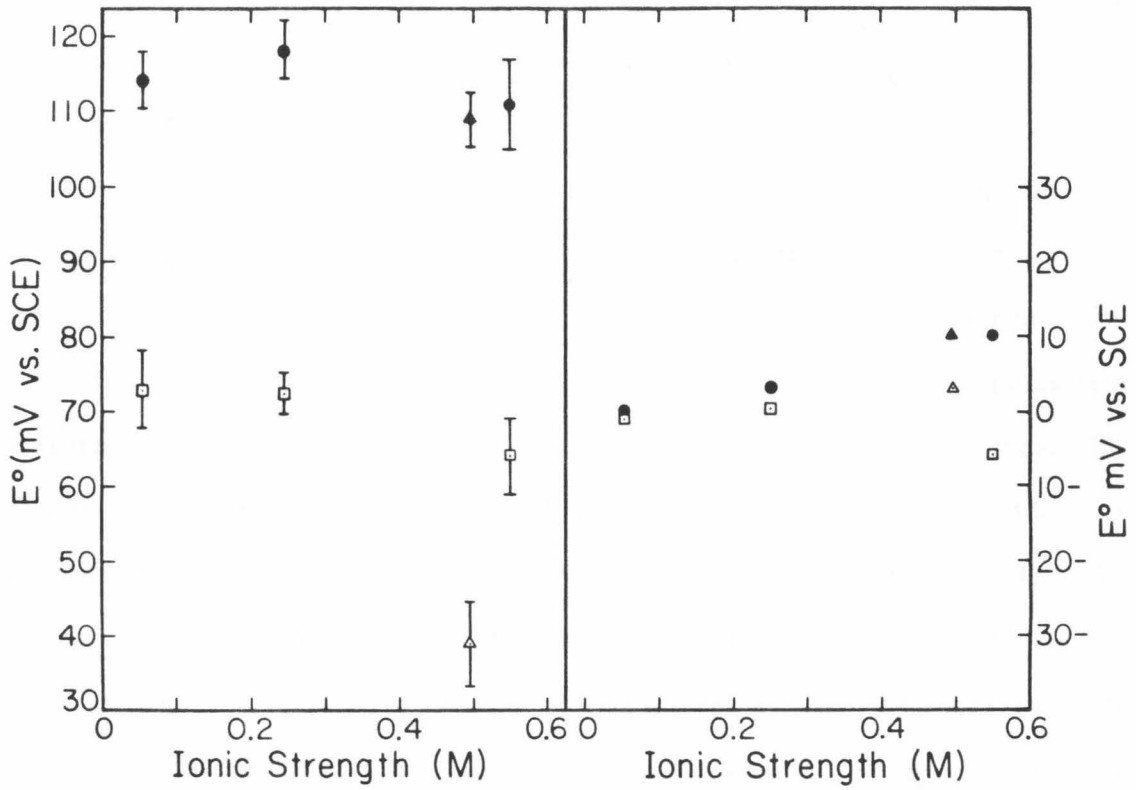
E°(mV vs. SCE)
120
110
100
90
80
70
60
50
40
30
0
0.2
0.4
0.6
Ionic Strength (M)
30
20
10
0
10-
20-
30-
E° mV vs. SCE
0
0.2
0.4
0.6
Ionic Strength (M)

with the studies on the enzyme inhibited with carbon monoxide. The potential of cytochrome $\underline{a}_3$ is also not significantly affected. As noted earlier, the potential of cytochrome $\underline{a}_3$ was significantly affected when KCl was used to raise the ionic strength; the upper asymptotic potential of cytochrome $\underline{a}_3$ decreased from ca. 70 mV vs. SCE to ca. 36 mV upon the addition of 0.25 M KCl. In this experiment, cytochrome $\underline{a}_3$ exhibited only 36 mV of interaction, while cytochrome $\underline{a}$ exhibited ca. 99 mV. Hence, approximately 63 mV of the interactions expressed at cytochrome $\underline{a}$ in Batch B must involve factors other than the oxidation state of cytochrome $\underline{a}_3$ when the buffer is supplemented with KCl (Figure 14). The lower asymptotic potential varied by much less, so that the titration behavior of cytochrome $\underline{a}_3$ approached that expected for an isolated one-electron acceptor. The potentials measured in the presence of 0.25 M KCl are also noted in Figure 13. Similar results were previously obtained when 0.1 M KCl was added to the enzyme in potentiometric titrations monitored by MCD (38). By using phosphate buffer instead to raise the ionic strength, it is apparent that a specific chloride effect, rather than ionic strength (as suggested in Reference 38), is likely to be the cause of changes in the enzyme induced by KCl.

The weak dependence of the cytochrome reduction potentials upon ionic strength suggests that these sites are effectively shielded from the solvent by the protein, as was discussed previously for cytochrome $\underline{a}$ in the CO-inhibited enzyme. Other experiments, notably infrared absorbance (39) and resonance Raman (40) studies, have shown that cytochrome $\underline{a}_3$ is also in a relatively hydrophobic environment.

Figure 14. Nernst plots for cytochromes a (circles) and a_3 (squares) in a spectroelectrochemical titration of Batch B (10 ^{o}C, pH 7.66, 90 mM phosphate) to which 0.25 M KCl was added. The solid points were obtained on oxidation of the enzyme and the open points upon rereduction.

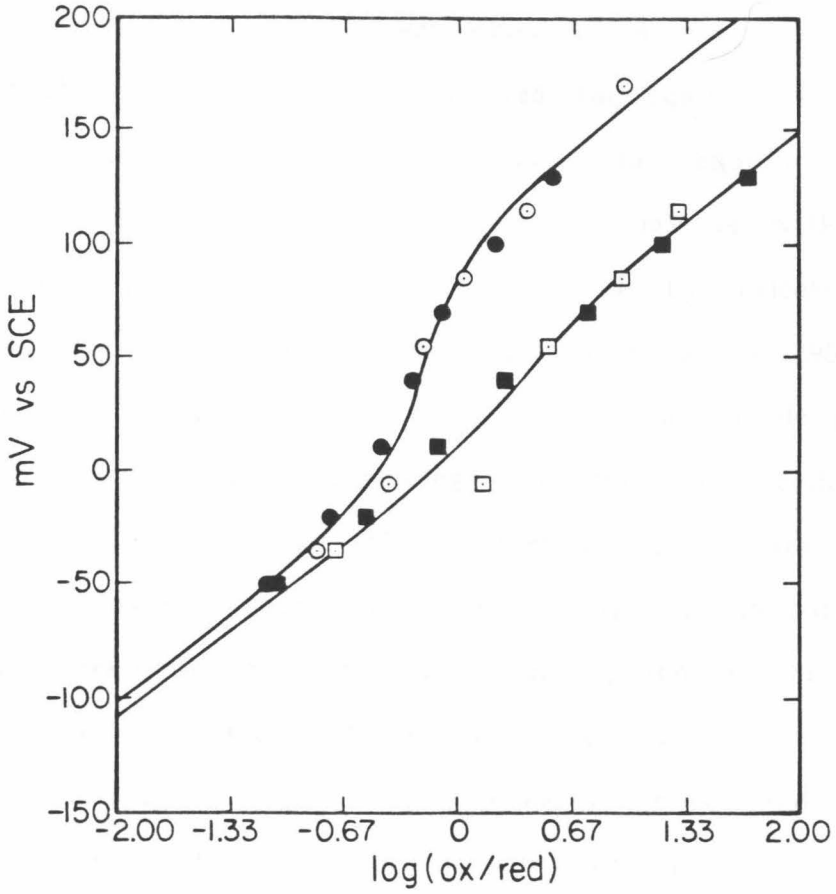
200
150
100
50
0
-50
-100
-150
mV vs SCE
-2.00
-1.33
-0.67
0
0.67
1.33
2.00
log(ox/red)

However, nothing is yet known of the possible effects of ionic strength upon the enthalpies and entropies of reduction of the cytochromes. In cytochrome c, significant compensating enthalpy-entropy effects have been observed (29), and this may also be true for cytochromes a and a_3 in the native enzyme.

Some degree of irreversibility was observed in the titrations even when as much as three hours was allowed for equilibration at each applied potential. Very slow approaches to equilibrium were ordinarily observed only at relatively high (> 300 mV vs. NHE) applied potentials. The irreversibility was characterized by calculating the absorbance difference spectrum of the sample poised at ca. 290 mV vs. NHE during the oxidative titration minus that of the sample poised at ca. 290 mV during the corresponding rereduction, for both enzyme batches (at pH 7.66, 10 ^{o}C). These difference spectra are displayed in Figure 15. This slow equilibration may be explained in part by the presence of interactions among the redox centers, and by the liklihood that equilibration with the mediator titrants occurs via only one or two of the sites (Fe_a or Cu_A) in the enzyme, whose potentials may not always be well matched to those of the other sites (cytochrome a_3 and Cu_B). However, the difference spectra which describe the hysteresis (Figure 15) indicate that multiple chemical forms of the oxidized enzyme, most likely the so-called pulsed and resting states, are involved. The equilibration between these states is known to be fairly slow (41). This problem typically appeared at high applied potentials, which indicates that partial reduction of the enzyme, probably just a single reducing equivalent, is sufficient to produce the pulsed

Figure 15. Absorbance difference spectra which characterize the hysteresis typically observed in the high potential portions of spectroelectrochemical titrations (pH 7.66, 10 ^{o}C) of native cytochrome oxidase. The two spectra were obtained from the two enzyme batches studied. Trace A, spectrum of a sample of Batch B poised at 145 mV vs. SCE during an oxidative titration minus the spectrum of the same sample poised at 145 mV during the corresponding rereduction. Trace B, spectrum of a sample of Batch A poised at 140 mV during an oxidative titration minus the spectrum of the same sample poised at 140 mV during the corresponding rereduction.

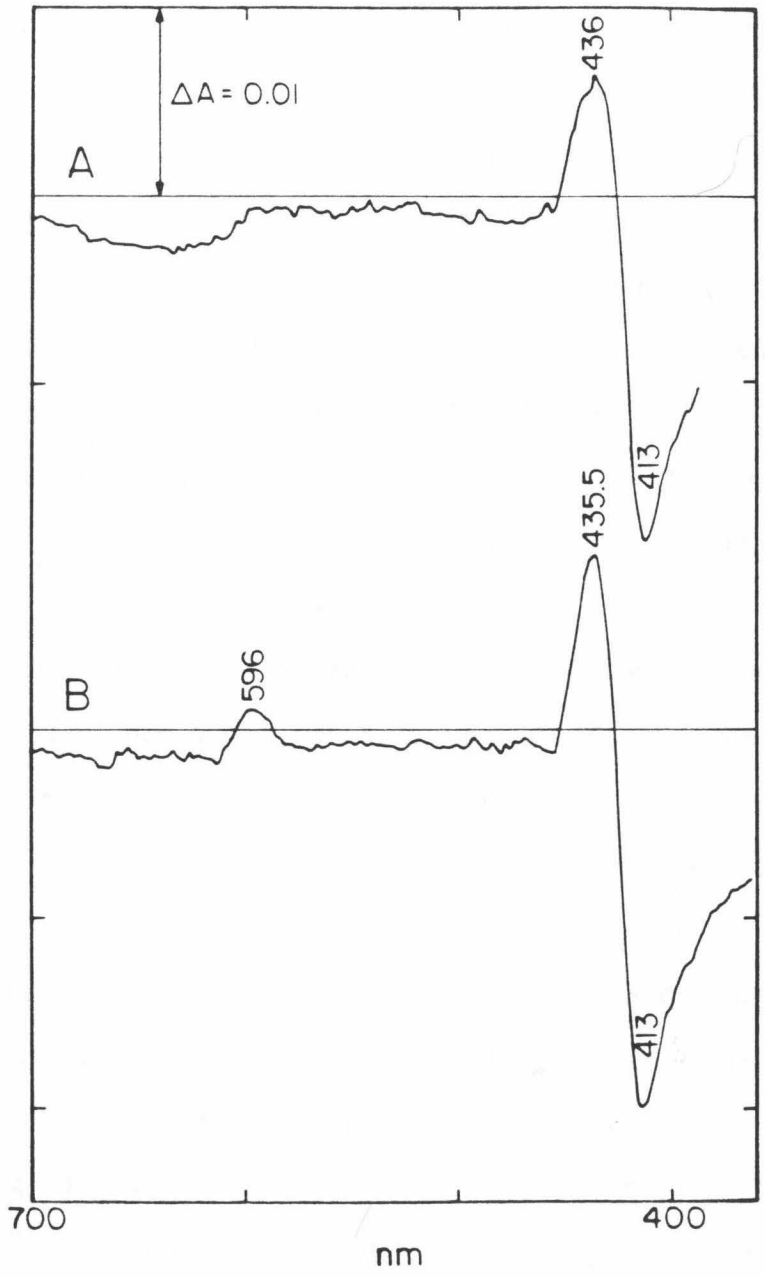
ΔA = 0.01
A
436
413
B
435.5
596
413
700
400
nm

state. The spectroscopic differences between these two states, and probably the largest structural differences, involve the cytochrome $\underline{a}_3/Cu_B$ binuclear site (35,41,42). Since MCD is comparatively insensitive to ferric high-spin hemes, this phenomenon should not be observed in redox titrations monitored by MCD, and it has not been (38). While not perfectly reversible, the titrations were slow enough that they should reflect most closely the potential of the more stable resting enzyme rather than the (nonequilibrium) effective potential of the pulsed enzyme. Assuming that the reduced state of the enzyme is the same regardless of whether it is derived from pulsed or resting enzyme, the reduction potential of cytochrome $\underline{a}_3$ in the resting enzyme will be lower than that of the more physiologically relevant pulsed enzyme, and possibly much lower (no reliable estimates of the equilibrium constant for the pulsed-resting interconversion are presently available). The pertinent reduction potentials of the cytochrome $\underline{a}_3/Cu_B$ binuclear site during dioxygen reduction, when different intermediates are bound at every step of the reaction, are likely to be much higher. These potentials cannot be measured by equilibrium methods. These considerations should be remembered when discussing the equilibrium thermodynamic properties of cytochrome $\underline{a}_3$, since these properties are of limited mechanistic relevance as a consequence.

Concluding Remarks. In this chapter, the redox thermodynamic properties of the optically visible sites (Cu_A, cytochrome $\underline{a}$, and cytochrome $\underline{a}_3$) are characterized in considerable detail. A significant batch dependence was noted in studies of the native enzyme and is attributed primarily to the cytochrome $\underline{a}_3$ center. The

properties of cytochrome a were found to be more nearly batch-invariant, and are in fact nearly the same within the uncertainty of the measurements. Both cytochrome a and Cu_A possess standard entropies of reduction that are much more negative than those for other metalloprotein heme and copper sites.

In contrast, nothing is known about the equilibrium redox behavior of the spectrally silent center, Cu_B. This unsatisfactory situation can now be rectified. Cytochrome oxidase has recently been chemically modified to yield a Cu_A-depleted derivative (43). A series of redox titration experiments employing the cyanide adduct of modified cytochrome oxidase should yield interesting results. Only two of the three sites would undergo oxidoreduction, cytochrome a and Cu_B. A reasonably accurate picture of the behavior of Cu_B would therefore be obtained from analyses of cytochrome a Nernst plots using an Fe_a/Cu_B interaction model.

REFERENCES

1. Ellis, W.R., Jr., Wang, H., Blair, D.F., Gray, H.B., and Chan, S.I. (1986) *Biochemistry* **25**, 161.

2. Wang, H., Blair, D.F., Ellis, W.R., Jr., Gray, H.B., and Chan, S.I. (1986) *Biochemistry* **25**, 167.

3. Blair, D.F., Ellis, W.R., Jr., Wang, H., Gray, H.B., and Chan, S.I. *J. Biol. Chem.*, accepted for publication.

4. Perrin, D.D., and Dempsey, B. (1974) *Buffers for pH and Metal Ion Control*, Chapman and Hall, London.

5. Taniguchi, V.T., Sailasuta-Scott, N.S., Anson, F.C., and Gray, H.B. (1980) *Pure & Appl. Chem.* **52**, 2275.

6. Taniguchi, V.T., Malmström, B.G., Anson, F.C., and Gray, H.B. (1982) *Proc. Natl. Acad. Sci. U.S.A.* **79**, 3387.

7. Gray, H.B., and Solomon, E.I. (1981) in *Copper Proteins*, Spiro, T.G., ed., Wiley-Interscience, New York, p. 1.

8. Corrin, A.F., Bersohn, R., and Cole, P.E. (1983) *Biochemistry* **22**, 2032.

9. Canters, G.W., Hill, H.A.O., Kitchen, N.A., and Adman, E.T. (1984) *Eur. J. Biochem.* **138**, 141.

10. van Gelder, B.F., van Rijn, J.L.M.L., Schilder, G.J.A., and Wilms, J. (1977) in *Structure and Function of Energy-Transducing Membranes*, Elsevier/North Holland, Amsterdam, p. 61.

11. Antalis, T.M., and Palmer, G. (1982) *J. Biol. Chem.* **257**, 6194.

12. Wilson, M.T., Greenwood, C., Brunori, M., and Antonini, E. (1975) *Biochem. J.* **147**, 145.

13. Ferguson-Miller, S., Brautigan, D.L., and Margoliash, E. (1976) *J. Biol. Chem.* **251**, 1104.

14. Wilms, J., Veerman, E.C.I., Konig, B.W., Dekker, H.L., and van Gelder, B.F. (1981) *Biochim. Biophys. Acta* **635**, 13.

15. Millet, F., Darley-Usmar, V.M., Capaldi, R.A. (1982) *Biochemistry* **21**, 3857.

16. Anderson, J.L., Kuwana, T., and Hartzell, C.R. (1976) *Biochemistry* **15**, 3847.

17. Wikström, M.K.F., Harmon, H.J., Ingledew, W.J., and Chance, B. (1976) *FEBS Lett.* **65**, 259.

18. Schroedl, N.A., and Hartzell, C.R. (1977) *Biochemistry* **16**, 4961; 4966.

19. Hinkle, P., and Mitchell, P. (1970) *J. Bioenerg.* **1**, 45.

20. Wikström, M., Krab, K., and Saraste, M. (1981) *Ann. Rev. Biochem.* **50**, 623.

21. Wikström, M., Krab, K., and Saraste, M. (1981) *Cytochrome Oxidase: A Synthesis*, Academic Press, London.

22. Babcock, G.T., and Callahan, P.M. (1983) *Biochemistry* **22**, 2314.

23. Blair, D.F., Gelles, J., and Chan, S.I. *Biophys. J.*, accepted for publication.

24. Sturtevant, J.M. (1977) *Proc. Natl. Acad. Sci. U.S.A.* **74**, 2235.

25. Urry, D.W., Wainio, W.W., and Grebner, D. (1972) *Biochem. Biophys. Res. Commun.* **27**, 625.

26. Cabral, F., and Love, B. (1972) *Biochim. Biophys. Acta* **283**, 181.

27. Taniguchi, V.T., Ellis, W.R., Jr., Cammarata, V., Webb, J., Anson, F.C., and Gray, H.B. (1982) in *Electrochemical and Spectrochemical Studies of Biological Redox Components*, Kadish, K.M., ed., Amer. Chem. Soc., Washington, D.C., p. 51.

28. Reid, L.S., Taniguchi, V.T., Gray, H.B., and Mauk, A.G. (1982) *J. Am. Chem. Soc.* **104**, 7516.

29. Margalit, R., and Schejter, A. (1970) *FEBS Lett.* **6**, 278.

30. Huang, Y.-Y., and Kimura, T. (1984) *Biochemistry* **23**, 2231.

31. Ohnishi, T., Blum, H., Leigh, J.S., Jr., and Salerno, J.C. (1979) in *Membrane Bioenergetics*, Lee, C.P. et al., eds., Addison-Wesley, Reading, Mass., p. 21.

32. Wilson, D.F., Lindsay, J.G., and Brocklehurst, E.S. (1972) *Biochim. Biophys. Acta* **256**, 277.

33. Artzatbanov, V.Y., and Grigor'ev, V.A. (1983) *Biokhimiya* **48**, 41.

34. Artzatbanov, V.Y., Konstantinov, A.A., and Skulachev, V.P. (1978) *FEBS Lett.* **87**, 180.

35. Brudvig, G.W., Stevens, T.H., Morse, R.H., and Chan, S.I. (1981) *Biochemistry* **20**, 3912.

36. Lanne, B., Malmström, B.G., and Vänngard, T. (1979) *Biochim. Biophys. Acta* **545**, 205.

37. Scott, R.A., and Gray, H.B. (1980) *J. Am. Chem. Soc.* **102**, 3219.

38. Kojima, N., and Palmer, G. (1983) *J. Biol. Chem.* **258**, 14908.

39. Fiamingo, F.G., Altschuld, R.A., Moh, P.P., and Alben, J.O. (1982) *J. Biol. Chem.* **257**, 1639.

40. Babcock, G.T., Callahan, P.N., Ondrias, M.R., and Salmeen, I. (1981) *Biochemistry* **20**, 959.

41. Antonini, E., Brunori, M., Colosimo, A., Greenwood, C., and Wilson, M.T. (1977) *Proc. Natl. Acad. Sci. U.S.A.* **74**, 3128.

42. Orii, Y., and King, T.E. (1976) *J. Biol. Chem.* **251**, 7487.

43. Gelles, J., Li, P.M., and Chan, S.I., unpublished results.

CHAPTER VI

REFLECTIONS AND CONCLUSION

There are a few caveats to consider when comparing literature E^o values. Many vary dramatically with pH, ionic strength, and temperature. Additionally, it is important to ascertain whether reduction of the prosthetic group in question yields titration data superimposable with data for oxidation of the prosthetic group. Most reduction potentials are measured by indirect methods of questionable reliability and may not be true equilibrium potentials. Failure to demonstrate reversibility has led to a number of erroneous conclusions, particularly in the iron-sulfur protein literature.

A prominent example is the case of titration data reported for Azotobacter vinelandii ferredoxin I. This iron-sulfur protein was originally thought to contain two (4Fe-4S) clusters, one that functions with E^o = -420 mV vs. NHE and one that functions with E^o = +320 mV (1,2). This work appeared to demonstrate that the reduction potentials of (4Fe-4S) clusters can be modulated by their protein environment by greater than 700 mV within a single protein. However, subsequent studies by X-ray crystallography (3,4) showed that this metalloprotein in fact contains only one (4Fe-4S) cluster, in addition to possessing a novel (3Fe-3S) cluster. More recently, the -420 mV potential has been verified by CD spectroelectrochemistry and assigned to the reduction of the (3Fe-3S) cluster (5). The +320 mV potential was reported (2) on the basis of a Nernst plot obtained by spectrophotometric titration with ascorbate after first oxidizing the protein with a fifteenfold excess of ferricyanide. Morgan et al. (6) have shown that ferricyanide oxidation of this protein leads to cluster destruction. Controlled potential electrolysis at +245 mV in

the absence of a mediator resulted in cluster degradation as well (7). The original conclusions (1,2) regarding the redox behavior of A. vinelandii ferredoxin I must therefore be discounted.

Despite the fact that reduction potentials have been reported for almost two hundred metalloproteins, virtually nothing is known about the factors that play a dominant role in their determination. Reduction potentials can vary by hundreds of millivolts even within a particular class of metalloproteins such as the blue copper proteins or cytochromes. Measurements of the reduction potentials of mutant proteins containing single amino acid replacements should prove helpful in elucidating the effects of protein structure on redox thermodynamics.

The single most obvious factor affecting redox potentials is ligand type. Properties such as charge, soft/hard characteristics, stereochemistry, and ligand field effects are expected to influence the redox potential. One of the few reliable estimations of a ligand effect is the comparison of the Fe(III/II) redox potentials of a bis-imidazole ligated heme (+5 mV for cytochrome b_5) with an imidazole-thioether ligated heme (+260 mV for cytochrome c). The soft thioether ligand, Met-80 in cytochrome c, stabilizes the Fe(II) state relative to the Fe(III) state (which has a much lower affinity for thioethers). Studies of metalloporphyrin model complexes show that, if all other factors are kept essentially constant, the substitution of one imidazole in a low-spin bis-imidazole complex with a thioether ligand increases the Fe(III/II) potential by approximately 160 mV (8).

The nature of the immediate environment surrounding the redox

center is another very important factor affecting reduction potentials (9,10). Two examples clearly illustrate this. There is the celebrated case of iron-sulfur proteins containing (4Fe-4S) clusters. Bacterial ferredoxins operate between the $(4Fe\text{-}4S)^{2+/1+}$ oxidation levels at very negative potentials, typically -350 to -500 mV vs. NHE. Conversely, high potential iron-sulfur protein (HiPIP) operates between the $(4Fe\text{-}4S)^{3+/2+}$ states at E^{o} ~ +350 mV. Since the (4Fe-4S) cluster cores are chemically identical it is apparent that the immediate protein environment exercises a major influence over the cluster reduction potential (11,12). The factors that mght contribute to this include protein constraint of geometry, NH····S hydrogen bonding, electrostatic effects, and dielectric effects (13,14). These factors are presumed to make the $(4Fe\text{-}4S)^{1+}$ state of HiPIP and the $(4Fe\text{-}4S)^{3+}$ state of bacterial ferredoxins inaccessible. Holm and coworkers (15) have reported a synthetic cluster model capable of expressing all three oxidation states; the difference between the (2+/1+) and (3+/2+) reduction potentials is very large, 1.3 V. This suggests that a given protein is unlikely to access all three cluster oxidation states.

The second notable case illustrating structural effects on redox states and potentials involves comparison of cytochromes _c_ and $\underline{c}_3$. One might naively conclude that cytochrome _c_ (E^{o} = +260 mV) exhibits a reduction potential approximately 150-250 mV more positive than one of the bis-histidine ligated cytochromes (E^{o} ~ -300 mV) in cytochrome $\underline{c}_3$, a tetraheme protein (16-19). The actual difference is ca. 550 mV, despite the heme groups being otherwise chemically similar. The

additional 300-400 mV must arise from hydrophobic encapsulation of the deeply buried heme in cytochrome _c_ (20). This is similar to generating a positive charge in a low dielectric medium. The heme groups of cytochrome $\underline{c}_3$ are much more exposed to the aqueous medium and the propionic acid groups are more free to ionize. Thus, the immediate environment of a heme in cytochrome $\underline{c}_3$ can more readily accommodate the overall positive charge of the ferric state.

It is clear that the ability of the protein backbone and solvent environment around a redox center to stabilize (or destabilize) charge is a critical determinant of the reduction potential of the metal center. The identification of the precise origin of electrode potential differences between chemically similar protein-bound species remains a difficult problem. The location of ionizable residues, H-bonding, protein dipole orientations, and the degree of solvent exposure are all factors that can be important in charge stabilization. The coupling of these environmental influences with ligand type serves to tune reduction potentials of biological systems over an impressive range.

Many studies have established that complementary electrostatic interactions (i.e., formation of intermolecular salt linkages) play an important role in facilitating reactions between electron transfer proteins. Albery and Knowles (21) have suggested that, for the most efficient enzymes, the free-energy difference between enzyme-bound species should approach zero. Applying this argument to redox proteins, one would expect that the reduction potential difference between donor and acceptor should approach zero in the protein-protein

complex. This requires that there be an asymmetric association of a protein to the oxidized and reduced forms of its partner in the complex. Data reported by Sligar and Gunsalus (22) indicates that the reduction potentials of putidaredoxin (-239 mV) and cytochrome P-450 (-170 mV) do approach each other upon formation of a putidaredoxin/cytochrome P-450 complex (-196 mV and -173 mV, respectively). There is currently no report of reduction potential measurements for structurally characterized redox proteins that form 1:1 protein-protein complexes, however. Recent computer graphics-modelling studies have been carried out on several putative reaction complexes of physiological relevance: cytochrome c/cytochrome b_5 (23), cytochrome c/cytochrome c peroxidase (24), and cytochrome b_5/hemoglobin (25). Electrochemical measurements for these protein-protein complexes would therefore be of more than casual interest.

Most of the presently known redox enzymes contain several redox centers, in contrast to the simple "electron transferases." Molecules containing multiple redox centers present additional experimental difficulties due to the potentially large number of redox states that must be dealt with. For example, a four center redox enzyme may exhibit up to 16 states, for which 32 Nernst equations can be written (for the 32 equilibria between pairs of states). An allosteric interaction between two or more of the redox cofactors, if sufficiently large, will lead to a marked deviation from simple Nernstian behavior in redox titrations. As discussed in Chapter IV, the reduction potential defined for Nernstian systems is not a meaningful measure of the intrinsic thermodynamic properties of a site

under these circumstances, since it depends critically upon the magnitude of the interactions and the potentials of the interacting partners. This effect is especially serious when redox titration data as a function of pH, temperature, or ionic strength must be analyzed.

A considerable effort has been made to characterize the electron transfer processes that occur in multisite redox proteins. The large number of parameters involved in describing the intramolecular electron distribution amongst the various redox centers contained within a multisite system will generally require several types of experimental approaches to the problem of obtaining microscopic reduction potentials, including optical and magnetic resonance spectroscopy, the use of exogenous ligands to stabilize selected oxidation states, and selective depletion of one or more redox sites. It is clear, however, that electrochemical measurements can only yield macroscopic potentials for multisite protein systems since the metal centers are typically interacting and nonidentical. One must therefore view reports for systems such an xanthine oxidase (26,27), laccase (28-30), cytochrome $\underline{cd}_1$ (31,32), and cytochrome $\underline{c}_3$ (18,19) with caution.

Much of our intuition about the functions of the components of biological electron transport chains stems from redox titration measurements. Any considered redox mechanism must, of course, be consistent with the thermodynamic constraints of the system. The assumption that thermodynamic data are relevant to mechanisms involving "electron transferases" seems secure. However, a serious problem arises when dealing with redox enzymes that shuttle electrons

into, or out of, substrates. Such enzymes are always out of equilibrium in vivo so that classical thermodynamics is only of limited applicability. As an example, consider cytochrome c oxidase. The cytochrome a and Cu_A sites of this enzyme function as electron carriers (we ignore the proton pumping question here). Hence equilibrium redox thermodynamic measurements for these sites are mechanistically important. The cytochrome a_3/Cu_B site binds molecular oxygen during enzymatic turnover and therefore anaerobic equilibrium measurements for this binuclear site appear to be an academic exercise. The reduction potentials of the suspected (33) oxygenated intermediates present during enzymatic turnover (for example, ferrylcytochrome a_3/Cu_B^{2+}-OH^-) are of far greater mechanistic relevance than the ferricytochrome a_3/Cu_B^{2+} reduction potentials. There is unfortunately little hope of obtaining such data from studies of the enzyme itself. In this regard, electrochemical studies of recently synthesized copper-iron model complexes (34,35) would perhaps be of interest.

REFERENCES

1. Sweeney, W.V., Yoch, D.C., and Rabinowitz, J.C. (1975) *J. Biol. Chem.* **250**, 7842.

2. Yoch, D.C., and Carithers, R.P. (1978) *J. Bacteriol.* **136**, 822.

3. Ghosh, D., Furey, W., O'Donnell, S., and Stout, C.D. (1981) *J. Biol. Chem.* **256**, 4185.

4. Ghosh, D., O'Donnell, S., Furey, W., Robbins, A.H., and Stout, C.D. (1982) *J. Mol. Biol.* **158**, 73.

5. Stephens, P.J., Morgan, T.V., Devlin, F., Burgess, B.K., Stout, C.D., Ellis, W.R., Jr., Gray, H.B., Beinert, H., and Emptage, M.H. *Biochemistry*, submitted for publication.

6. Morgan, T.V., Stephens, P.J., Devlin, F., Stout, C.D., Melis, K.A., and Burgess, B.K. (1984) *Proc. Natl. Acad. Sci. U.S.A.* **81**, 1931.

7. Ellis, W.R., Jr., and Morgan, T.V., unpublished results.

8. Marchon, J.-C., Mashiko, T., and Reed, C.A. (1982) in *Electron Transport and Oxygen Utilization*, Ho, C., ed., Elsevier Biomedical, New York, p. 67.

9. Stellwagen, E. (1978) *Nature* **275**, 73.

10. Kassner, R.J. (1973) *J. Am. Chem. Soc.* **95**, 2674.

11. Carter, C.W., Jr. (1977) *J. Biol. Chem.* **252**, 7802.

12. Carter, C.W., Jr. (1977) in *Iron-Sulfur Proteins, Vol. 3*, Lovenberg, W., ed., Academic Press, New York, p. 157.

13. Sweeney, W.V., and Rabinowitz, J.C. (1980) *Ann. Rev. Biochem.* **49**, 139.

14. Sheridan, R.P., Allen, L.C., and Carter, C.W., Jr. (1981) *J. Biol. Chem.* **256**, 5052.

15. DePamphilis, B.V., Averill, B.A., Herskovitz, T., Que, L., Jr., and Holm, R.H. (1974) *J. Am. Chem. Soc.* **96**, 4159.

16. Pierot, M., Haser, R., Frey, M., Payan, F., and Astier, J.-P. (1982) *J. Biol. Chem.* **257**, 14341.

17. Higuchi, Y., Kusunoki, M., Matsuura, Y., Yasuoka, N., and Kakudo, M. (1984) *J. Mol. Biol.* **172**, 109.

18. Santos, H., Moura, J.J.G., Moura, I., LeGall, J., and Xavier, A.V. (1984) *Eur. J. Biochem.* **141**, 283.

19. Sokol, W.F., Evans, D.H., Niki, K., and Yagi, T. (1980) *J. Electroanal.*

Chem. **108**, 107.

20. Kassner, R.J. (1972) *Proc. Natl. Acad. Sci. U.S.A.* **69**, 2263.

21. Albery, W.J., and Knowles, J.R. (1976) *Biochemistry* **15**, 5631.

22. Sligar, S.G., and Gunsalus, I.C. (1976) *Proc. Natl. Acad. Sci. U.S.A.* **73**, 1078.

23. Salemme, F.R. (1976) *J. Mol. Biol.* **102**, 563.

24. Poulos, T.L., and Kraut, J. (1980) *J. Biol. Chem.* **255**, 10322.

25. Poulos, T.L., and Mauk, A.G. (1983) *J. Biol. Chem.* **258**, 7369.

26. Spence, J.T., Barber, M.J., and Siegel, L.M. (1982) *Biochemistry* **21**, 1656.

27. Porras, A.G., and Palmer, G. (1982) *J. Biol. Chem.* **257**, 11617.

28. Farver, O., Goldberg, M., Wherland, S., and Pecht, I. (1978) *Proc. Natl. Acad. Sci. U.S.A.* **75**, 5245.

29. Taniguchi, V.T., Malmström, B.G., Anson, F.C., and Gray, H.B. (1982) *Proc. Natl. Acad. Sci. U.S.A.* **79**, 3387.

30. Wynn, R.M., Knaff, D.B., and Holwerda, R.A. (1984) *Biochemistry* **23**, 241.

31. Blatt, Y., and Pecht, I. (1979) *Biochemistry* **18**, 2917.

32. Carson, S.D., Ching, Y.C., Wells, C.A., Wharton, and Ondrias, M.R. (1986) *Biochemistry* **25**, 787.

33. Blair, D.F., Witt, S.N., and Chan, S.I. (1985) *J. Am. Chem. Soc.* **107**, 7389.

34. Gunter, M.J., Mander, L.S., Murray, K.S., and Clark, P.E. (1981) *J. Am. Chem. Soc.* **103**, 6784.

35. Gunter, M.J., Berry, K.J., and Murray, K.S. (1984) *J. Am. Chem. Soc.* **106**, 4227.